A ROLE FOR p107 IN MUSCLE SATELLITE CELL SELF-RENEWAL

VICKY SHAH

A DISSERTATION SUBMITTED TO THE FACULTY OF GRADUATE STUDIES IN PARTIAL FUFILLMENT OF THE REQUIREMENTS FOR THE DEGREE OF MASTER OF SCIENCE

GRADUATE PROGRAM IN BIOLOGY

YORK UNIVERSITY
TORONTO, ONTARIO
JANUARY, 2023

Abstract

It is well established that skeletal muscle homeostasis is dependent on the activity of the muscle resident stem cells termed satellite cells (SCs). Many neuromuscular dystrophies and complications brought on from ageing are associated with decline to the SC population. Thus, there is a critical need to investigate the control mechanisms that dictate SC fate decisions for self-renewal that are crucial to maintain the SC population. A fundamental regulator of SC fate decisions is mitochondrial metabolism and thereby mitochondrial ATP generation via oxidative phosphorylation (OXPHOS). In our study we uncover a potential novel role for the transcriptional co-repressor retinoblastoma susceptibility protein like 1(Rbl1 or p107) in manipulating the self-renewal capacity of SCs through its mitochondrial localization under the control of the NAD^+/NADH ratio. An investigation of this role for p107 function establishes a new mechanism to target SC decline and improve muscle regeneration that is required in muscular dystrophies and ageing.

Acknowledgements

First and foremost, I would like to thank my supervisor, **Dr. Anthony Scimè**, for giving me this amazing opportunity 2 years ago. I will forever be grateful to you for providing me the chance to push myself and pursue research. Although, we have not always seen eye to eye, I cannot thank you enough for continuing to push me to worker harder each and every day. There have been many ups and downs throughout this journey, and I can say with certainty that I would not have been able to continue going without your constant motivation and encouragement. I admire and respect your love for research and ability to inspire your students to want to find the next groundbreaking result. It is something that I want to replicate and apply to my own life. I appreciate the countless number of hours you have put into reviewing my work to helping me improve my technical and writing skills. Again, I cannot stress this enough, but I really do thank you for taking a chance on an inexperienced student and sticking by my side through everything.

I would also like to thank **Dr. John C. McDermott** for being a part of my supervisory committee. Thank you for showing interest in my research work throughout every step of the way. In addition, I want to thank **Dr. Tara Haas** for her insights and suggestions on improving my experimental protocol and techniques. Moreover, I am grateful to Dr. Haas for allowing me to borrow reagents at the shortest notice without hesitation.

To all the lab volunteers and my lab mates, **Joy**, **Debasmita**, **Lucas**, **Justin**, **Kira**, **Marissa** and **Kyra** thank you all of your contributions towards my success, and for making the lab such an inviting place to be. I would like to give special thanks to Joy and Debasmita for all their guidance and taking time out of there busy schedules to teach and help me without hesitation. To Lucas, Justin and Kira I want to thank the three of you for being so kind and willing to help with experiments. I would like to specifically thank **Jaryeon** and **Nadeem** for not just helping with my experiments but for going out of their way to make my day better. I cannot thank you enough and I am forever indebted to you. I am happy to have got the chance to work beside you all and I am delighted to consider you, my friends.

I would like to thank my loving girlfriend **Cassandra** for always being there and giving me the support, I needed. I am proud to have you by my side and I cannot thank you enough for all that you have sacrificed over the years to let me pursue my academic journey. It is very enduring to know that I have someone like you who will always be by my side no matter what. I thank you for continuing to push me to achieve more and I wish to do the same for you.

Finally, I would like to thank my **parents** and **sister** for encouraging me to take this opportunity. If it wasn't for you three, I might have not taken this opportunity and would be living with regret. I thank you for teaching me to stand up for myself and fight for what I want. Thank you for always supporting me and allowing me to explore all my interests. I wish to make you all proud by achieving my dream.

Table of Contents

List of Figures

Chapter 1:

Introduction:

Chapter 4:

Results:

Chapter 5:

Discussion:

List of Publications

1. Bhattacharya, D., **Shah, V**., Oresajo, O., Scimè, A. (2021). p107 mediated mitochondrial function controls muscle stem cell proliferative fates. *Nat Commun* **12,** 5977

Data for figures **4.3**, **4.4**, **4.5** and **4.26** were from the above publication.

List of Abbreviations

SC	Satellite cells
Pax7	Paired homeobox transcription factor 7
MyoD	Myogenic determining factor 1
Myf5	Myogenic factor 5
Myog	Myogenin
RNA	Ribonucleic acid
DNA	Deoxyribonucleic acid
Wnt7A	Wingless-type MMTV integration site 7A
Fzd7	Frizzled 7
ATP	Adenosine tri-phosphate
NADH	Reduced nicotinamide adenine dinucleotide
NADPH	Reduced nicotinamide adenine dinucleotide phosphate
ETC	Electron transport chain
TCA	Tri-carboxylic acid cycle
Pdh	Pyruvate dehydrogenase
Ldha	Lactate dehydrogenase
OXPHOS	Oxidative phosphorylation
UQ	Ubiquinone
Cyt c	Cytochrome c
$FADH_2$	Reduced flavin adenine dinucleotide
NAD^+	Nicotinamide adenine dinucleotide
mtDNA	Mitochondrial deoxyribonucleic acid

mRNA	Messenger ribonucleic acid
rRNA	Ribosomal ribonucleic acid
tRNA	Transfer ribonucleic acid
LSP	Light strand promoter
HSP1	Heavy strand promoter 1
HSP2	Heavy strand promoter 2
Tfam	Transcription factor A of mitochondria
Polrmt	Mitochondrial DNA-directed RNA polymerase
Tfb2m	Transcription factor B2 of mitochondria
p107	Rbl1
Rb	Rb1
p130	Rbl2
p107KO	p107 genetically deleted
Sirt1KO	Sirt1 genetically deleted
SDS-PAGE	Sodium dodecyl sulfate polyacrylamide gel electrophoresis
PGC-1	Peroxisome proliferator-activated receptor gamma coactivator-1
MP	Myogenic progenitor

CHAPTER 1

LITERATURE REVIEW

1.1 Satellite cells

Skeletal muscle, comprising a large portion of total body mass, is a major organ crucial for physical movement (Díaz-Vegas et al., 2019). This is made possible by muscle contraction of thousands of multinucleated muscle fibers. In addition to physical movement, skeletal muscle is a major source for glucose and fatty acid metabolism. Importantly, skeletal muscle demonstrates a remarkable ability to undergo complete myofiber regeneration to maintain its normal physiology over its entire lifetime. This is due to its inherent ability to respond to changes in contractile activity, substrate availability and crucially to injury (Gundersen, 2011; Nguyen et al., 2019; Yin et al., 2013).

Successful myofiber regeneration is made possible by the presence of muscle resident adult myogenic stem cells termed satellite cells (SCs) (Mauro, 1961; Sousa-Victor et al., 2022). From their discovery over half a century ago (Mauro, 1961), SCs have been a major focus of skeletal muscle research. Due to their peripheral localization, SCs were originally hypothesized to be dormant cells that are involved in myofiber regeneration (Mauro, 1961). This hypothesis was later confirmed with advancements in skeletal muscle research revealing that SCs are the primary myogenic stem cells responsible for skeletal muscle maintenance and regeneration (Moss & Leblond, 1970; Reznik, 1969).

The SC population consists of 2% to 10 % of total myonuclei that are located between the basal lamina of myofiber sarcolemma, which allows the signals to be received from the surrounding microenvironment in a timely manner (Yin et al., 2013) (Dumont, Bentzinger, et al., 2015). As in other stem cells, the SCs can self-renew to replenish their population or commit to

differentiate, adding nuclei to existing myofibers or altogether forming new myofibers. Unfortunately, malfunctioning of the SC population is associated with the buildup of fibrotic tissue from poor skeletal muscle regeneration and results in a progressive loss of muscle strength (Mann et al., 2011; Sousa-Victor et al., 2022).

SC malfunction is commonly associated with the decline of skeletal muscle that is observed in neuromuscular disorders such as muscular dystrophies and muscle complications associated with ageing (N. C. Chang et al., 2016; W. Chen et al., 2020; Hwang & Brack, 2018). In muscular dystrophies there is a malfunction to SC divisions which leads to poor regeneration (N. C. Chang et al., 2016). In Duchenne muscular dystrophy, the absence of dystrophin causes SCs to give rise to progenitors that have reduced transcription of myogenic regulatory factors (N. C. Chang et al., 2018). This in turn leads to a diminished population of SCs required for sufficient muscle regeneration. Research on aged skeletal muscle indicates that in both uninjured and injured muscle there is a decline in the function and number of SCs (**Fig. 1.1**) (Cosgrove et al., 2014). Moreover, the age-related changes to the microenvironment are thought to influence quiescent SCs, by reducing their self-renewal capacity and activation potential (Chakkalakal et al., 2012; Hwang & Brack, 2018). This contributes to the diminished skeletal muscle regeneration from the smaller initial starting population of SCs with reduced proliferative ability that is observed in aged muscle (**Fig. 1.1**) (Shefer et al., 2006).

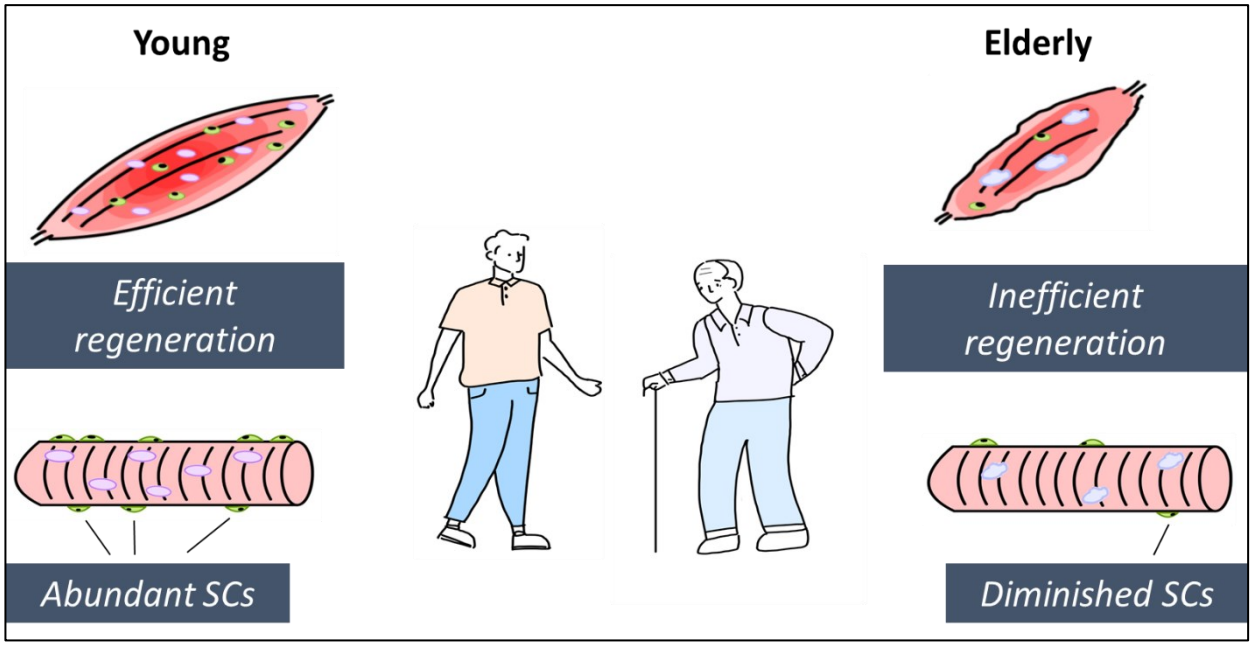

Figure 1.1: Schematic of SC decline observed through ageing. Compared to young skeletal muscle, aged skeletal muscle is associated with poor regeneration and a diminished SC population.

1.2 Satellite cell fate decisions

It is well established that SCs exist as a quiescent adult stem cell population that can become activated upon the introduction of stimuli, for example from muscle injury (**Fig. 1.2**) (Yin et al., 2013). Upon activation, SCs begin to proliferate to eventually generate new quiescent stem cells or commit to differentiate (**Fig. 1.2**) (Almada & Wagers, 2016; Giordani et al., 2018; Zammit et al., 2006). SCs are known to have differing protein and gene expression profiles during quiescence, activation, and differentiation, which allows for the discrimination of each of these states (Giordani et al., 2018). Quiescent SCs are characterized by the expression of paired homeobox transcription factor 7 (Pax7) (**Fig. 1.3**) (Zammit et al., 2006). Upon the introduction of stimuli from injury, the quiescent SCs activate and begin protein expression of myogenic determining factor 1 (MyoD) and might also express myogenic factor 5 (Myf5) (Kuang et al., 2007; Zammit et al., 2006). In quiescent SCs, MyoD and Myf5 ribonucleic acid (RNA) transcripts are stored in structures known as granules (Crist et al., 2012). The granules are comprised of non-

translating messenger RNA (mRNA) that is ready for release and translation upon activation to instigate a rapid start to the myogenic program (Crist et al., 2012; de Morrée et al., 2017). Correspondingly, SC activation is followed by a rapid increase in MyoD gene and protein expression which promotes rapid entry to proliferation (Yablonka-Reuveni, 2011; Zammit et al., 2006). Once activated, SCs enter a proliferative state, rapidly dividing to generate enough cells for differentiation and for maintenance of the quiescent SC population (**Fig. 1.3**). A small subset of the proliferating SCs will discontinue MyoD protein expression and become quiescent SCs (**Fig. 1.3**) (Zammit et al., 2006). Whereas most will differentiate, terminating Pax7 expression and initiating the expression of various muscle specific genes that include other myogenic regulatory factors (MRFs) such as Myogenin (Myog) and structural proteins (Dumont, Bentzinger, et al., 2015). Thus, based on Pax7 and MyoD protein expression, SCs can be discriminated as quiescent (Pax7+/MyoD-), activated/proliferating (Pax7+/MyoD+), or differentiating (Pax7-/MyoD+) (**Fig. 1.3**) (Olguin et al., 2007; Yin et al., 2013; Zammit et al., 2004, 2006).

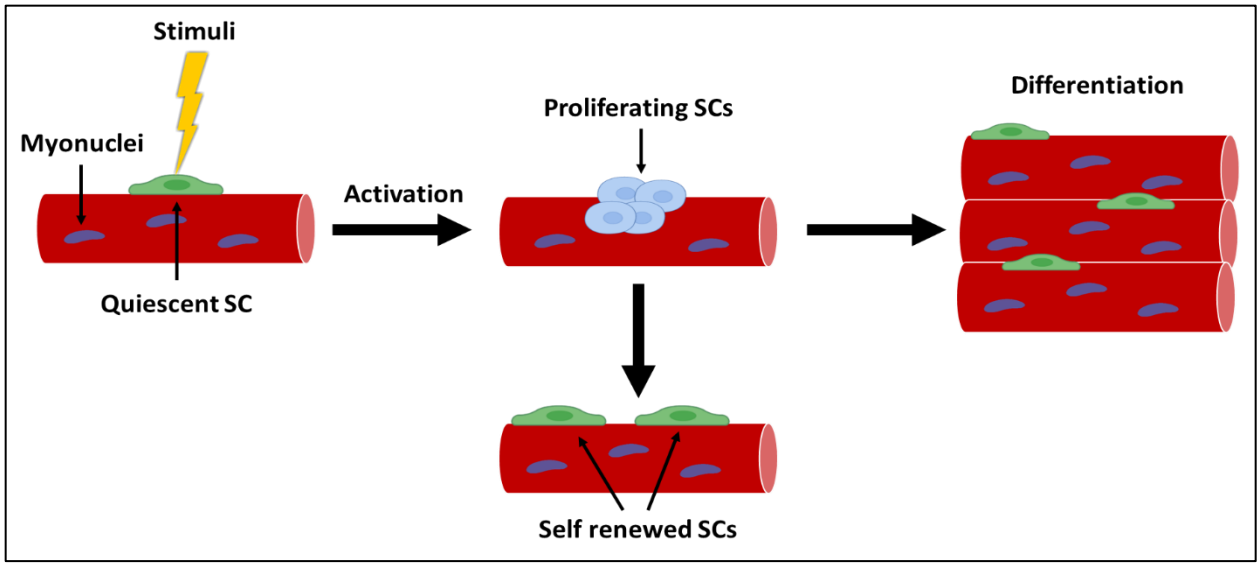

Figure 1.2: Schematic of SC fates. SCs are normally quiescent and become activated after the introduction of a stimuli. SCs then rapidly proliferate to generate sufficient progeny for differentiation. A small portion of the proliferating SCs replenish the quiescent SC pool.

SCs isolated from tissue or ex vivo from myofibers that are cultured in vitro can proliferate and be induced to differentiate into myotubes (Yin et al., 2013). In vitro, the proliferating cells are referred to as myoblasts or myogenic progenitors (MPs), which correspond to myofiber associated proliferating SCs (**Fig. 1.4**) (Snow, 1978). Additionally, MPs that are induced to undergo differentiation but maintain their myogenic potential are referred to as reserve cells (**Fig. 1.4**). Reserve cells can become activated and differentiate, thus are thought to be analogous to a myofiber associated quiescent SC population (Pax7+/MyoD-) (**Fig. 1.3**) (Nalbandian et al., 2021; Yoshida et al., 1998).

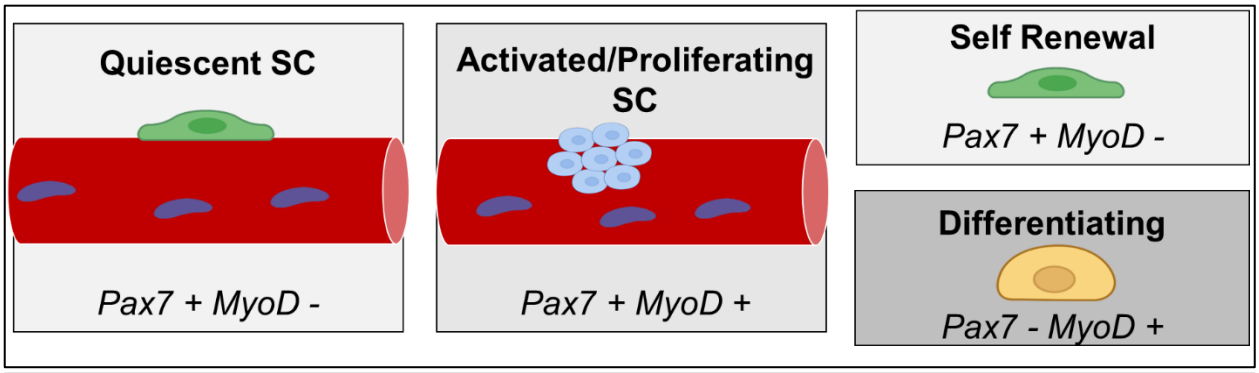

Figure 1.3: Pax7 and MyoD expression profile in SC fate. All quiescent SCs exclusively express Pax7 and only begin to express MyoD once activated. Some activated SCs can lose their Pax7 expression and differentiate to form myofibers. Self-renewal occurs when activated SCs downregulate MyoD and return to quiescence.

Quiescent SCs are thought to exist as a heterogenous population, Kuang et al showed that roughly 90% of SCs are a committed population that have expressed Myf5 at some point during their lifetime before returning to quiescence, and 10% being an uncommitted population that has never expressed Myf5 (Feige et al., 2018; Kuang et al., 2007). The latter population can undergo asymmetric division which produces Myf5 positive and negative cells. Moreover, both populations can undergo symmetric division, which is responsible for expanding their populations, resulting in two Myf5 positive or two Myf5 negative cells (Dumont, Bentzinger, et al., 2015; Kuang et al., 2007; Yin et al., 2013).

The regulation of symmetric and asymmetric SC division that is required for the maintenance of the SC population is preserved by Wingless-type MMTV integration site 7A (Wnt7A) signaling and its receptor Frizzled 7 (Fzd7) (le Grand et al., 2009). Recently, the dystrophin glycoprotein complex has also been implicated in regulating SC asymmetric division (N. C. Chang et al., 2018; Dumont, Wang, et al., 2015). Studies on mdx mice revealed that dystrophin controls Carm1 phosphorylation which effects Pax7 methylation and thereby Myf5 transcription (N. C. Chang et al., 2018). In addition, dystrophin is shown to control the expression of Mark2 a kinase known to regulate cell polarity (Dumont, Wang, et al., 2015). Both regulatory pathways function by dictating the polarity of the cell and thus causing a parallel (symmetric) or perpendicular (asymmetric) division to occur with respect to the basal lamina (N. C. Chang et al., 2018; Dumont, Wang, et al., 2015; le Grand et al., 2009).

1.3 Glycolysis and OXPHOS in energy metabolism

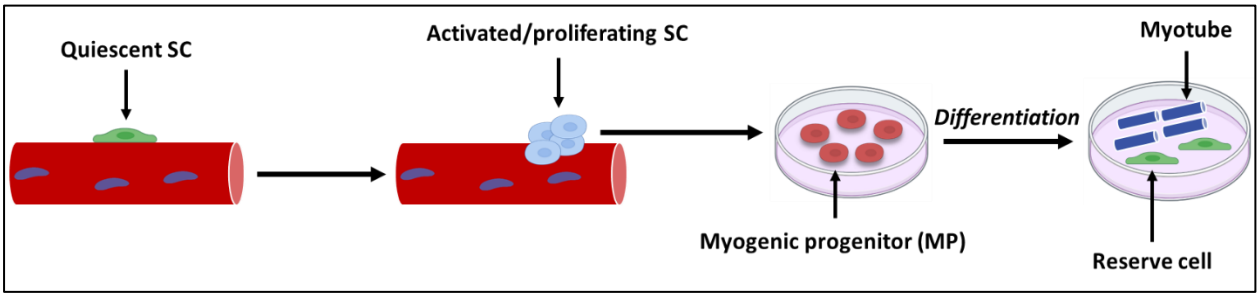

Figure. 1.4 Schematic of myogenic progenitor and reserve cell generation from SCs. In vitro SCs become myogenic progenitors (MPs) that are analogous to the myofiber bound activated/proliferating SCs. MPs have the ability to differentiate and form new myotubes or to become reserve cells that are analogous to quiescent SCs. The reserve cells can be activated to proliferate leading to myotube formation and/or more reserve cells. Figure created with BioRender.

Crucial to SC function is the interplay between glycolysis and oxidative phosphorylation (OXPHOS) that generate ATP (Bhattacharya & Scimè, 2020). Glycolysis rapidly generates two molecules of ATP and glycolytic intermediates that might be used to make nucleotides, lipids, amino acids, reduced nicotinamide adenine dinucleotide (NADH) and reduced nicotinamide

adenine dinucleotide phosphate (NADPH) (Lunt & vander Heiden, 2011). The NADH produced from glycolysis can remain in the cytoplasm or be transported into the mitochondria via the malate-aspartate shuttle to be serve as a reducing agent for OXPHOS (Kane, 2014). Pyruvate, the end product of glycolysis can form acetyl-coA via pyruvate dehydrogenase (Pdh) or oxaloacetate via pyruvate carboxylase. Acetyl-coA and oxaloacetate might be shuttled into the tri-carboxylic acid cycle (TCA), which is present in the mitochondria, where the reducing agents NADH and reduced flavin adenine dinucleotide ($FADH_2$) are produced (**Fig. 1.5**) (DeBerardinis et al., 2008; Martínez-Reyes et al., 2016). Alternatively, pyruvate can be converted to lactate in the cytosol with oxidation of NADH by lactate dehydrogenase (Ldha) (**Fig. 1.5**). Lactate formation typically occurs in the absence of oxygen and is known as anaerobic glycolysis. However, aerobic glycolysis occurs if lactate is formed in the presence of oxygen when the need for rapid ATP supply is required (Lunt & vander Heiden, 2011).

OXPHOS, which takes place in the mitochondria produces more ATP than glycolysis at a slower rate (Pfeiffer et al., 2001). The mitochondria are a cellular organelle comprised of an outer and inner double membrane (Chandel, 2018). The area between the membranes is termed the intermembrane space, while the matrix is designated as the area enclosed by the inner membrane (Chandel, 2018). Mitochondrial ATP generation via OXPHOS occurs on the inner membrane where the electron transport chain (ETC) accepts electrons from reducing agents produced mainly from the TCA cycle or NADH from glycolysis. The ETC is comprised of 5 major complexes (I through to V) and a lipid soluble electron carrier between complexes I/II and III called ubiquinone (UQ) and a water-soluble carrier between complexes III and IV called cytochrome c (Cyt c) (Martínez-Reyes & Chandel, 2020). NADH and $FADH_2$ enter the ETC through complexes I and II respectively where they are oxidized and their electrons are passed through the chain and travel

to the final electron acceptor oxygen at complex IV (**Fig. 1.5**) (Martínez-Reyes & Chandel, 2020). The passing of electrons through the ETC results in the pumping of protons by complexes I, III, and IV from the matrix to the inter-membrane space (Martínez-Reyes & Chandel, 2020). The movement of protons generates the mitochondria membrane potential (ψ) (Martínez-Reyes et al., 2016; Martínez-Reyes & Chandel, 2020) that causes protons to funnel through complex V, which is an ATP synthase causing the production of ATP from ADP (**Fig. 1.5**) (Martínez-Reyes & Chandel, 2020).

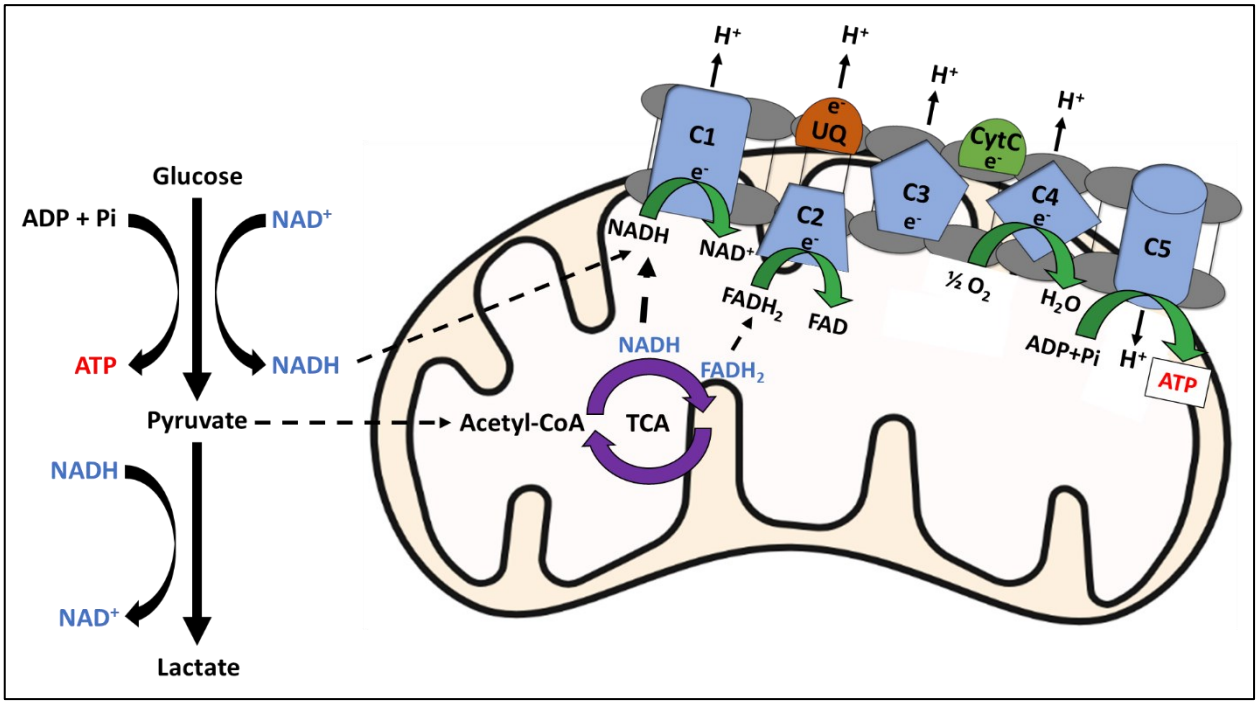

Figure 1.5: Diagram of glycolysis and OXPHOS. In the cytoplasm, glucose is converted to pyruvate via glycolysis, which enters the mitochondria and TCA cycle as acetyl-CoA. The NADH and $FADH_2$ generated from glycolysis and the TCA cycle is oxidized in the ETC by donating electrons. The electrons (e^-) are funneled through the complexes and transported via ubiquinone (UQ) and cytochrome C (CytC) eventually contributing to the generation of ATP via OXPHOS. Protons are pumped out of matrix at complex 1 (C1), complex 3 (C3) and complex 4 (C4) and pumped back into the matrix at complex 5 (C5).

1.4 Mitochondrial DNA

The mitochondria contain their own DNA within the matrix. The mitochondrial DNA (mtDNA) contains about 16,600 base pairs of double stranded DNA (D'Souza & Minczuk, 2018). It consists of a regulatory non-coding D-loop region and encodes 13 messenger RNAs (mRNAs), which are translated into subunits of the ETC complexes, 2 ribosomal ribonucleic acids (rRNA) and 22 transfer ribonucleic acids (tRNA) (**Fig 1.6**) (D'Souza & Minczuk, 2018). The two strands of mtDNA can be subdivided into a heavy and light strand. The light strand only contains one gene promotor element (LSP), whereas the heavy strand contains two unique promoters (HSP1) and (HSP2) from where transcription can be initiated (**Fig. 1.6**) (D'Souza & Minczuk, 2018). LSP is associated with the transcription of Nd6, a subunit of complex I in addition to 8 tRNAs (Guja & Garcia-Diaz, 2012). HSP1 encodes 16S and 12S rRNA and HSP2 generates a polycistronic RNA that encodes 12 mRNAs and 12 tRNAs (**Fig. 1.6**) (D'Souza & Minczuk, 2018; Guja & Garcia-Diaz, 2012).

For the initiation of mtDNA transcription to occur, transcription factor A of mitochondria (Tfam), mitochondrial DNA-directed RNA polymerase (Polrmt) and transcription factor B2 of mitochondria (Tfb2m) are recruited (Farge & Falkenberg, 2019; Gustafsson et al., 2016). Tfb2m is thought to interact with Polrmt to facilitate a transition to an open promoter, which is required for transcription initiation (Ramachandran et al., 2017). There are two major hypotheses regarding the role of Tfam in the transcription complex. In one hypothesis Tfam acts as a transcriptional activator and detaches from the Tfb2m and Polrmt complex once transcription has begun (Gustafsson et al., 2016; Hillen et al., 2017; Morozov et al., 2015). In another, Tfam is part of the Tfb2m and Polrmt complex throughout transcription (Lodeiro et al., 2012; Zollo et al., 2012). Intriguingly, in proliferating myogenic cell line C2C12 Tfam protein expression remains relatively

low and rapidly increased during differentiation (Collu-Marchese et al., 2015). This suggests that in SCs Tfam might not be an active member of the mitochondrial transcription complex during proliferation.

Importantly, the mtDNA is a regulator of ATP synthesis rates, as it is responsible for the expression of the mitochondrial genes that make up functional components of 4 out of 5 of the ETC complexes (**Fig. 1.6**) (Gustafsson et al., 2016). This is apparent in some diseases and with ageing where mutations in the mtDNA reduces mitochondrial efficiency resulting in decreasing ATP generation capacity (Carelli & Chan, 2014; Ryzhkova et al., 2018).

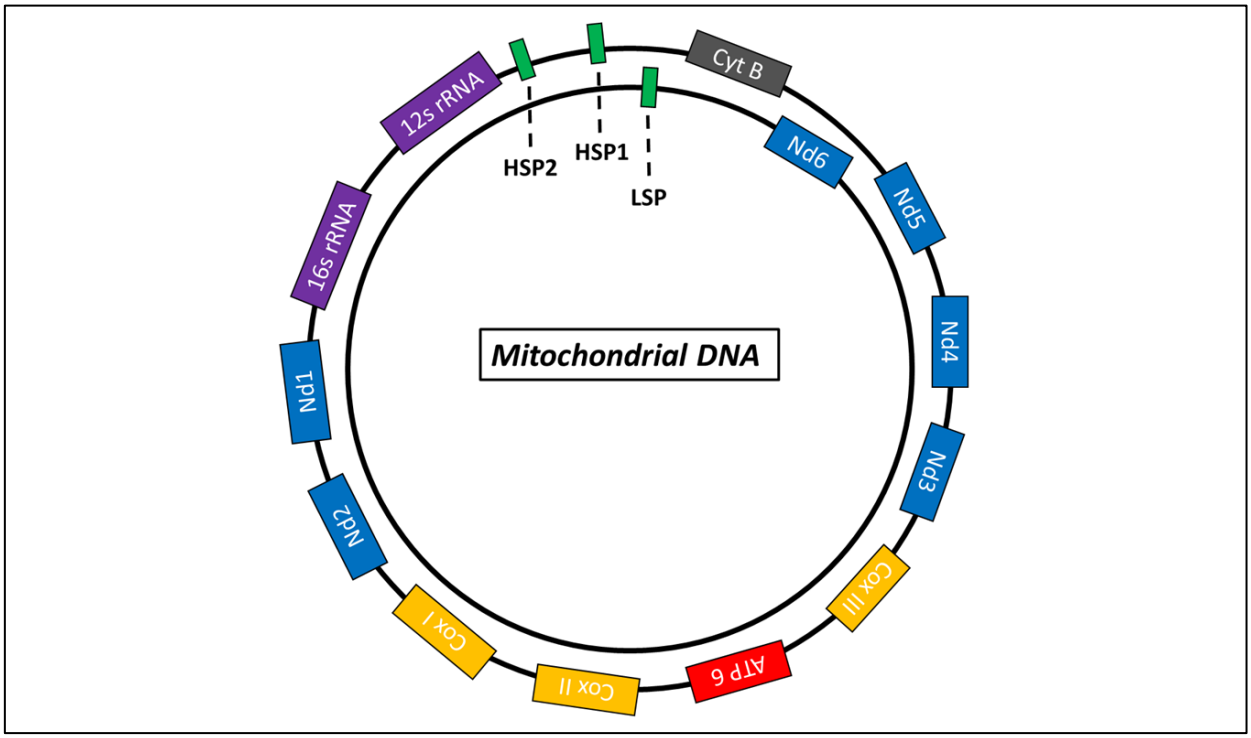

Figure 1.6: Schematic of mitochondrial DNA. The mitochondrial DNA is comprised of two heavy strand promoters (HSP1 and HSP2) and one light strand promoter (LSP) (green). The ETC subunit genes encoded are for complex I, Nd1, Nd2, Nd3, Nd4, Nd5, Nd6 (blue), complex III, Cyt B (grey), complex IV, CoxI, CoxII, CoxIII (yellow), and complex V, ATP 6 (red) and two rRNA genes, 16s rRNA and 12s rRNA (purple). Eight other tRNAs are not visualized.

1.5 The NAD^+/NADH redox ratio and Sirtuins in SC fate choices

The NAD^+/NADH ratio can act as a measure of the relative contribution of glycolysis and OXPHOS to ATP generation (Cantó et al., 2015). A low NAD^+/NADH ratio is associated with an increased reliance on glycolysis for ATP generation, whereas a high NAD^+/NADH ratio is indicative of a greater contribution from OXPHOS (**Fig. 1.7**) (Lunt & vander Heiden, 2011). The phenomena of a low NAD^+/NADH ratio is a common feature of cells that undergo high levels of proliferation, such as cancers cells and cells that are exposed to hypoxic environments, where glycolysis is the driving force for ATP production (Eales et al., 2016; vander Heiden & DeBerardinis, 2017). Likewise, in conditions of hyperglycemia where the NAD^+/NADH ratio is low, there is a reduction to OXPHOS in favor of glycolysis for ATP production (Xiao et al., 2018). In contrast, in conditions of caloric deficit or glucose starvation which increase the NAD^+/NADH ratio, there is a reliance on OXPHOS in place of glycolysis for ATP production (Xiao et al., 2018). Overall, ATP production in a cell is a balance between glycolysis and OXPHOS, and an important parameter that measures the contribution of either pathway is the NAD^+/NADH ratio (Cantó et al., 2015; Eales et al., 2016; Xiao et al., 2018).

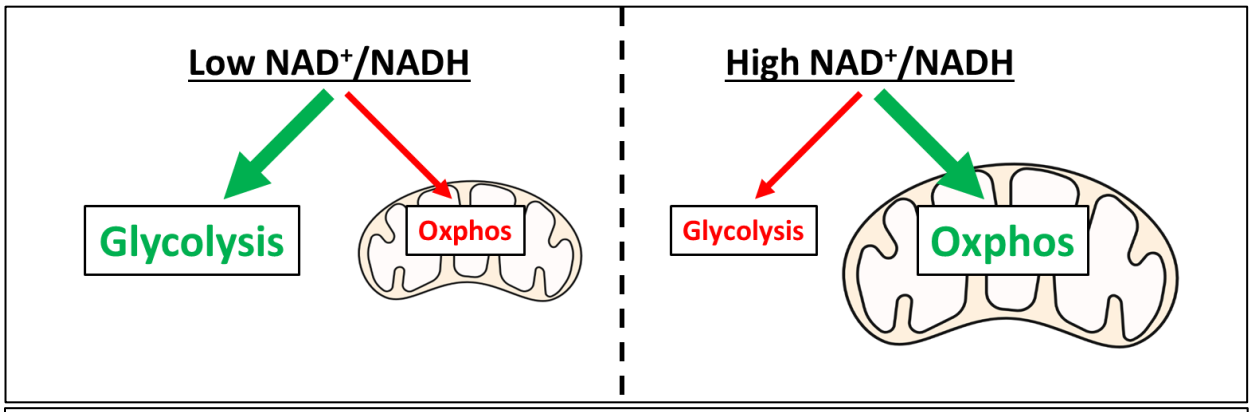

Figure 1.7: Schematic of relative contribution of glycolysis and OXPHOS with low or high NAD^+/NADH ratio. When the NAD^+/NADH ratio is low there is shift to a more glycolytic metabolism where glycolysis becomes the main source of ATP generation. In contrast, when the NAD^+/NADH ratio is high there is a reliance on OXPHOS for ATP generation in place of glycolysis.

In SCs, there is a gradual decline in mitochondrial content and thereby activity that occurs with ageing (García-Prat et al., 2016). This is thought to be modulated by the decline to NAD^+ levels that occurs alongside mitochondrial decline in ageing (Frederick et al., 2016). Intriguingly, the replenishment of NAD^+ to aged mice saw improvements to SC activation and skeletal muscle regeneration following injury (H. Zhang et al., 2016). Moreover, the replenishment of NAD^+ in SCs and C2C12 MPs improved mitochondrial function and reduced the expression of cellular senescence markers (H. Zhang et al., 2016).

NAD^+ is involved in many cellular reactions and is known to exert its metabolic effect through its function as a positive cofactor for the sirtuin (Sirt) family of deacetylases (Boutant & Cantó, 2014). The Sirts are known to act as cellular energy sensors through the NAD^+/NADH, as their activity increase when the ratio is high and there is more NAD^+ available (Boutant & Cantó, 2014; Cerutti et al., 2014). Sirt1 is known to enhance mitochondrial activity by its NAD^+ dependent interaction with peroxisome proliferator-activated receptor gamma coactivator-1α (PGC-1), which enhances mitochondrial biogenesis (Cantó et al., 2012; Gerhart-Hines et al., 2007). Due to the reliance on NAD^+ for Sirt1 to exert its effects on metabolism, any manipulation to the NAD^+/NADH ratio influences Sirt1 activity (Boutant & Cantó, 2014; Cerutti et al., 2014). This is demonstrated in conditions of soaring glucose or fat availability which lower the NAD^+/NADH ratio and decrease Sirt1 activity or in conditions of caloric restriction, which do the opposite. (Anderson et al., 2017; Cantó et al., 2015).

Sirt1 is thought to play a crucial role in SC fate decisions. Its activity during SC activation is debated and there are opposing views. On one hand Sirt1 has been shown to upregulate autophagy to provide the energy required for SC proliferation (Tang & Rando, 2014). Moreover, the deletion of SC specific Sirt1 has been shown to delay SC activation and reduce muscle

regeneration, whereas its overexpression has been shown to improve muscle regeneration in elderly mice (Myers et al., 2019; Tang & Rando, 2014). On the contrary, Sirt1 has been shown to become less active during SC activation due to the decrease in free NAD^+ from the metabolic shift to glycolysis from OXPHOS (Ryall et al., 2015). Moreover, the absence of Sirt1 has been shown to deregulate SC activation and promote premature differentiation (Ryall et al., 2015). Consistent with these findings, the activation of Sirt1 via caloric restriction is strongly linked with enhanced SC self-renewal and enhanced proliferative capacity (Cerletti et al., 2012).The diverging role of Sirt1 explained by these groups might be due to differences in the time point considered for SC activation and the use of whole body versus SC specific Sirt1KO models (Ryall et al., 2015; Tang & Rando, 2014). Intriguingly, Sirt1 and SCs both decline with age, which suggests that Sirt1 activity might have a protective affect against the age-related decline in SC regenerative capacity (Myers et al., 2019). Notably, SCs with a Sirt1 deletion fail to activate, decrease mitochondrial function, and reduce skeletal muscle regeneration capacity post injury (H. Zhang et al., 2016).

Sirt2, another Sirt family member, is also known to regulate SC fate choices by enhancing SC self-renewal via its deacetylation of Pax7 (Sincennes et al., 2021). Sirt2 knockdown increased asymmetric divisions resulting in the expansion of the Myf5 positive SC population and enhanced Myf5 expression (Sincennes et al., 2021). In addition, Sirt2 activity is shown to be necessary to maintain MP proliferation and repress differentiation by complexing with MyoD (Fulco et al., 2003; Massenet et al., 2021). Indeed, cells with decreased Sirt2 expression had a greater propensity to prematurely differentiate (Fulco et al., 2003).

Sirt3, is known to function solely in the mitochondria and is considered to control mitochondrial metabolism through its NAD^+ dependent deacetylase activity (Costa-Machado & Fernandez-Marcos, 2019). In the mitochondria Sirt3 has been shown to regulate the acetylation

levels of many mitochondrial proteins involved in transcription, translation, lipid metabolism, ETC, OXPHOS and the TCA cycle (J. Zhang et al., 2020). Moreover, Sirt3 decline has been shown to negatively affect mitochondrial OXHPOS activity and is a characteristic of the age-related mitochondrial decline observed in muscle (Costa-Machado & Fernandez-Marcos, 2019; J. Zhang et al., 2020). Though there is not much research on the role of Sirt3 in SC fate choices, Sirt3 has been shown to regulate myoblast differentiation (Abdel Khalek et al., 2014). Abdel et al, show that in C2C12 cells Sirt3 expression peaks at the onset of differentiation and the inhibition of Sirt3 expression results in diminished terminal differentiation (Abdel Khalek et al., 2014). Moreover, the reduced differentiation capacity is evidenced by the low expression levels of Myog and decline of the myofusion index (Abdel Khalek et al., 2014).

The NAD^+/NADH ratio can be used as a tool to gauge the level of free acetyl-coA. When the NAD^+/NADH ratio is low (glycolytic flux is high) there is an increase of acetyl-coA formation (Klimova et al., 2019; Yucel et al., 2019). Contrarily, when the NAD^+/NADH ratio is high (OXPHOS is favoured) then acetyl-coA is used in the TCA cycle to generate the reducing agents required for the ETC causing a decline in free acetyl CoA levels (Klimova et al., 2019; Yucel et al., 2019). In SCs, acetyl-coA has been shown to promote SC activation and myogenic progression through its control over histone and Pax7 acetylation levels (Massenet et al., 2021; Sincennes et al., 2021). Moreover, with the onset of differentiation SCs are characterized by hyperacetylation of histones H3 and H4 which are associated with the promotion of differentiation related genes (Massenet et al., 2021). Intriguingly, the reduction of acetyl-coA mediated Pax7 acetylation results in a significant decline to Myf5 expression and promoted an expansion of the quiescent SC population (Sincennes et al., 2021). These findings indicate that increased acetyl-coA levels

promote SC activation and myogenic progression while a decline to acetyl-coA mediated acetylation promotes SC self-renewal.

1.6 Satellite cell metabolism

SCs have a dynamic metabolic profile that is manifested during their various fate decisions (Bhattacharya & Scimè, 2020). They are predominately OXPHOS reliant during quiescence, which is followed by an upregulation of glycolysis during activation and finally, a switch back to OXPHOS during differentiation (**Fig. 1.8**). Notably, during quiescence SCs have greater levels of OXPHOS related gene expression (Ryall et al., 2015). In quiescence this coincides with the heavy reliance on ß-oxidation of fatty acids that are utilized to generate ATP via OXPHOS, and the very low metabolic rate observed in SCs (Latil et al., 2012). Despite their reliance on OXPHOS for ATP generation, quiescent SCs are generally characterized with having few mitochondria that are concentrated around the nucleus (Latil et al., 2012).

Based on their mitochondrial content, quiescent SCs are divided into two subpopulations that are inversely related to their Pax7 expression (Rocheteau et al., 2012). The subpopulation of SCs with higher levels of Pax7 and lower levels of mitochondrial content are shown to have a lower metabolic rate than the SCs with lower levels of Pax7 and higher mitochondrial content (Rocheteau et al., 2012). The population with higher levels of Pax7 expression maintain their quiescence for a longer time before activating (Rocheteau et al., 2012).

Recent studies show that enhanced mitochondrial fusion promotes SC quiescence and delays entry into the cell cycle (Baker et al., 2022; Hong et al., 2022). The deletion of the mitochondrial fusion protein OPA1 shift SCs into a G-alert quiescent state, which causes them to prematurely activate in response to stimuli. Conversely, the overexpression of OPA1 was shown to promote a deeper quiescence due to the increased mitochondrial fusion and thereby

mitochondrial activity (Baker et al., 2022). The deeper quiescence observed in SCs with enhanced mitochondrial fusion appears to mimic the phenotype observed in the population of SCs with higher levels of Pax7 (Baker et al., 2022; Rocheteau et al., 2012). Ultimately, OXPHOS and thereby mitochondrial activity appear to be essential for the preservation of SC quiescence.

During activation, SCs switch from a reliance on OXPHOS to glycolysis (**Fig. 1.8**) (Bhattacharya & Scimè, 2020; Ryall et al., 2015). A study on the gene expression profile of activated SCs indicated there is an increase in the expression of glycolysis related genes and a decline in OXPHOS related gene expression (Yucel et al., 2019). The switch to glycolysis is thought to be necessary to provide metabolites and the rapid generation of ATP that is required to facilitate the high rate of proliferation. Moreover, an analysis of skeletal muscle three days post injury, a time point when SCs are activated, revealed there was a massive increase in glycolysis (Pala et al., 2018). The switch favouring glycolysis for activation is hypothesized to be partially facilitated by mitochondrial fission that occurs in response to stimuli from injury (Hong et al., 2022). However, as proliferating SCs transition to differentiation there is a steady increase to mitochondrial content and OXPHOS related gene expression despite a continued reliance on glycolysis for ATP production. (Ryall et al., 2015). Furthermore, the reduced reliance on OXPHOS for ATP generation observed in activated SCs is thought to possibly protect them from mitochondrial ROS production that promotes early differentiation (Baker et al., 2022; Folmes et al., 2012).

As in quiescence, when SCs exit proliferation and enter differentiation, glycolysis begins to subside in favour of OXPHOS for ATP generation which is supported by changes to OXPHOS related gene expression (**Fig. 1.8**) (Bhattacharya & Scimè, 2020; Hoffmann et al., 2018). Thus, pyruvate is preferentially shuttled into the TCA cycle as acetyl-coA to provide sufficient flux for

the ETC instead of forming lactate through Ldha activity in the cytoplasm (Hoffmann et al., 2018). This is corroborated by the conditional deletion of Pdh in proliferating SCs that results in poor myoblast differentiation and skeletal muscle regeneration (Hori et al., 2019). The increase to ETC gene expression observed during MP differentiation is thought to occur through MyoD activity (Hoffmann et al., 2018; Shintaku et al., 2016). This is due to the interaction between MyoD with PGC-1β, and other metabolic genes involved in promoting mitochondrial biogenesis and ETC function (Shintaku et al., 2016). Overall, there is a shift to OXPHOS for ATP generation during differentiation.

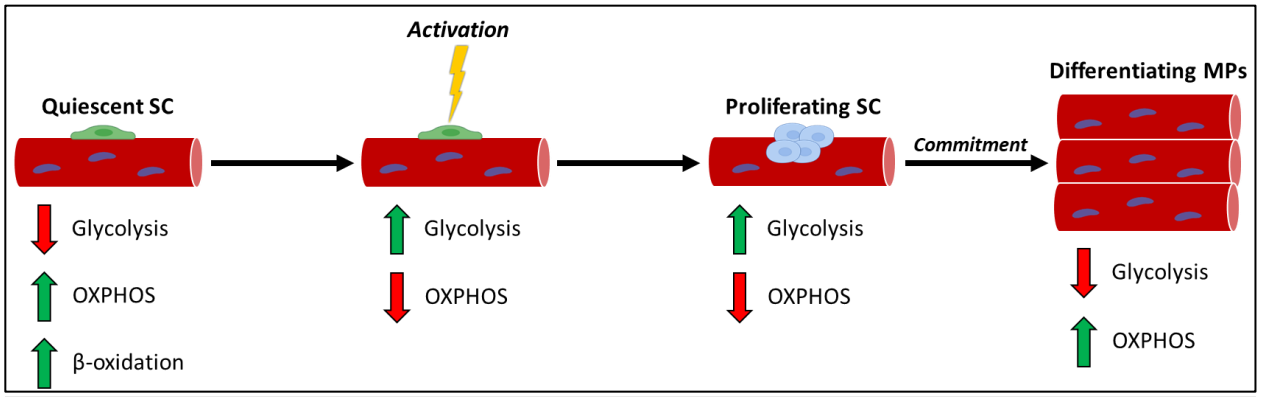

Figure 1.8: Diagram of the metabolic shift that occurs in SCs as they transition from quiescence to differentiation. Quiescent SCs are characterized with having relatively low glycolytic rate and a high reliance on OXPHOS via β-oxidation for ATP generation. Activated and proliferating SCs shift to a reliance on glycolysis in place of OXPHOS. The transition to differentiation is marked by a shift back to a reliance on OXPHOS for ATP generation.

1.7 The role of p107 in SC metabolism

Rbl1 (p107), a transcriptional co repressor, is a member of the retinoblastoma susceptibility (Rb) gene family, which also consists of Rb1 (Rb) and Rbl2 (p130). Along with its family members, p107 is implicated as a cell cycle regulator (Fischer & Müller, 2017; Henley & Dick, 2012). Studies for nuclear localized p107 show that it does not directly bind to the DNA but rather interacts with the transcription factors E2f4 or E2f5 (**Fig. 1.9**) (Wirt & Sage, 2010). The interruption of this interaction by cyclin/Cdk phosphorylation of p107 is thought to derepress gene

expression (Beijersbergen et al., 1995). p107 is almost always expressed only in proliferating cells and absent in quiescent and differentiated cells (Wirt & Sage, 2010).

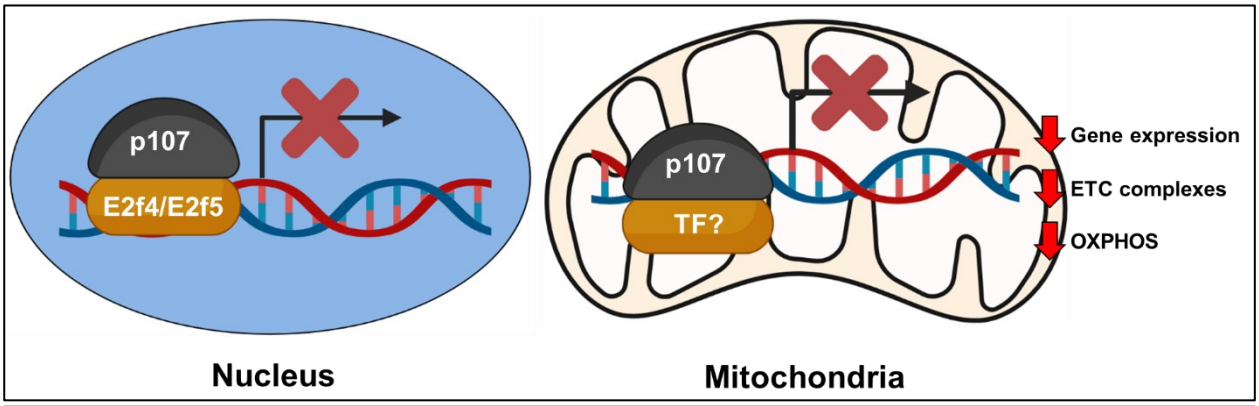

Figure 1.9: Schematic diagram of p107 nuclear and mitochondrial function. p107 interacts with E2f4 and E2f5 to repress transcription in the nucleus. p107 in the mitochondria decreases mitochondrial gene expression, ETC complex formation and OXPHOS capacity but its interacting transcription factor partner (TF?) is unknown. Figure created with BioRender.

Aside from its cell cycle regulatory role, p107 is shown to have a considerable influence on cellular metabolism. p107 genetically deleted (p107KO) mice were shown to preferably develop thermogenic highly oxidative brown and beige adipose tissue, rather than white (de Sousa et al., 2014; Scimè et al., 2005). In vivo and in vitro p107KO adipogenic progenitors present in the stromal vascular fraction of mice as well as p107KO murine embryonic fibroblasts (MEF) readily differentiated into the oxidative thermogenic adipocytes (de Sousa et al., 2014). Importantly, it was revealed that p107 regulates adipocyte lineage fates via its control over determining an oxidative metabolic state (Porras et al., 2017). p107 depleted adipogenic progenitors develop a aerobic glycolysis with the potential for high OXPHOS to drive commitment to thermogenic adipocytes (Porras et al., 2017). This was confirmed with growth arrested p107KO MEFs that were shown to have significantly greater oxygen consumption compared to their wildtype counterparts (de Sousa et al., 2014; Porras et al., 2017). These findings strongly suggesting that p107 limits the capacity for oxidative energy production.

In skeletal muscle p107 was shown to influence muscle fiber type differentiation. Skeletal muscle from p107 deficient mice display higher levels of oxidative type I and type IIA muscle fibers (Scimè et al., 2010). Additionally, the differentiation of primary myogenic progenitors from p107KO mice resulted in highly oxidative myotubes compared to controls (Scimè et al., 2010). These findings suggested that p107 might regulate the metabolism and cell fate decisions of SCs as it does in adipocyte progenitors. Recently, we established a novel mitochondrial role of p107 in C2C12 cells that reveals its effect on reducing OXPHOS capacity (**Fig. 1.9**) (Bhattacharya et al., 2021). Bhattacharya et al determined that p107 interacts with the mtDNA to represses its transcriptional activity (Bhattacharya et al., 2021). Indeed, p107KO C2C12 cells exhibited higher levels of OXPHOS, greater mitochondrial activity and enhanced mitochondrial gene expression compared to controls (Bhattacharya et al., 2021). Moreover, p107 mitochondrial function is regulated by Sirt1 activity through the NAD^+/NADH ratio, as p107 mitochondrial localization was inversely correlated with NAD^+/NADH in C2C12 cells (**Fig. 1.10**) (Bhattacharya et al., 2021). These findings establish p107 as a metabolic regulator in muscle progenitors that might have an influence in SC fate decisions. However, the role for p107 in metabolic regulation in SCs and fate decisions has not been investigated.

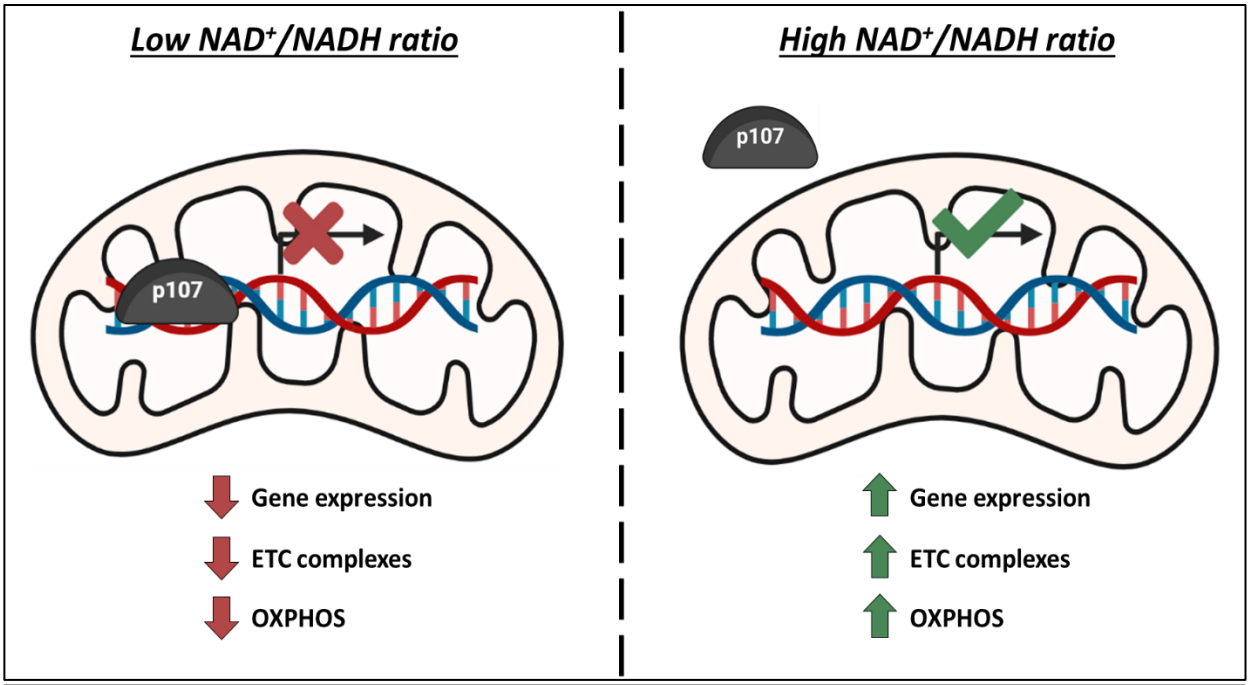

Figure 1.10: Schematic diagram of NAD^+/NADH ratio mediated control of p107 mitochondrial activity. p107 mitochondrial activity is inversely correlated to the NAD^+/NADH ratio. When the NAD^+/NADH ratio is low, p107 mitochondrial activity increased and there is a decline to mitochondrial function. When the NAD^+/NADH ratio is high, p107 mitochondrial activity is reduced and mitochondrial activity is enhanced (Bhattacharya et al., 2021). Figure created with BioRender.

CHAPTER 2

RATIONALE, HYPOTHESIS AND OBJECTIVES

Rationale

SC fate decisions, which are associated by dynamic changes in metabolism, are essential to the maintenance of skeletal muscle homeostasis, (Bhattacharya & Scimè, 2020). There is evidence that the transcriptional corepressor p107 influences the metabolism of adipose and muscle progenitors (de Sousa et al., 2014; Porras et al., 2017; Scimè et al., 2005). Our lab has shown that p107 is implicated in the white versus beige adipocyte lineage fate decision and oxidative muscle fiber type formation (de Sousa et al., 2014; Porras et al., 2017; Scimè et al., 2005). More recently, our lab has established a novel role for p107 in regulating OXPHOS and mitochondrial efficiency (Bhattacharya et al., 2021). We have shown that p107 when localized to the mitochondria represses mtDNA transcription, which consequently reduces mitochondrial OXPHOS capacity (Bhattacharya et al., 2021). Conversely, mitochondrial absence of p107 increases mitochondrial gene expression causing OXPHOS capacity to increase (Bhattacharya et al., 2021). However, these findings primarily focus on primary proliferating myogenic progenitors and C2C12 cells. Indeed, the mitochondrial role of p107 in in SC fate decisions are unknown. This investigation of p107 in SCs might provide new insights to combating muscle deficiencies associated with neuromuscular diseases and ageing.

Hypothesis

We hypothesize that p107 contributes to SC fate decisions through a mitochondrial metabolic function.

Objectives

The primary ambition of this research project is to determine a potential metabolic role of p107 in primary SC activation and self-renewal by 3 specific objectives.

Aim 1: To corroborate p107 mitochondrial function

Aim 2: To determine a role for p107 in SC- self-renewal and activation

Aim 3: To determine the metabolic role of p107 in SC self-renewal and activation

CHAPTER 3

MATERIALS AND METHODS

Mice

All animal experiments were performed in accordance with the guidelines approved by the Animal Care Committee of York University, which are based on the guidelines of the Canadian Council on Animal Care. Wild type (WT) and p107 genetically deleted (p107KO) mice (LeCouter et al., 1998) used for all animal experiments are on a mixed strain (NMRI, C57/Bl6, FVB/N) background (D. Chen et al., 2004). All mice were aged 6 to 8 weeks except for those involved in cardiotoxin (Ctx) induced muscle regeneration experiments (9 to 12 week old). p107KO mice on average were smaller in size than WT mice.

Cell culture

The C2C12 myogenic progenitor (MP) cell line was purchased from the American Tissue Type Culture (ATCC). The cells were grown in 25mM glucose Dulbecco's Modified Eagle Medium (DMEM) (Wisent Bioproducts) supplemented with 10% fetal bovine serum (FBS) (Wisent Bioproducts) and 1% penicillin streptomycin (P/S) (Wisent Bioproducts) at 37°C with 5% CO2.

Primary myofiber isolation and culture

Primary extensor digitorum longus (EDL) myofibers were isolated from WT or p107KO mice. EDL muscles were dissected tendon to tendon and digested in filter sterilized 0.2% type 1 collagenase in serum free DMEM for 45 minutes at 37°C. Upon sufficient unravelling, the muscles were transferred to prewarmed cell culture dishes containing DMEM with 1% P/S. The muscles were then gently flushed to induce the release of single myofibers with intermittent incubation at 37°C every 5-10 minutes. Myofibers were then moved to 24 well plates containing pre warmed

25mM glucose DMEM supplemented with 20% FBS, 1% P/S, 1% chick embryo extract (CEE) (MP Biomedicals) and 7.5ng/ml basic fibroblast growth factor (bFGF) (Peprotech) and cultured for various times.

For nutrient specific experiments, myofibers were cultured for 72 hours in stripped DMEM (ThermoFisher Scientific) lacking glucose, sodium pyruvate, HEPES and L-glutamine supplemented with 5.5mM or 25mM glucose, 20% FBS, 1% P/S, 1% CEE and 7.5ng/ml bFGF.

A minimum of 60 myofibers were analyzed for all timepoints and nutrient condition with atleast 15 myofibers from each mouse with atleast 4 WT and p107KO mice respectively. Quiescent Pax7+MyoD-), activated (Pax7+MyoD+) and differentiating (Pax7-MyoD+) SCs were counted and expressed as a fraction of the total SC population per myofiber. Dividing clusters were described as 3 or more SCs in close proximity on the myofiber. Data were expressed as a fold change of the fraction of quiescent, activated or committed SCs per myofiber or the fold change of SCs in cluster per myofiber.

Reserve cells and myofusion index

After 3 days in culture 60 myofibers from each WT or p107KO mouse were washed in phosphate buffer saline (PBS) and transferred to rat tail collagen I (ThermoFisher Scientific) coated Nunc Lab-Tek™ II chambered tissue culture plates (ThermoFisher Scientific). For reserve cell determination, the fibers were cultured for 3 additional days before processing for immunostaining the cells (MPs) derived from the SCs on the fibers with 4′,6-diamidino-2-phenylindole (Dapi), Pax7 and MyoD. The number of reserve cells (Pax7+MyoD-) were expressed as a fraction of the total MPs observed that is Pax7+MyoD-, Pax7+MyoD+ and Pax7-MyoD+ and displayed as a fold change between WT and p107KO. At least 7 different fields per mouse for 5 WT and 5 p107KO mice were used to collect data.

For evaluation of myofusion index, the fibers were cultured for 3 days as per above and then differentiated for an additional 3 days by incubating cells in 25mM DMEM supplemented with 5% horse serum (Wisent Bioproducts) and 1% P/S. Differentiated cells were immunostained with Dapi and Myosin heavy chain (Myh). Myofusion index was determined as a fraction of the number of nuclei inside myotubes (Myh positive) divided by the total number of myotubes expressing Myh in at least 5 different fields per mouse for 3 WT and 3 p107KO mice. Data were expressed as a fold change between WT and p107KO.

Whole cell protein lysis

Cells were lysed in RIPA buffer (0.5% NP-40, 0.1% sodium deoxycholate, 150mM NaCl, 50mM Tris-Cl pH 7.5, 5mM EDTA) containing 1mg/ml of pepstatin, aprotinin, and leupeptin protease inhibitors on ice for 10 minutes. To remove cellular debris, the lysate was centrifuged at 21000g for 15 minutes at 4°C.

Cytosolic and mitochondrial isolation

For mitochondrial and cytoplasmic isolation, cells were washed in PBS, pelleted, dissolved in 150µl of mitochondrial isolation buffer (0.25M sucrose, 0.1% BSA, 0.2mM EDTA, and 10mM HEPES pH 7.4, with 1mg/ml of pepstatin, leupeptin, and aprotinin protease inhibitors). A Dounce homogenizer was used to homogenize cells with a loose rod (6 times) followed by tight rod (6 times) on ice. The homogenate was transferred to 1.5ml centrifuge tubes and spun at 1000g for 10 minutes at 4°C. The supernatant was then centrifuged at 14000g for 15 minutes at 4°C and the resulting supernatant, the cytoplasmic fraction, was transferred to a new tube. The pellet, the mitochondrial fraction, was purified by washing 3 times in 150µl of mitochondrial isolation buffer with centrifugation at 14000g for 15 minutes at 4°C each time. The mitochondria were lysed by repeated freeze thaw cycles (3 times) using dry ice.

Western blot analysis

For Western blot analysis protein lysates from whole cell, cytosolic, or mitochondrial lysates were loaded onto gradient gels (6-15%), 6% or 10% SDS-PAGE gels. Samples were first boiled for 4 minutes in loading buffer containing 4% SDS, 10% 2-mercaptoethanol, 20% glycerol, 0.004% bromophenol blue, 0.125M Tris HCl and 1mM DTT. The samples were then loaded onto a gel and run in 1X running buffer (10X running buffer contains 25mM Tris base, 192mM glycine and 0.1% SDS powder and 90% ddH_2O) and proteins were separated by electrophoresis for 1 hour and 45 minutes at 30 milliamps. After separation, proteins from the gel were transferred onto 0.22µM pore size nitrocellulose membrane (Santa Cruz Biotechnology) at 100V for 80 minutes at 4°C in transfer buffer (1x transfer buffer contains 50mM Tris base, 384mM glycine, 20% methanol). Afterwards, the membranes were blocked for 1 hour at room temperature in 5% non-fat milk in Tris-buffered saline (TBS) (50mM Tris-base and 150mM NaCl) with 0.1% Triton X-100 (TBST) and then washed for 3 minutes in TBST. The membranes were then probed overnight at 4°C with primary antibodies diluted in 1% BSA in TBST. The next day, membranes were washed three times with TBST and secondary antibodies, goat anti-rabbit or goat anti-mouse (Bio-Rad Laboratories), conjugated with horseradish peroxidase diluted in 5% non-fat milk in TBST were added for 1 hour at room temperature with gentle rocking. After the incubation, membranes were washed in TBST 3 times for 5 minutes with a final wash in TBS for 10 minutes. The membranes were visualized with chemiluminescence Clarity Western ECL Substrate (Bio-Rad Laboratories) on photographic UltraCruz Nitrocellulose Pure Transfer film (Santa Cruz Biotechnology). Protein levels were evaluated by densitometry using Image J software. All representative Western blot experiments were conducted at least 3 independent times with similar results.

Antibodies used

α-tubulin (66031-1-Ig Proteintech); Cox4 (ab16056, Abcam); E2f4 (E2F4-E3G2G Cell Signaling); E2f5 (E2F5-C8 Santa Cruz Biotech); Histone H3 (histone H3-D1H2 Cell Signaling); Laminin (NB300-14455 Novus Biologicals); Myh B-5 (sc-376157 Santa Cruz Biotech); MyoD (NBP1-54153 Novus Biologicals); Pax7 (sc-81648 Santa Cruz Biotech); Pax7 (20570-1-AP Proteintech); p107 (13354-1-AP Proteintech); p107 (p107-SD9 Santa Cruz Biotech); p130 (RBL2-D9T7M Cell Signaling); Rb (Rb-D20 Cell Signaling); Sirt1 (Sirt1-D1D7 Cell Signaling); Sirt1 (Sirt1-B7 Santa Cruz Biotechnology); Tfam1 (22586-1-AP Proteintech); Tom20 (11802-1-AP Proteintech); IgG (IgG-D7 Santa Cruz Biotechnology); Goat anti-rabbit IgG (H+L) HRP Conjugate (170-6515 BioRad); Goat Anti-Mouse IgG (H+L) HRP Conjugate (170-6516 BioRad); Goat Anti-Rabbit IgG (H+L) Cross-Adsorbed secondary antibody, Alexa Fluor 594 (A11012 Life Technologies); Donkey Anti-Mouse IgG Secondary Antibody NL 493 conjugated (NL009 Novus Biologicals); Donkey Anti-Mouse IgG Secondary Antibody NL 557 conjugated (NL007 Novus Biologicals); Donkey Anti-Rabbit IgG Secondary Antibody NL 637 conjugated (NL005 Novus Biologicals)

Co-immunoprecipitation

For immunoprecipitation (IP), 40µl of PureProteome protein A/G mix magnetic beads (EMD Millipore Corp) were pelleted using a magnetic separation rack (S1506S New England BioLabs) and washed with 200µl PBS 3 times. Next, the beads were incubated with 10ug of antibody; p107-SD9, Sirt1-B7 or IgG-D7 for 30 minutes while rocking at 4°C. After, cytosolic protein lysates were added to the bead-antibody complexes for incubation overnight at 4ºC while rocking. The following day, the beads were washed with E1A wash buffer (50mM HEPES pH 7.0, 150mM NaCl and 0.1% NP-40), denatured in loading buffer and loaded onto SDS-PAGE gels.

For co-IP, the gels were Western blotted for p107 (13354-1-AP) or Sirt1 (D1D7). Inputs represent 10% of cytosolic protein lysates that were immunoprecipitated. All co-immunoprecipitation experiments were conducts at least three independent times with similar results.

p107KO and Sirt1KO cell line derivation

For co-immunoprecipitation experiments, Crispr/Cas9 was used to generate p107 and Sirt1 genetically deleted C2C12 cell lines used. These cell lines were used as negative controls to test our antibodies to confirm that they specific for western blotting p107 or Sirt1. For p107KO cells, C2C12 cells were transfected with 3 pLentiU6-sgRNA-SFFV-Cas9-2A-Puro plasmids each containing a different sgRNA to target p107 sequences 110 CGTGAAGTCATCCAGGGCTT, 156 GGGAGAAGTTATACACTGGC and 350 AGTTTCGTGAGCGGATAGAA (Applied Biological Materials), and for Sirt1KO with 2 Double Nickase plasmids each containing a different sgRNA to target sequences 148 CGGACGAGCCGCTCCGCAAG and 110 CCATGGCGGCCGCCGCGGAA (Santa Cruz Biotechnology). For cell transfections, 10ug of each plasmid, 2.5M $CaCl_2$, and double distilled water (ddH_2O) to a volume of 500µl was added dropwise to HEBS buffer (274mM NaCl, 10mM KCl, 1.4mM Na_2HPO_4, 15mM D-glucose and 42mM HEPES), incubated at room temperature for 1 hour and then added to C2C12 cells plated at 20% confluency.

For clonal selection, at 18 hours post transfection, the cells were passaged into 96 well tissue culture plates and treated the next day and every 2 days for a total of 3 times with 2mg/ml of puromycin in DMEM. Any surviving clones were grown and tested via Western blotting. For control cells, C2C12 cells were transfected with an empty vector, pLentiU6-sgRNA-SFFV-Cas9-2A-Puro and selected as above.

p107 percent occupancy in mitochondria and cytoplasm

To determine the percentage of p107 occupancy in total, mitochondrial and cytoplasmic fractions, 25% and 75% of $2x10^6$ C2C12 cells were used to generate whole cell and mitochondrial/cytoplasmic lysates respectively. The lysates were loaded onto polyacrylamide gels and Western blotted for p107 (13354-1-AP, Proteintech), α-tubulin (66031-1-Ig, Proteintech) and Cox4 (ab16056, Abcam). The percent of mitochondrial or cytoplasmic p107 occupancy was ascertained by the ratio of p107:Cox4 and p107:α-tubulin for whole cell representing the total, and for the mitochondrial and cytoplasmic protein lysates, respectively, by densitometry using the ImageJ software.

p107 internal mitochondria targeting signal-like (iMTS-L) sequence prediction

The p107 protein sequences that were analyzed for a potential iMTS-L sequence were the polypeptides resulting from a sequential removal of a single amino acid from the N terminus end of p107 (Backes et al., 2018; Emanuelsson et al., 2007; Rahbani et al., 2021). The polypeptides were assessed for the presence of an iMTS-L sequence using the TargetP prediction algorithm with the options set to non-plant organism, without cut-off and cleavage site prediction (Emanuelsson et al., 2007). The mitochondrial targeting peptide probability (mTP) values obtained from the TargetP algorithm were plotted against the corresponding amino acid. A threshold mTP value of 0.75 was used to define the presence of a potential iMTS sequence (Backes et al., 2018; Emanuelsson et al., 2007; Rahbani et al., 2021).

Quantitative chromatin immunoprecipitation assay (qChIP)

Mitochondrial fractions collected as described above were washed twice in PBS by centrifugation at 14000g for 15 minutes at 4ºC. The samples were then resuspended in 200µl of PBS containing 1% formaldehyde and rocked at room temperature for 30 minutes to fix the cells.

The fixation was stopped with the addition of 125mM glycine in PBS and rocked for 5 minutes at room temperature. The fixed mitochondrial pellet was washed twice in PBS containing 100mM NaF and 1mM Na_3VO_3 via centrifuging at 14000g for 5 minutes at 4ºC. The pellet was dissolved in 500µl of ChIP lysis buffer (40mM Tris, pH 8.0, 1% Triton X-100, 4mM EDTA, 300mM NaCl) and sonicated at 24% amplitude with 15 second intervals on and off for 3 cycles. After sonication, the samples were centrifuged at 13000 rpm for 10 minutes at 4ºC. The supernatant was transferred to a new tube containing 100µl of dilution buffer 1 (40mM Tris, pH 8.0, 4mM EDTA). Input controls were removed from the samples and 150µl of dilution buffer 2 (40mM Tris, pH 8.0, 0.5% Triton X-100, 4mM EDTA, 150mM NaCl) was added. Samples were precleared with 50µl of protein A/G agarose beads (Santa Cruz Biotechnology) while being rocked for 90 minutes at 4ºC. Next, the beads were pelleted, and the supernatant was transferred to a new tube. To the samples E2f4 (E2F4-E3G2G Cell Signaling), Tfam (22586-1-AP Proteintech) or IgG antibody (IgG-D-7 Santa Cruz Biotechnology) were added. The mixture was rocked overnight at 4ºC and the following day, 50µl of protein A/G agarose beads were added to the samples and rocked for 90 minutes at 4ºC.

The beads were then washed with the following buffers in sequential order: a low salt wash buffer (0.1% SDS, 1% Triton X-100, 2mM EDTA, 20mM Tris HCl, pH 8.0, 150mM NaCl), high salt wash buffer (0.1% SDS, 1% Triton X-100, 2mM EDTA, 20mM Tris HCl, pH 8.0, 500mM NaCl), LiCl wash buffer (0.25M LiCl, 1% NP-40, 1% deoxycholic acid, 1mM EDTA, 10mM Tris, pH 8.0) and 2 washes with TE buffer (10mM Tris HCl, pH 8.0, 1mM EDTA). Following the final wash, the mtDNA-protein complexes were isolated by suspending the beads in 250µl of elution buffer (1% SDS, 0.1M $NaHCO_3$), vortexing, rocking for 15 minutes at room temperature and centrifuging at 400g for 2 minutes. The supernatant was transferred to a new tube and the isolation

step was repeated on the remaining beads. For isolation of mtDNA fragments, 20µl of 5M NaCl was added to the 500µl of mtDNA-protein complexes in elution buffer and incubated at 65ºC overnight. The next day, the DNA was isolated using a DNA purification kit (Qiagen), and its concentration determined using the NanoDrop 2000 (ThermoFisher Scientific). The isolated DNA was amplified using qPCR with D-loop region primer sets GCGTTATCGCCTCATACGTT and GGTGCGTCTAGACTGTGTG having an amplicon length of 173bp. The qPCR assays were performed on Light cycler 96 (Roche) using SYBR green Fast qPCR master mix (Bimake) according to the MIQE (Minimum Information for Publication of Quantitative Real-Time PCR Experiments) guidelines (Bustin et al., 2009). The relative occupancy was determined by the ΔCt method to obtain Ct values that are normalized to IgG Ct values.

Cardiotoxin-induced muscle regeneration

2-month-old anesthetized Wt and p107KO mice were injected intramuscularly in the tibialis anterior (TA) muscle with 40µl of Ctx (Latoxan) that was prepared as a 10µM stock dissolved in water. TA muscles, including uninjured contralateral muscles were harvested on the 21st day following Ctx injection and immersed in a 1:2 ratio of 30% sucrose:optimal cutting temperature compound (OCT) (ThermoFisher Scientific). The immersed samples were slowly frozen in liquid nitrogen-cooled isopentane. Following muscle freezing, samples were cross sectioned at 10µm thickness using a cryostat onto positively charged microscope slides (FroggaBio) for immunohistochemistry.

Immunohistochemistry of muscle cross sections

TA muscle tissue cross sections were washed with PBS and fixed with 4% paraformaldehyde (PFA) for 15 minutes at room temperature. The samples were then washed with PBS to remove excess PFA and blocked with blocking buffer (5% goat serum, 5% donkey serum,

0.1% Triton X-100 in PBS) for 45 minutes. Next, the tissues were incubated with primary antibody anti-laminin (NB300-14455 Novus Biologicals) in blocking buffer at a 1:100 ratio for 90 minutes. After three washes in 0.05% Tween 20 in PBS (PBST), tissues were incubated with secondary antibody goat anti rabbit IgG Alexa Fluor 594 (ThermoFisher Scientific) in blocking buffer for 1 hour at a 1:200 ratio. The tissues were then washed 3 times with PBST and re incubated with primary antibody Pax7 (sc-81648 Santa Cruz Biotech) in blocking buffer at a ratio of 1:100 for 90 minutes. The tissues were again washed 3 times with PBST and incubated with secondary antibody donkey anti mouse IgG NL493 conjugated (R and D Systems) in blocking buffer at a ratio of 1:200 for 1 hour. After, the tissues were washed 3 times with PBST, Dapi was added. Vectasheild mounting media (Vector) was added before the placement of the coverslip. Digital images were taken with the Axio Scope.A1 using the EC Plan-Neofluar 20x/0.5 or EC Plan-Neofluar 40x/0.75 (Zeiss). At least, six fields per muscle section from 4 to 5 different mice for uninjured and Ctx injury recovered conditions were used for analysis. Quiescent SCs were identified by counting the Pax7+ nuclei per muscle fiber for uninjured and Ctx injury recovered WT and p107KO mice. Data were expressed as a fold change of the Pax7+ per fiber.

To determine muscle cross sectional area, uninjured and Ctx injury recovered WT and p107KO TA muscle cross sections were immunostained according to the above protocol for Dapi and laminin. At least, 5 fields were used per muscle section from 3 different mice per condition for both WT and p107KO to gather data. Cross sectional area was measured using ImageJ software to outline each muscle fiber in a field and measure its area. ImageJ was calibrated to convert pixel length to um^2 based on image scale to ensure accurate measurements. Data are expressed as a fold change of cross-sectional area.

Immunocytochemistry and confocal imaging

Immunocytochemistry for reserve cells, and myfusion index, the cells were fixed for 10 minutes with 4% paraformaldehyde (PFA) and permeabilized for 30 minutes at room temperature in blocking buffer (3% BSA, 0.3% Triton X-100, 5% goat serum and 5% donkey serum in PBS). After blocking, cells were incubated with primary antibody Pax7 (sc-81648 Santa Cruz Biotech) or MYH B-5 (sc-376157 Santa Cruz Biotech) at 1:100 dilution in blocking buffer for 1 hour. After 3 washes with PBST, cells were incubated with secondary antibody donkey anti-mouse IgG NL493-conjugated (R and D Systems) at a 1:200 dilution in blocking buffer. Cells were then washed with PBST 3 times and re incubated with primary antibody MyoD (NBP1-54153 Novus Biologicals) or Pax7 (20570-1-AP Proteintech) at a 1:100 dilution in blocking buffer for 1 hour. Cells were then washed 3 times with PBST and incubated with secondary antibody goat anti rabbit IgG Alexa Fluor 594 (ThermoFisher Scientific) at a 1:200 dilution for 1 hour. After 3 washes with PBST the cells were incubated with Dapi and Vectashield mounting media (Vector) was added before placing the coverslip. Confocal images were obtained using the Axio Observer.Z1 microscope with alpha Plan-Apochromat 20x/0.8 M27 (Zeiss). Digital images were captured using the Axiocam MR R3 and the Axio Scope.A1 using the EC Plan -Neofluar 20x/0.5 or EC Plan-Neofluar 40x/0.75 (Zeiss).

For visualizing myofiber associated SCs, myofibers were fixed for 10 minutes with prewarmed 2% PFA in PBS while rocking at room temperature. Myofibers were then washed 3 times with PBS and incubated with permeabilization buffer (0.3% Triton X-100 and 0.1M glycine in PBS) for 10 minutes while rocking. Next, myofibers were incubated with blocking buffer (2% BSA, 5% donkey serum, 5% goat serum and 0.1% Triton X-100 in PBS) for 1 hour at room temperature while rocking. After blocking, myofibers were incubated with primary antibody Pax7

(sc-81648 Santa Cruz Biotech) or p107 (p107-SD9 Santa Cruz Biotech) in blocking buffer at a 1:100 dilution overnight at 4ºC. Myofibers were then washed 3 times with PBS and incubated with secondary antibody donkey anti-mouse IgG NL493-conjugated (R and D Systems) or donkey anti-mouse IgG NL557-conjugated (R and D Systems) at a 1:1000 dilution for 1 hour at room temperature. Then myofibers were washed 3 times with PBS and re-incubated over night with primary antibody MyoD (NBP1-54153 Novus Biologicals) or Pax7 (20570-1-AP Proteintech) or Tom20 (11802-1-AP Proteintech) at a dilution of 1:100 overnight at 4ºC. The next day, myofibers were washed 3 times with PBS and incubated with secondary antibody goat anti rabbit IgG Alexa Fluor 594 (ThermoFisher Scientific) or donkey anti-rabbit IgG NL637 (R and D Systems) at a 1:1000 dilution for 1 hour at room temperature. After 3 washes with PBS myofibers were incubated with Dapi for 10 minutes and washed 3 more times with PBS before they were mounted to positively charged microscope slides (FroggaBio). Vectashield mounting media (Vector) was added before placing the coverslip and sealing the slide. Confocal images and z-stacks were obtained using the Axio Observer.Z1 microscope with alpha Plan-Apochromat 100x/1.46 Oil DIC (UV) M27 (Zeiss). Digital images were captured using the Axiocam MR R3 and Axio Scope.A1 with the EC Plan-Neofluar 20x/0.5 or EC Plan-Neofluar 40x/0.75 (Zeiss). Optical sections were then stacked or merged to create high resolution z-series images. A line was drawn through a representative cell to indicate relative intensity of RGB signals for co-localization analysis using the Zen Blue software (Zeiss).

Statistics and Reproducibility

All experiments were performed with at least three biological replicates as indicated in the figure legends, and results are presented as the mean +/- standard deviation (SD). The immunoblot (**Fig. 4.3, Fig. 4.4A, Fig. 4.4B, Fig. 4.4C and Fig. 4.26B**), co-immunoprecipitation (**Fig 4.26A**)

experiments have been performed at least three independent times with similar results. Statistical analysis was performed by GraphPad Prism 5 or Microsoft Excel. Statistical comparisons between groups were made using two-tailed unpaired Student's t-test. Results were considered statistically significant when $p<0.05$. Some data were analyzed using an appropriate two-way analysis of variance (ANOVA) with criterion of $p<0.05$. All significant differences for ANOVA testing were evaluated using a Tukey post hoc test.

CHAPTER 4

RESULTS

Percentage of total p107 in mitochondrial and cytoplasmic compartments

p107 has recently been shown in the mitochondria of primary MPs and the MP cell line C2C12, where it influences the metabolic state of the cells (Bhattacharya et al., 2021; Porras et al., 2017). To gauge a functional importance of mitochondrial p107 in MPs, we sought to determine its proportion within this organelle. For this, the percentage of cytoplasmic and mitochondrial p107 was established from total protein lysates of proliferating C2C12 cells by of Western blotting. We found the percentage of p107 protein that was expressed in the proliferating cells was about 28% and 45% in the mitochondrial and cytoplasmic compartments respectively (**Fig. 4.1A and 4.1B**). Thus, the high levels of p107 in the mitochondria suggest an important role in MPs that might be applicable to SCs.

p107 has an internal mitochondrial targeting sequence

To further confirm that p107 is a bona fide mitochondrial functional protein we considered how it might enter the mitochondria. It is unclear if p107 is imported into the mitochondrial matrix by the mitochondrial import machinery because it lacks an N-terminal mitochondrial targeting signal (MTS) (Wiedemann & Pfanner, 2017;). However, recent research utilizing the TargetP prediction algorithm for MTS has revealed the presence of internal MTS (iMTS) like sequences that might act to facilitate the mitochondrial import of proteins that lack a conventional N-terminal MTS (Backes et al., 2018; Rahbani et al., 2021). We used this algorithm to determine if p107 has an iMTS sequence(s). Importantly, for p107, the TargetP algorithm for iMTS revealed two regions of very strong scores (<0.75) (Emanuelsson et al., 2007). They are from amino acids 70-95 with a

score of 0.837 and amino acids 770-795 with a score of 0.844 (**Fig. 4.2**). These data suggest that p107 mitochondrial import is likely facilitated by the presence of iMTS sequences.

Rb family mitochondrial presence in MPs is exclusive to p107

As with p107, family members Rb and p130 are also known to enter the mitochondria of some cell lines (Ferecatu et al., 2009; Oresajo, 2021), hence they might also influence mitochondrial function in MPs (Hansen et al., 2004; Scimè et al., 2005). Thus, we assessed if the mitochondrial presence of the Rb family is exclusive to p107 in proliferating MP cells. Western blotting for Rb and p130, showed that unlike p107, Rb is not expressed in the mitochondria. p130 is not expressed at all in proliferating C2C12 cells, but was expressed in contact inhibited growth arrested (GA) cells (**Fig. 4.3**). These findings highlight the exclusivity of Rb family member p107 for a mitochondrial role in MPs and a potential mitochondrial function in SCs.

p107 might interact with E2f4 in the mitochondria of MPs

p107 is known to not directly interact with DNA, requiring an interaction partner to facilitate its transcriptional repressor role (Wirt & Sage, 2010). Therefore, we assessed the potential mtDNA interaction partners of p107. We evaluated the known mitochondrial transcription factor Tfam (Gustafsson et al., 2016) and the p107 interacting nuclear transcription factors E2f4 and E2f5 (C.-R. Chen et al., 2002; Ginsberg et al., 1994) as potential candidates. By Western blotting of mitochondrial lysates, Tfam was found to be present in negligible levels in proliferating cells but was highly expressed in GA cells (**Fig. 4.4A**). E2f5 was completely absent in the proliferating MP mitochondrial fractions but was expressed in whole cell, cytoplasmic and GA samples (**Fig. 4.4B**). Contrarily, E2f4 was revealed to be present in proliferating MP mitochondrial lysates in addition to the other cellular compartments and GA samples, suggesting

that it might have a mitochondrial function and potentially interact with p107 in the mitochondria (**Fig. 4.4C**).

To confirm that E2f4 is the potential p107 binding partner on the mtDNA, we performed quantitative chromatin immunoprecipitation (qCHIP) analysis of mitochondria lysates from proliferating and GA MPs, which do not express p107 (Bhattacharya et al., 2021). qCHIP revealed that E2f4 interacted with the mtDNA of proliferating C2C12 cells and not Tfam, but the opposite finding was observed in growth arrested MPs (**Fig. 4.5**). Together, these findings suggest that E2f4 might be the mitochondrial binding partner of p107 in proliferating MPs.

p107 is expressed only in activated primary SCs

To begin delineating a possible p107 mitochondrial role in SCs we used an ex vivo model relying on cultured primary myofibers from extensor digitorum longus (EDL) muscle of mice (**Fig. 4.6A**). First, we assessed when p107 is first expressed in SCs using early timepoints (0, 4, 6 and 8 hours) of cultured primary myofibers from Wild Type (WT) and negative control p107KO mice. By immunostaining for p107 and SC marker Pax7, (Dumont, Bentzinger, et al., 2015; Zammit et al., 2006) we found that p107 expression was not present in myofibers nor quiescent SCs but was first observed at 8 hours only in SCs of the WT myofibers (**Fig. 4.6B)**. It was not expressed at all in the negative control p107KO myofibers **(Fig. 4.7**). Immunofluorescence of MyoD, whose protein expression is used to distinguish quiescent from activated SCs (Dumont, Bentzinger, et al., 2015; Zammit et al., 2006), revealed that MyoD was not expressed at all at 0 hours of culture (**Fig. 4.8A**), but was expressed before p107 within the first 6 hours of culture. Thus, indicating the activation of SCs can occur within the first 6 hours of culture in our model (**Fig. 4.8B**). Together, these data suggest that p107 expression is limited to activated SCs and is not involved in activation, as it is detectable a short time after they had become activated.

p107 influences the timing of SC activation

To determine whether p107 influences SC activation, we enumerated the number of activated SCs on myofibers 24 hrs after incubation. As 6hrs represents a sufficient time for MyoD protein expression in our model (**Fig. 4.8**), 24hrs would represent a time frame that has allowed for a substantial amount of activation to occur. WT and p107KO myofibers were fixed and stained for Pax7 and MyoD (**Fig. 4.9A**). The quiescent (Pax7+MyoD-) and activated SC populations (Pax7+MyoD+) were determined as a fraction of the total SCs (Pax7+) observed per myofiber. We found that p107KO myofibers have almost 3.5 times more SCs that remain quiescent (Pax7+MyoD-) after 24 hours in culture compared to WT (**Fig. 4.9B**). In accordance, there is a decrease in the fraction of activated SCs (Pax7+MyoD+) in p107KO compared to WT myofibers (**Fig. 4.9C**). Overall, these findings signify that the absence of p107 results in a delay of activation.

p107 regulates SC proliferation

As p107 expression is found only in the activated SCs, it suggests that p107 has a potential SC specific function during proliferation. Recently published data from our lab revealed that it has a role in MP proliferation (Bhattacharya et al., 2021), Thus, we assessed if the same relationship is conserved in proliferating SCs that are present in clusters on myofibers. For this, primary myofibers were cultured after isolation for 42 and 72 hours. Despite the lag time in activation (**Fig. 4.9**), immunofluorescence of Pax7 and MyoD of dividing SCs revealed that there was at least a 2-fold greater number of cells at 42 hours in p107KO compared to WT, suggesting a greater proliferative capacity (**Fig. 4.10**). Additionally, myofibers cultured for 72 hours revealed as much as 2.5 times greater number of SCs per myofiber and 1.4 times greater number of SCs per cluster for p107KO compared to their WT counterparts (**Fig. 4.11**). Together this date suggests that p107 affects SC proliferation as in MPs (Bhattacharya et al., 2021).

p107 has a role in regulating SC numbers

Next, we investigated a possible effect of p107 on SC fate decisions. For this, we harvested TA muscle from WT and p107KO mice and enumerated the quiescent SC population by immunostaining for Pax7 and laminin (**Fig. 4.12A and 4.12B**). Immunofluorescence revealed there is an increased number of quiescent SCs by as much as 1.5 times in p107KO muscle compared to WT (**Fig. 4.12C**).

The increased number of SCs in p107KO muscle compared to WT in vivo was confirmed ex vivo using EDL myofibers. Isolated WT and p107KO myofibers from EDL were immediately fixed and immune stained for Pax7 and MyoD to enumerate the quiescent population of SCs. Confocal microscopy revealed that there is an almost 2-fold increase in the quiescent SC population in p107KO myofibers compared to WT controls (**Fig. 4.13**). Together these data suggest that p107 might have a role in dictating SC self-renewal.

p107 regulates SC numbers during regeneration

To further assess the potential that p107 is involved in self renewal, we compared the SC number in uninjured muscle to fully recovered contralateral muscle post Ctx injury. A greater number of SCs in p107KO muscle after injury recovery would strongly support the presence of enhanced SC self-renewal. Twenty-one days post injury, to ensure total muscle recovery had occurred, (**Fig. 4.14A**) the injured muscle was cross sectioned and immune stained for Pax7 and laminin to enumerate the SC population (**Fig. 4.14B**). The immunofluorescence and microscopy revealed there were nearly 2-fold greater SC numbers in the recovered p107KO compared to WT muscle (**Fig. 4.14C**). Moreover, the p107KO muscle had about 1.3-fold increased number of SCs after recovery from injury compared to the uninjured contralateral limb (**Fig. 4.15A**). There did not appear to be a change to the SC count of the WT muscle after injury recovery (**Fig. 4.15B**).

Overall, these findings strongly suggest that p107 has a role in SC self-renewal wherein its absence is associated with a greater propensity for self-renewal.

p107 regulates SC self-renewal

Next, we assessed if p107 regulates SC fate decisions by assessing if the increase in the SC population in p107KO muscle is a result of enhanced self-renewal. For this, WT and p107KO myofibers were immune stained for Pax7 and MyoD at 42 and 72 hours post isolation. In this way the quiescent (Pax7+MyoD-), activated (Pax7+MyoD+) and differentiating (Pax7-MyoD+) population of SCs could be enumerated (**Fig. 1.3**). These timepoints were chosen to ensure that SC division had occurred, so as to visualize newly formed quiescent and differentiating SCs (Dumont, Bentzinger, et al., 2015; Sincennes et al., 2021). We found that there is a significantly greater fraction of quiescent SCs in clusters of p107KO myofibers compared to WT at both 42 (**Fig.4.16**) and 72 hours (**Fig. 4.17A and Fig.4.17B**) by as much as 10 and 6.5 times respectively. Additionally, there was no difference in the fraction of proliferating SCs (Pax7+MyoD+) (**Fig. 4.17D**), but there was a significant decline to the fraction of differentiating SCs (Pax7-MyoD+) (**Fig. 4.17C**) in the p107KO myofibers at 72 hours. Moreover, at 72 hours the fraction of activated SCs in the p107KO have caught up to the WT despite the delay in activation that was observed at 24 hours of culture (compare **Fig. 4.17D** with **Fig. 4.9A**) These findings suggest that p107 activity reduces SC self-renewal and might promote SC commitment to differentiation.

p107 activity limits reserve cell production

We next considered the role of p107 in SC self-renewal by enumeration of the reserve cell population that are the progeny of SCs dispersed from myofibers denoted as MPs that might become quiescent despite being forced to differentiate (Abou-Khalil et al., 2013; Yoshida et al., 1998). They are an indicator of the self-renewal capacity as the reserve cells can be reactivated

and differentiate (Furuichi et al., 2021; Laumonier et al., 2017). Hence, to enumerate the number of reserve cells we transferred WT and p107KO myofibers 72 hours post isolation to collagen coated plates for another 72-hour incubation to allow SCs to be dispersed from myotubes (**Fig. 4.18A**). These MPs were stained for Pax7 and MyoD and the fraction of reserve cells, which are Pax7+MyoD- from the total number of primary MPs, were tabulated. We found that the p107KO MPs generate a significantly greater fraction of reserve cells compared WT cells with nearly a 3.5-times increase. (**Fig 4.18B**). Together, with the previous ex vivo data, the increase in reserve cell population for p107KO indicate that p107 affects SC self-renewal.

p107 activity does not affect differentiation

For proper muscle regeneration to occur, there is a balance between SC self-renewal and differentiation (Dumont, Bentzinger, et al., 2015). Indeed, an increase in SC self-renewal can negatively affect differentiation capacity and reduce muscular regeneration capacity (Abou-Khalil et al., 2009; Wen et al., 2012). Thus, as our findings show that p107KO promotes SC self-renewal we tested the capacity of SC differentiation and muscular regeneration. (**Fig. 4.17**). First we investigated the differentiation capacity in vivo by measuring the cross-sectional area of uninjured and contralateral recovered (21 days after Ctx administration) TA muscles from WT and p107KO mice. The muscles were stained for Laminin to allow for the measuring cross sectional area per myofiber. Importantly, the results showed that there was no significant difference in cross sectional area between uninjured and recovered p107KO TA muscle (**Fig. 4.19**). As expected, there was also no significant difference in cross sectional area of uninjured and recovered WT TA (**Fig. 4.19**). These findings suggest that the increased self-renewal observed in p107KO mice does not hinder their differentiation and regenerative capacity.

To corroborate these findings, we next assessed the potential to generate myotubes in vitro of MPs derived from SCs of myofibers from WT and p107KO mice. This was accomplished by differentiating the MPs and measuring the myofusion index, which is an in vitro measure of the differentiation capacity (Furuichi et al., 2021). Myofusion index was measured by counting the number of nuclei present within myotubes per myotubes present. We found that there was no significant difference to the myofusion index between WT and p107KO MPs (**Fig. 4.20**). Together these findings suggest that p107 has a role in SC fates for self-renewal without affecting their differentiation capacity.

p107 mitochondrial localization in SCs is controlled by NAD+/NADH ratio

Recently published work from our lab shows that p107 has a mitochondrial function in MPs by localizing within the organelle (Bhattacharya et al., 2021) (Bhattacharya et al., 2021). We confirmed that p107 is in the mitochondria of SCs by culturing EDL myofibers isolated from WT and p107KO mice for 72 hours and immunostaining for p107 and the mitochondrial translocase of the outer membrane complex (Tom20). Confocal microscopy and subsequent analysis of generated Z-stacks showed that p107 and the mitochondrial protein Tom20 co-localize in SCs (**Fig. 4.21A**). p107 and Tom20 co-localization was confirmed by matching fluorescence intensity peaks of a line scanned for red, green, and blue (RGB) profile of a representative image (**Fig. 4.21B**). As expected, negative control p107KO myofibers had no immunofluorescent signal for p107.

We also recently showed that p107 mitochondrial localization in MPs is manipulated by the NAD^+/NADH ratio which is inversely related to the glucose concentration (**Fig. 1.10**). MPs cultured in 5.5mM glucose which elicits a high NAD^+/NADH ratio saw negligible mitochondrial p107 levels compared to the cells cultured in 25mM glucose, which illicit a low NAD^+/NADH

ratio (Bhattacharya et al., 2021). Thus, we wanted assessed if NAD^+/NADH p107 localization in SCs. We affected NAD^+/NADH levels by culturing myofibers isolated from WT mice for 72 hours in stripped media with either 5.5mM or 25mM glucose as the sole nutrient without pyruvate and glutamine. Confocal microscopy and subsequent analysis of generated Z-stacks showed p107 and mitochondrial protein Tom20 have enhanced co-localization in the myofibers cultured in 25mM compared to 5.5mM (**Fig. 4.22**) As before, p107 and Tom20 co-localization was confirmed by matching fluorescence intensity peaks of a line scanned for RGB profile of a representative image for the myofibers grown in 25mM. (**Fig. 4.23**). These findings strongly suggest that that p107 mitochondrial localization in SCs is regulated by the NAD^+/NADH ratio.

p107 mitochondrial localization manipulated by the NAD^+/NADH ratio regulates SC self-renewal

We next determined if self-renewal fate decisions by p107 is a result of its mitochondrial function. To test this, we cultured myofibers isolated from WT and p107KO mice for 72 hours in stripped media with 5.5mM or 25mM glucose as the sole nutrient. The 5.5mM condition would result in SCs that have minimal mitochondrial p107 localization and the 25mM condition would result in SCs that contain p107 within the mitochondria (**Fig. 4.22 and Fig. 4.23**). The myofibers were immune stained for Pax7 and MyoD and the fraction of quiescent SCs (Pax7+MyoD-) was determined (**Fig. 4.24**). We found that WT myofibers cultured in 5.5mM glucose when p107 is outside the mitochondria had significantly greater fraction of quiescent SCs compared to those grown in 25mM glucose (**Fig.4.25A**). Moreover, we determined that there was no change to the fraction of quiescent SCs for p107KO myofibers when comparing their growth in 5.5mM to 25mM groups (**Fig. 4.25A**). When comparing WT and p107KO myofibers cultured in 5.5mM there was

no difference in the fraction of quiescent SCs (**Fig. 4.25B**). Together, these findings strongly suggest that p107 mitochondrial localization regulates SC self-renewal.

p107 interacts with Sirt1 in the cytoplasm of C2C12 MPs

As mitochondrial p107 localization in SCs is controlled by the NAD^+/NADH ratio (**Fig 4.23**) it suggests that the Sirt family might control p107 function. Sirt1 is one of the two sirtuins active in the cytoplasm of cells that is known to control mitochondrial metabolism through its activation by cytoplasmic NAD^+ (Cantó et al., 2015). In addition, Sirt1 has been shown to target transcription factors and co-activators (H.-C. Chang & Guarente, 2014; Costa-Machado & Fernandez-Marcos, 2019). Therefore, we chose to assess if Sirt1 controls p107 mitochondrial function by interacting with it in the cytoplasm of MPs. For this, reciprocal immunoprecipiatation (IP)/ Western blot analysis for endogenous p107 and Sirt1 was conducted on cytoplasmic lysates from C2C12 cells grown at 5.5mM (**Fig. 4.26A**) when p107 is known to be predominately in the cytoplasm instead of the mitochondria (**Fig. 4.22**). The results revealed that Sirt1 and p107 interacted in the cytoplasm (**Fig 4.26A**). 1/10th of the lysates that were used in the IP reactions were Western blotted for p107 and Sirt1 to provide an estimate of the input protein lysate that were IPed. Moreover, we confirmed that the specificity of the antibodies used were accurate by Western blotting for p107 on p107KO cells and Sirt1 on Sirt1KO cells (**Fig. 4.26B**). These findings suggest that p107 mitochondrial localization is mediated by Sirt1 interaction in the cytoplasm and can be controlled by manipulation of Sirt1 activity via the NAD^+/NADH ratio.

Figure 4.1

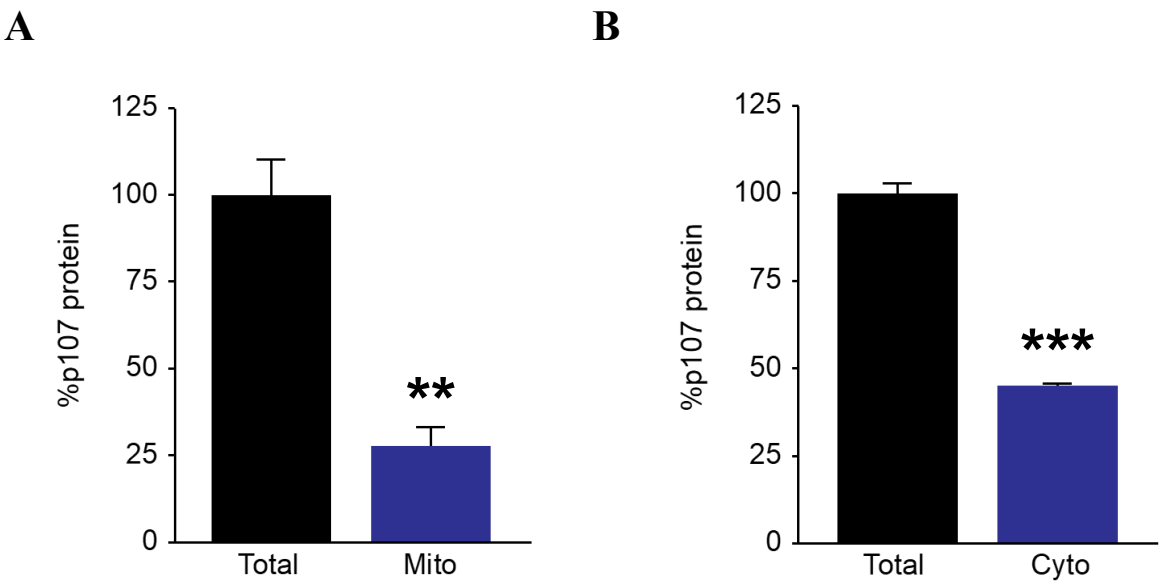

Figure 4.1. p107 mitochondrial and cytoplasmic percent occupancy. Percentage of cellular p107 protein distribution in C2C12 cells for **(A)** mitochondria (Mito) and **(B)** cytoplasm (Cyto). Data are presented as mean values +/- SD. n = 3 biologically independent samples. Two-tailed unpaired Student T-test, $^{**}p = 0.001$, $^{***}p < 0.001$.

Figure 4.2

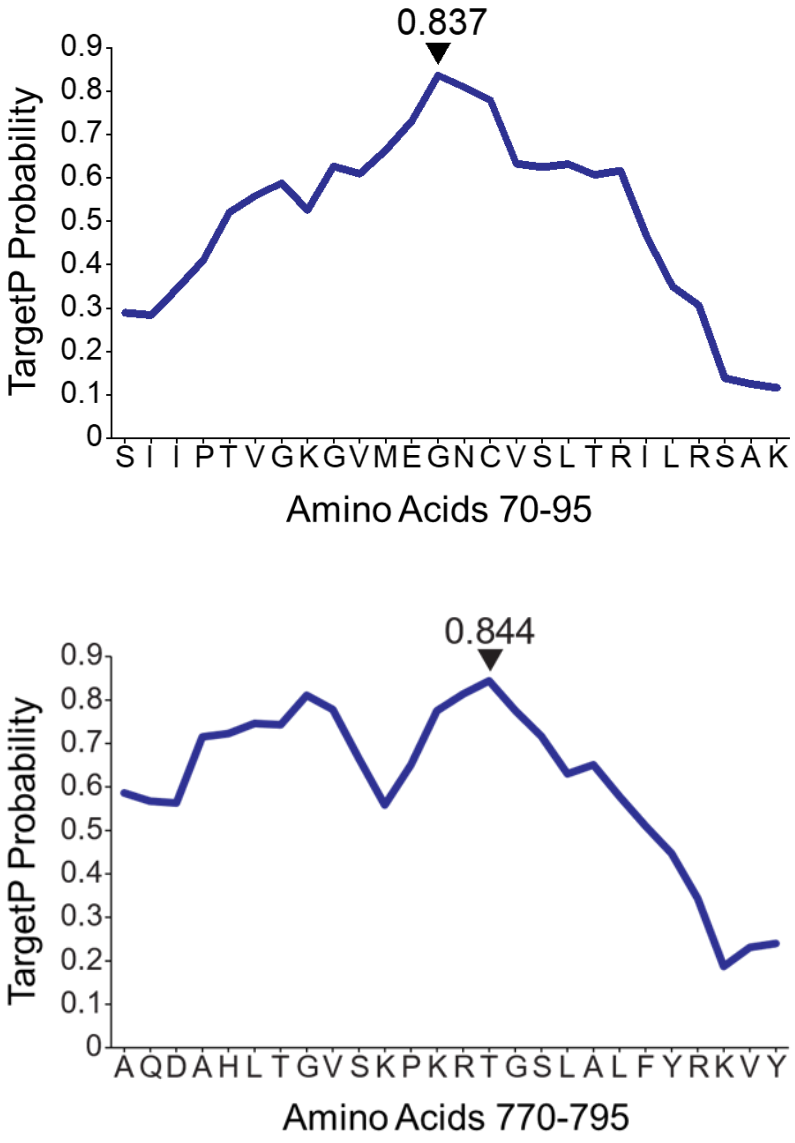

Figure 4.2. p107 mitochondrial import is likely mediated by iMTS recognition. iMTS probability scores for p107 from amino acids 70-95 and 770-795 using the TargetP prediction algorithm for mitochondrial targeting signal detection. Black arrows denote peak probability scores of 0.837 and 0.844 (>0.75 is a strong predicator for localization).

Figure 4.3

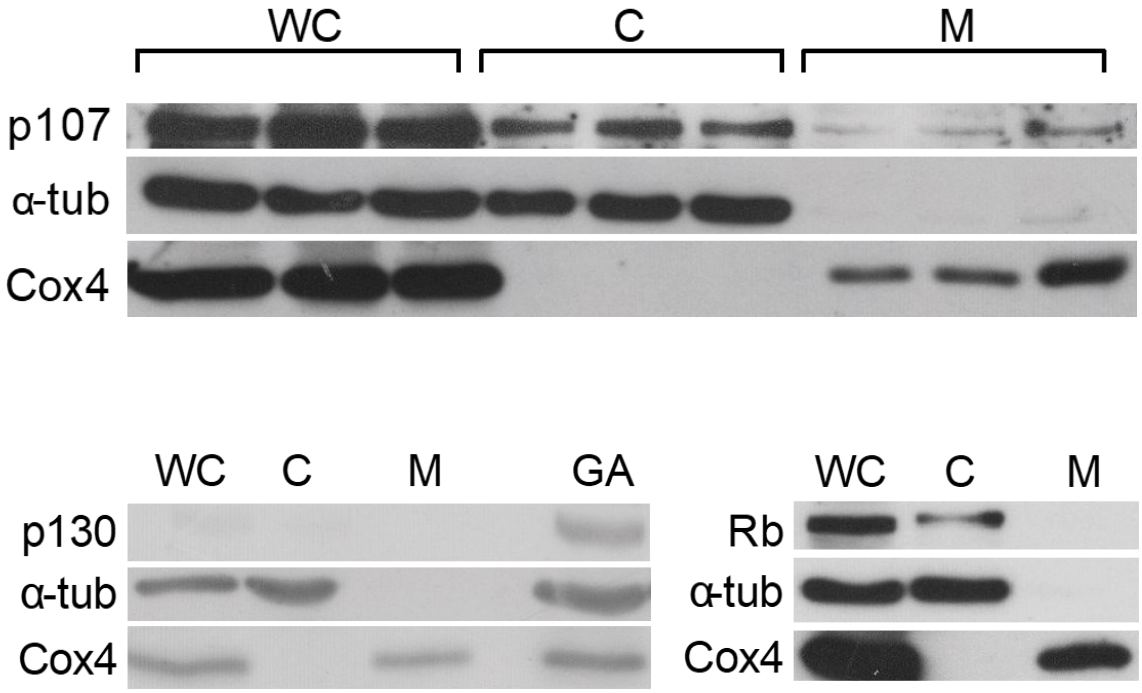

Figure 4.3. Rb family mitochondrial function in MPs is exclusive to p107. Representative Western blots of whole cell (WC), cytoplasmic (C) and mitochondrial (M) and contact inhibited growth arrested (GA) C2C12 cellular fractions for p107, p130, Rb, cytoplasmic loading control α-tubulin (α-tub) and mitochondrial loading control Cox4. (Bhattacharya et al., 2021)

Figure 4.4

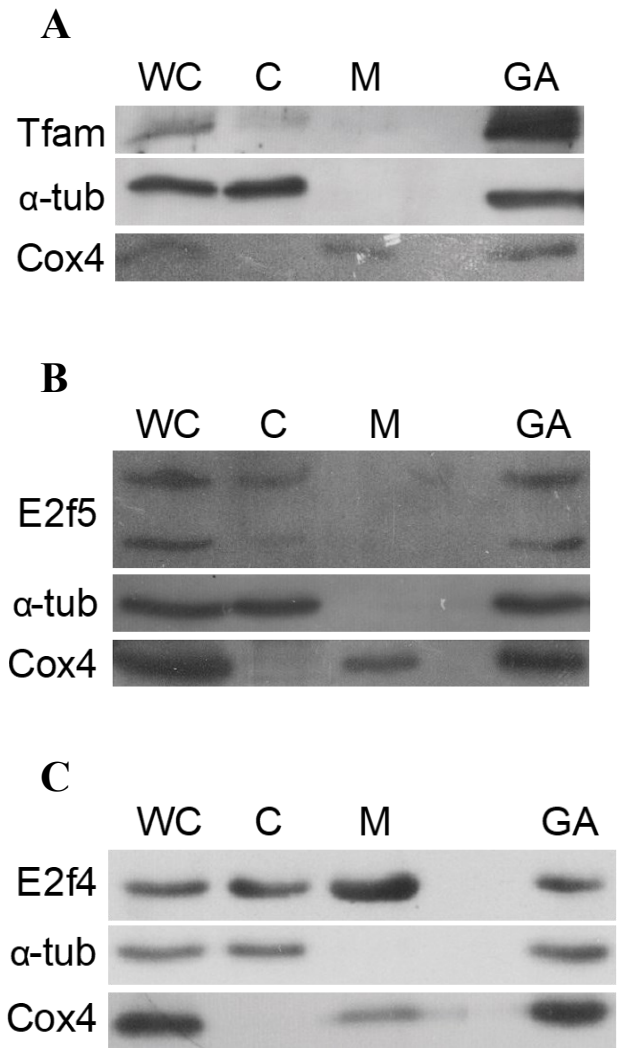

Figure 4.4. E2f4 is present in the mitochondria of proliferating MPs. (A), (B), (C) Representative western blots of whole cell (WC), cytoplasmic (C), mitochondrial (M) and growth arrested (GA) C2C12 cellular fractions for Tfam, E2f4, E2f5, α-tub, and Cox4. (Bhattacharya et al., 2021)

Figure 4.5

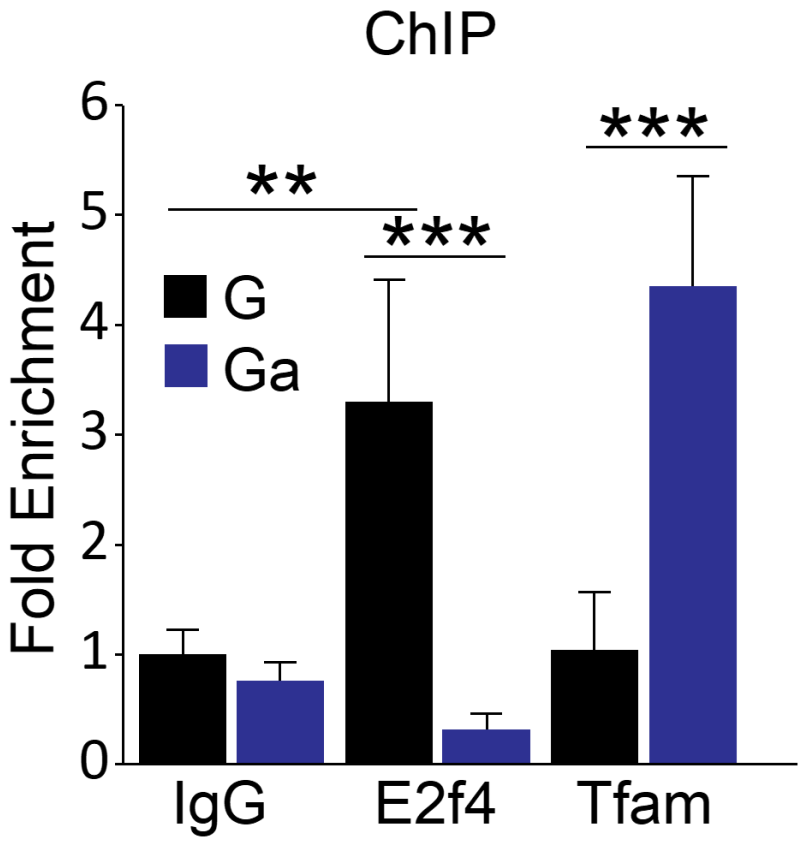

Figure 4.5. E2f4 interacts with the mitochondrial DNA in proliferating MPs. Graphical representation of qChIP analysis of IgG, E2f4 and Tfam mitochondrial DNA occupancy during proliferation (G) and growth arrest (Ga). n=4 biologically independent samples, $^{**}p < 0.01$ and $^{***}p < 0.001$. Data are presented as mean values +/- SD. Two-way Anova and post hoc Tukey test. (Bhattacharya et al., 2021)

Figure 4.6

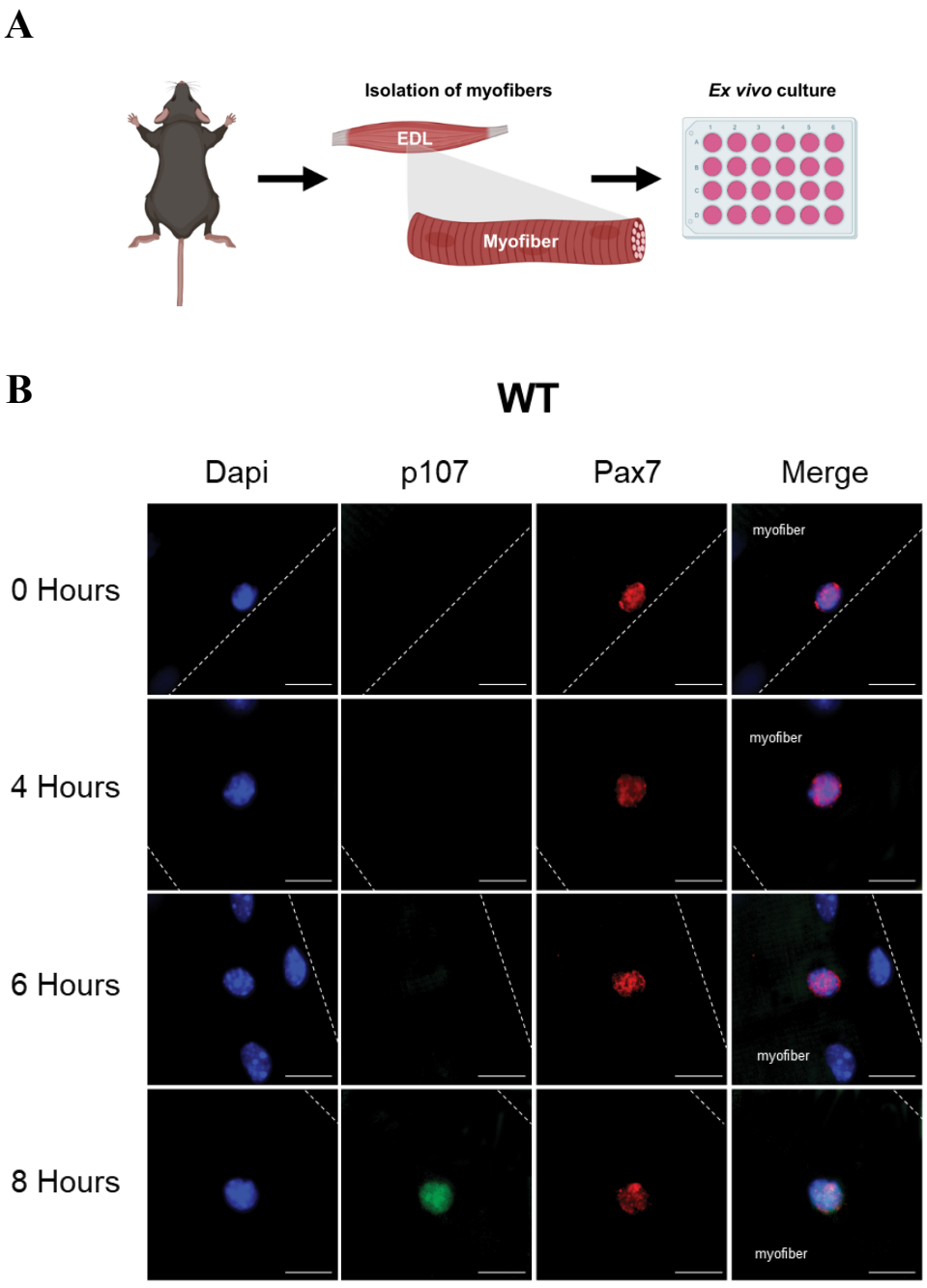

Figure 4.6. p107 is expressed in SCs after 8 hours of culture. (A) Schematic showing the methodology of EDL myofiber isolation and culture. Schematic created with BioRender. **(B)** Representative immunohistochemistry for Dapi, p107, Pax7 and merged image of WT EDL myofibers at 0, 4, 6, and 8 hours. Note p107 is first observed at 8 hours in culture. Scale bar represents 10µm. Hashed line is an outline of the myofiber.

Figure 4.7

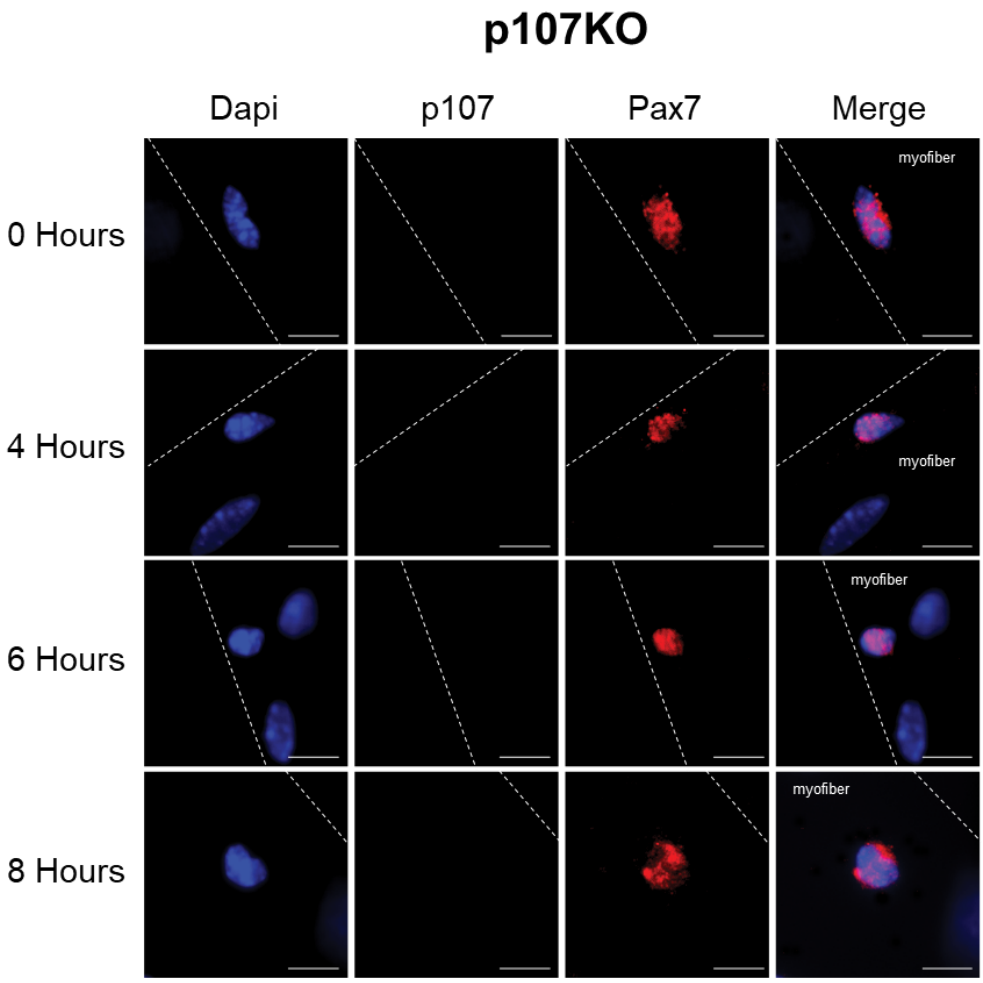

Figure 4.7. p107 is not expressed in p107KO myofibers. Representative immunohistochemistry for Dapi, p107, Pax7 and merged image of p107KO EDL myofibers at 0, 4, 6, and 8 hours. Scale bar represents 10μm. Hashed line is an outline of the myofiber.

Figure 4.8

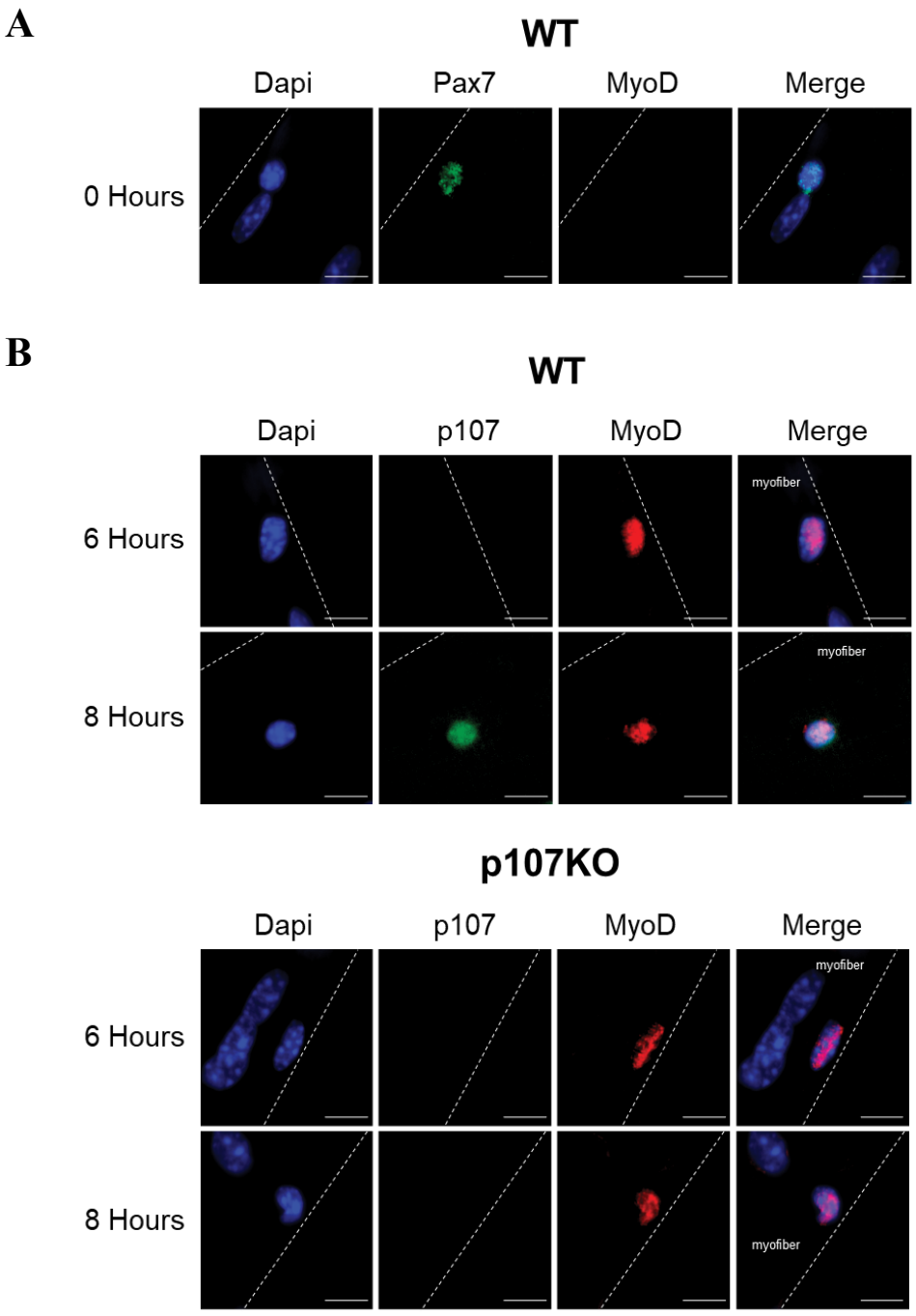

Figure 4.8. p107 is expressed after SC activation. (A) Representative immunohistochemistry for Dapi, pax7, MyoD and merged image of WT EDL myofibers at 0 hours. **(B)** Representative immunohistochemistry for dapi, p107, MyoD and merged image of WT and p107KO EDL myofibers at 6, and 8 hours. Note p107 is first observed at 8 hours after MyoD which is observed within 6 hours. Scale bar represents 10μm. Hashed line is an outline of the myofiber.

Figure 4.9

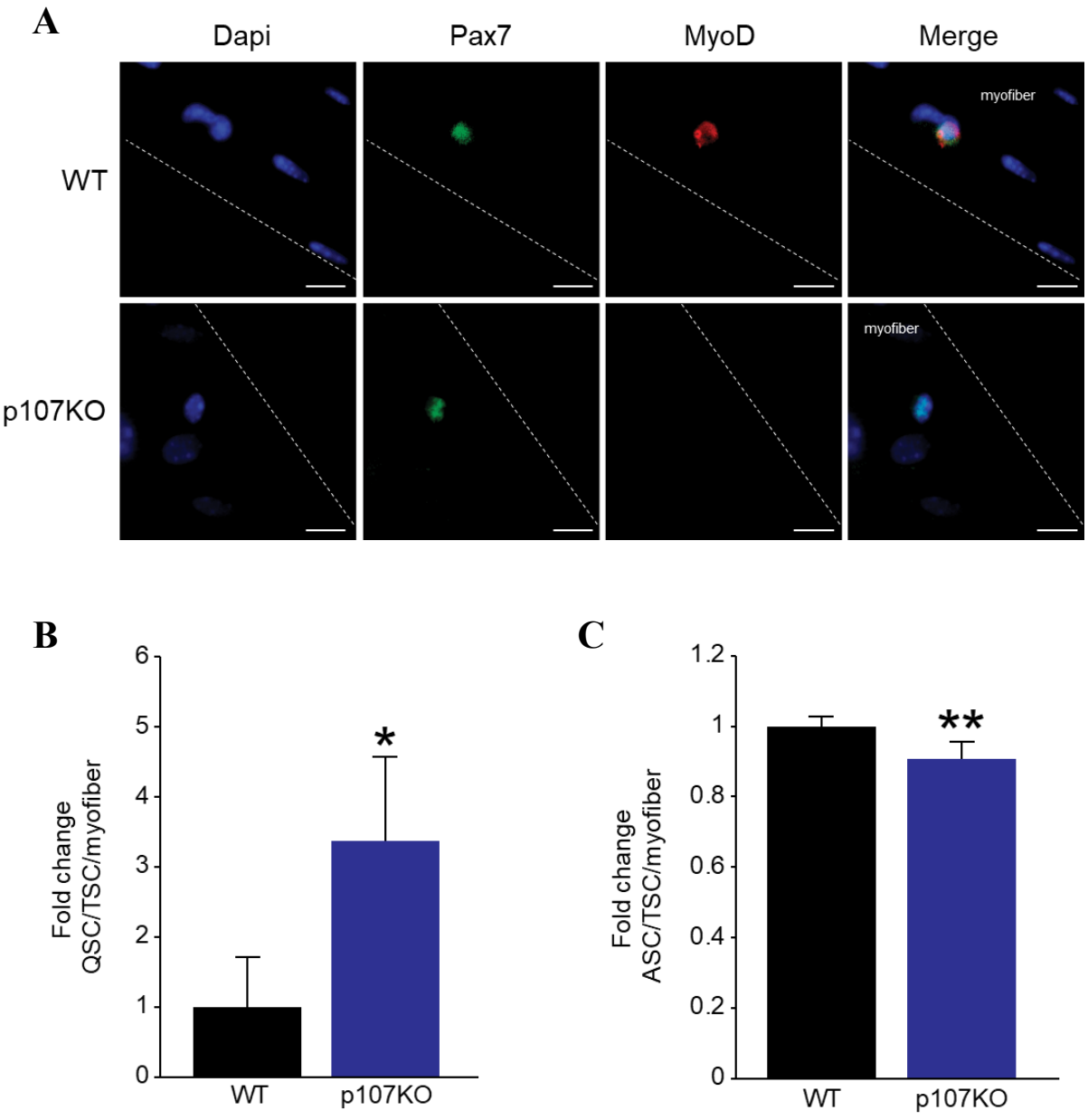

Figure 4.9. p107 is important for SC activation timing. (A) Representative immunohistochemistry for Dapi, Pax7 and MyoD merge of WT and p107KO myofibers at 24 hours post isolation. Scale bars are 10um and hashed line is an outline of myofiber. Graphical representation of fold change for fraction of **(B)** quiescent Pax7+MyoD- (QSC) and **(C)** activated Pax7+MyoD+ (ASC) SCs from WT and p107KO myofibers. TSC is total satellite cells (Pax7+). Data are presented as mean values +/- SD. n=5 mice for each WT and p107KO. Two-tailed unpaired Student T-test, *p<0.05, **p <0.01.

Figure 4.10

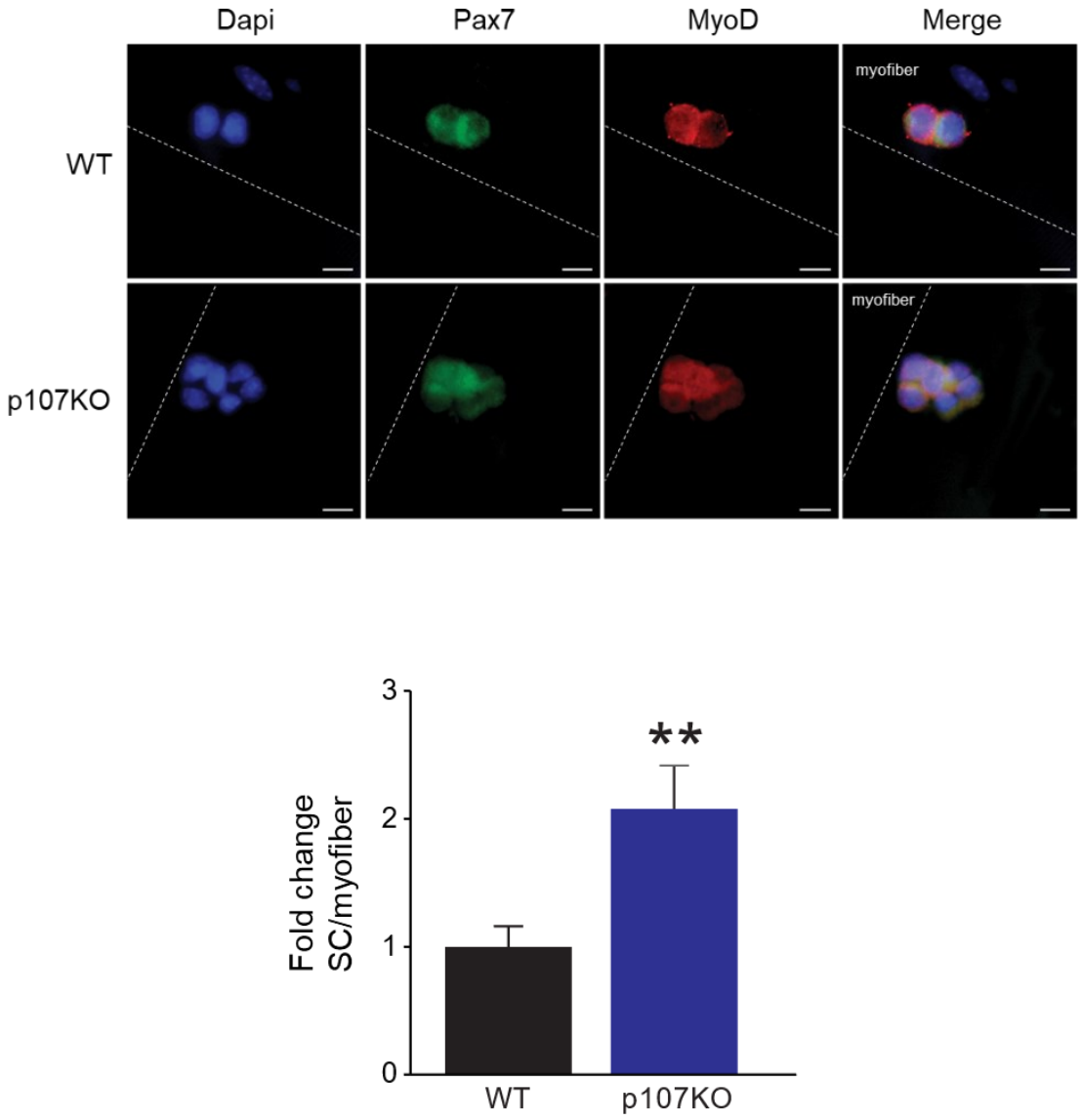

Figure 4.10. p107 has a role in SC proliferation. Representative immunohistochemistry for Dapi, Pax7, Myod and merge of WT and p107KO myofiber at 42 hrs of culture. Scale bars are 10um and hashed line is an outline of myofiber. Graphical representation of fold change for total SCs per myofiber for WT and p107KO at 42 hrs culture. Data are presented as mean values +/- SD. n=5 mice for each WT and p107KO. Two-tailed unpaired Student T-test, $**p<0.01$.

Figure 4.11

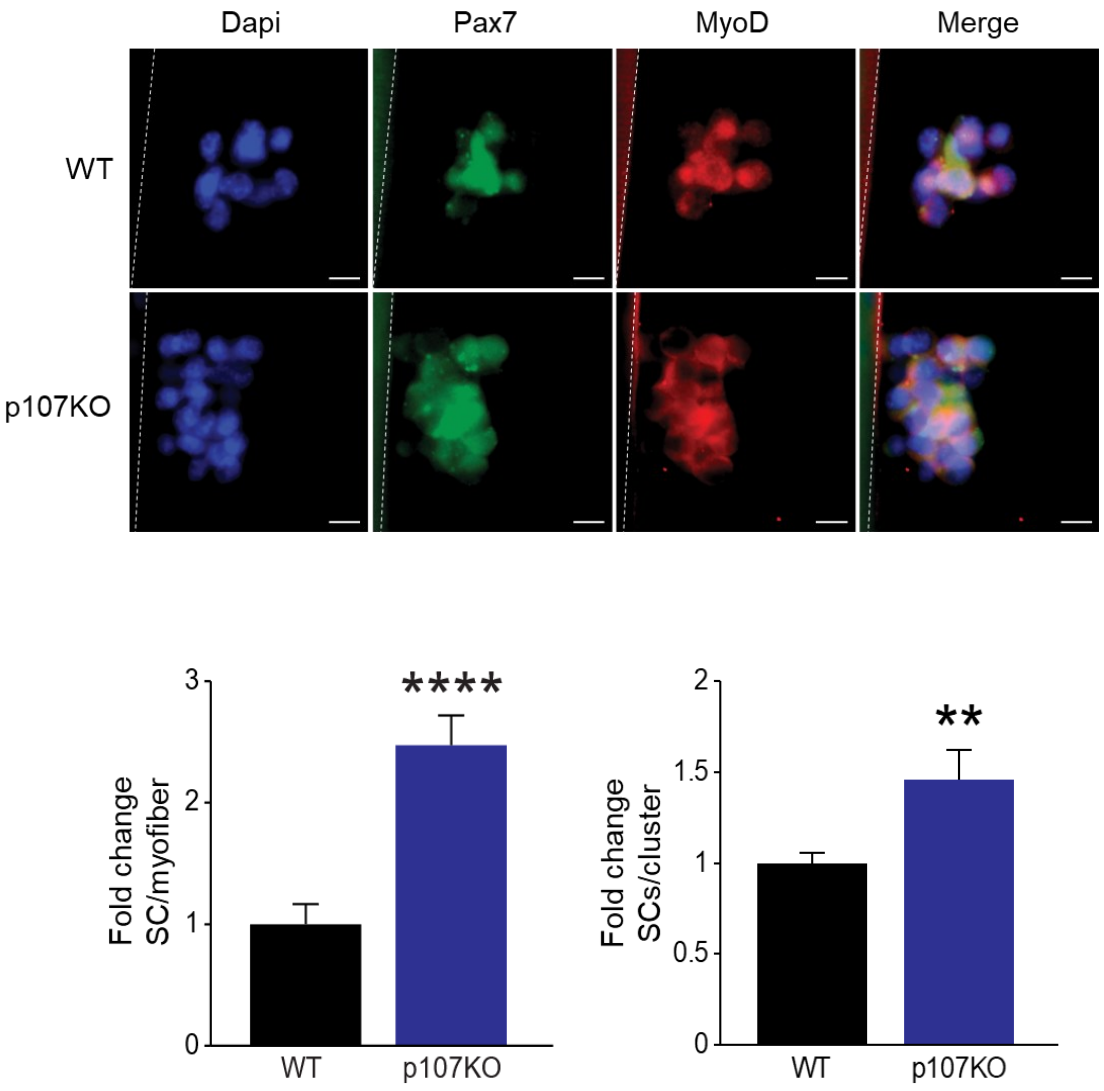

Figure 4.11. p107 has a role in SC proliferation. Representative immunohistochemistry for Dapi, Pax7, Myod and merge of WT and p107KO myofiber at 72 hrs of culture. Scale bars are 10um and hashed line is an outline of myofiber. Graphical representation of fold change for total SCs per myofiber and fold change for SCs in clusters per myofiber for WT and p107KO at 72 hrs culture. Data are presented as mean values +/- SD. n=5 mice for each WT and p107KO. Two-tailed unpaired Student T-test, $^{**}p<0.01$, $^{****}p<0.0001$.

Figure 4.12

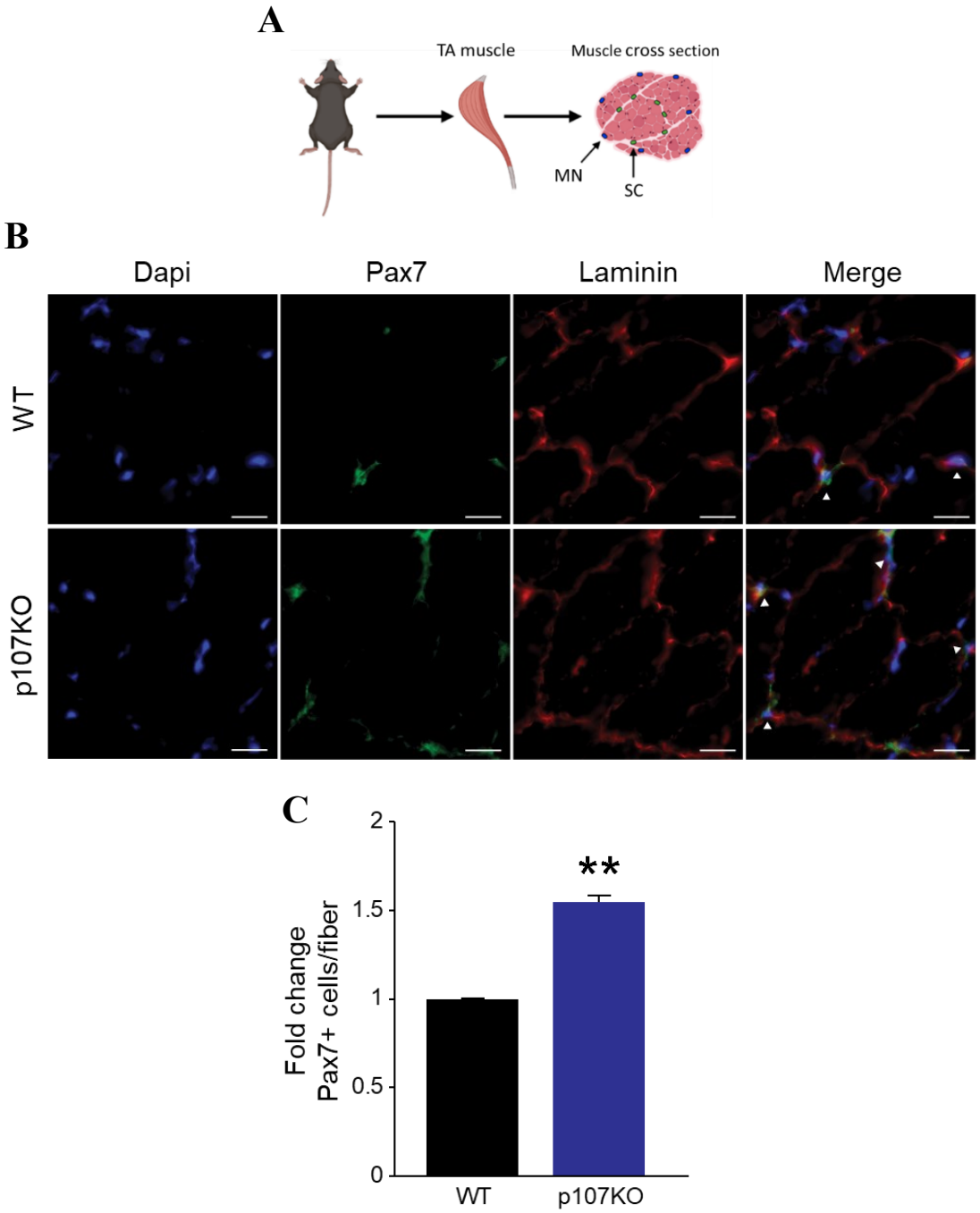

Figure 4.12. Uninjured p107KO muscle exhibits greater SC count. (A) Diagram of TA muscle harvesting and cross sectioning. MN is myonuclei. Diagram created with BioRender. **(B)** Representative immunohistochemistry of Dapi, Pax7, Laminin and merged images for WT and p107KO TA muscle. **(C)** Graphical representation of fold change of Pax7+ cells per fiber for WT and p107KO. Arrows denote Pax7+ SCs. Scale bar represents 10μm. Data are presented as mean values +/- SD. n=4 mice for each WT and p107KO. Two-tailed unpaired Student T-test, $^{**}p < 0.01$.

Figure 4.13

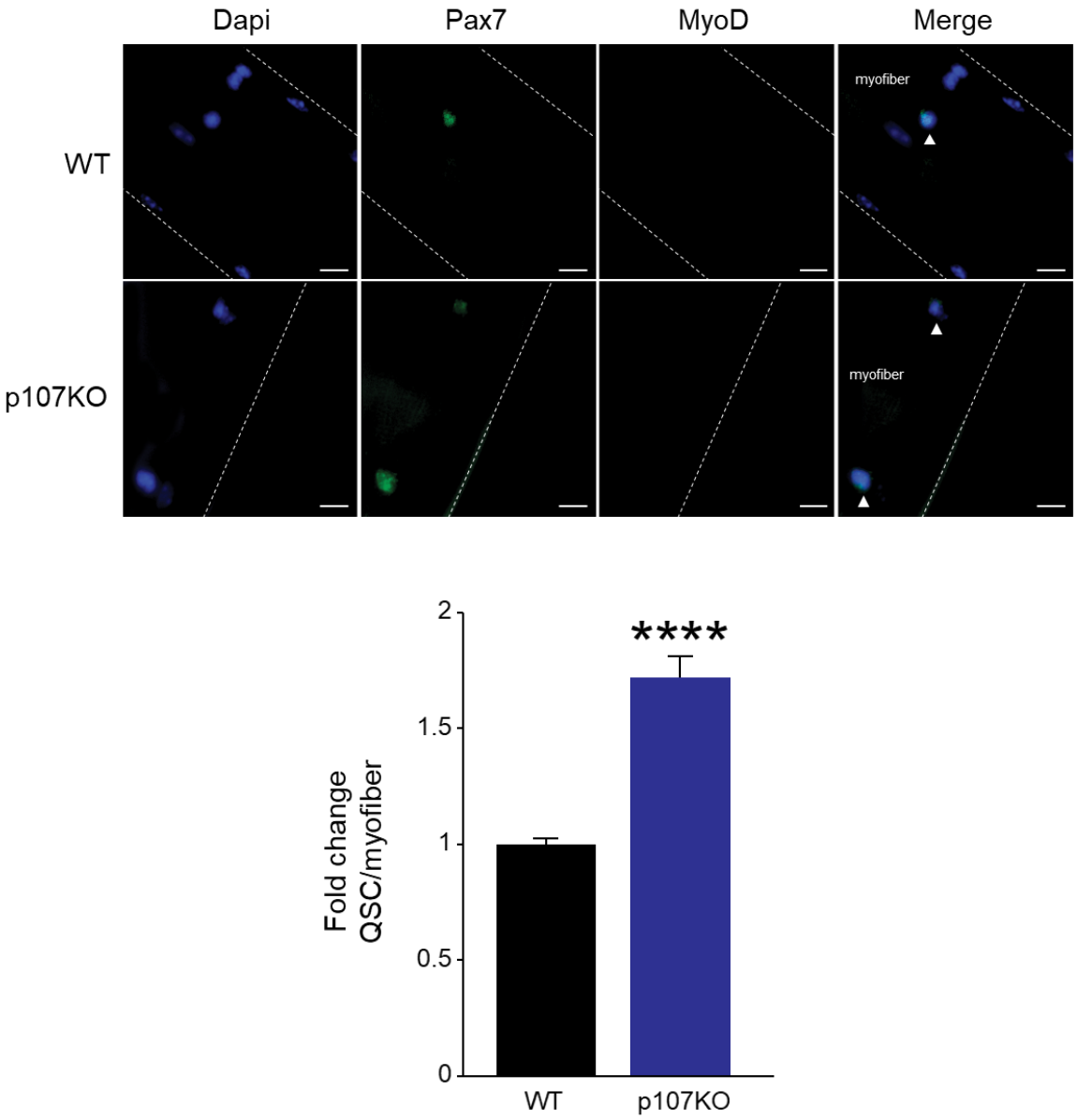

Figure 4.13. p107KO myofibers have more SCs. Representative immunohistochemistry for Dapi, Pax7, MyoD and merge of WT and p107KO and graphical representation of fold change for quiescent (Pax7+MyoD-) SCs (QSC) per myofiber at 0 hrs. Arrows denote quiescent SCs (Pax7+MyoD-). Scale bar represents 10μm and hashed line is an outline of myofiber. Data are presented as mean values +/- SD. n=5 mice for each WT and p107KO. Two-tailed unpaired Student T-test, ****p <0.0001.

Figure 4.14

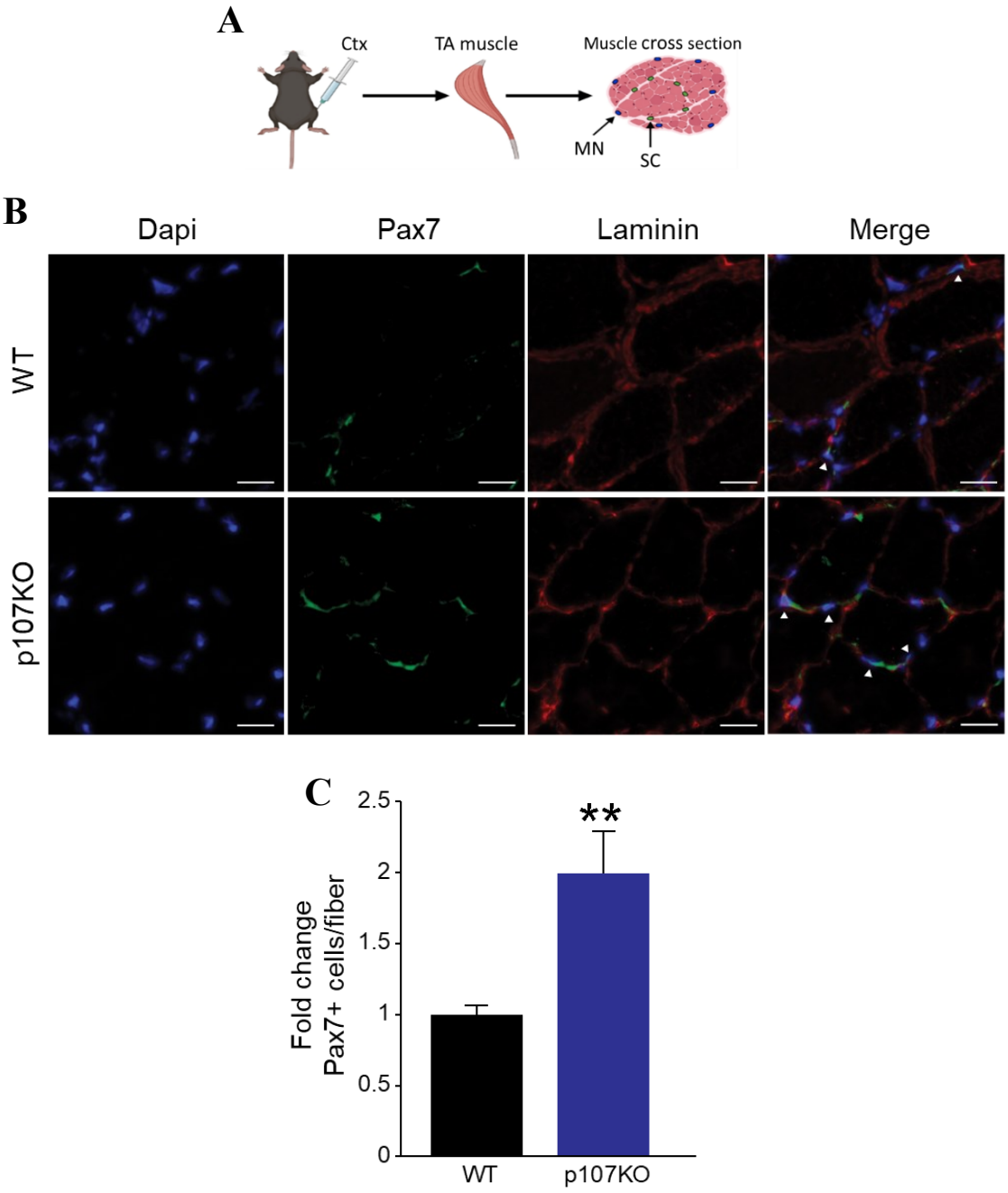

Figure 4.14. p107 regulates SC numbers during regeneration. (A) Diagram of Ctx induced muscle injury methodology (MN is myonuclei). Diagram created with BioRender. **(B)** Representative immunohistochemistry after 21 days post recovery with Ctxinjury with Dapi, Pax7, Laminin and merged images for WT and p107KO TA muscle. Arrows denote Pax7+ SCs. **(C)** Graphical representation of fold change of Pax7+ cells per fiber for WT and p107KO. Scale bar represents 10µm. Data are presented as mean values +/- SD. n=4 mice for each WT and p107KO. Two-tailed unpaired Student T-test, $^{**}p < 0.01$.

Figure 4.15

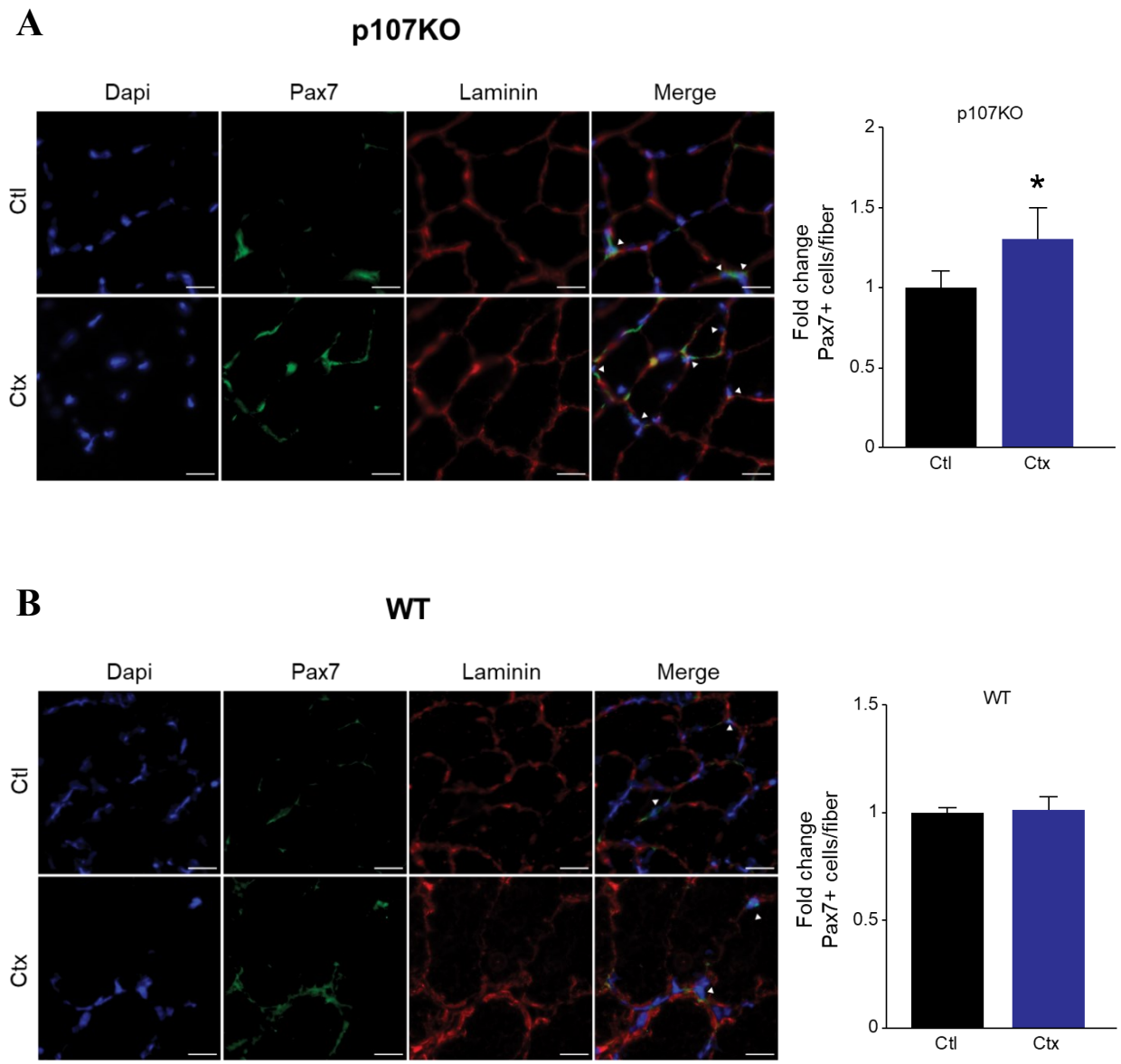

Figure 4.15. p107 deletion causes quiescent SC expansion in vivo. Representative immunohistochemistry of Dapi, Pax7, Laminin and merged images for TA of uninjured (Ctl) and contralateral recovered (Ctx) post 21 days injury with CTX for **(A)** p107KO and **(B)** WT TA muscles and graphical representations of fold change of Pax7+ cells per fiber for uninjured (Ctl) and contralateral recovered (Ctx) TA. Arrows denote Pax7+ SCs. Scale bar represents 20μm. Data are presented as mean values +/- SD. n=4 mice for each WT and p107KO. Two-tailed unpaired Student T-test, *p<0.05.

Figure 4.16

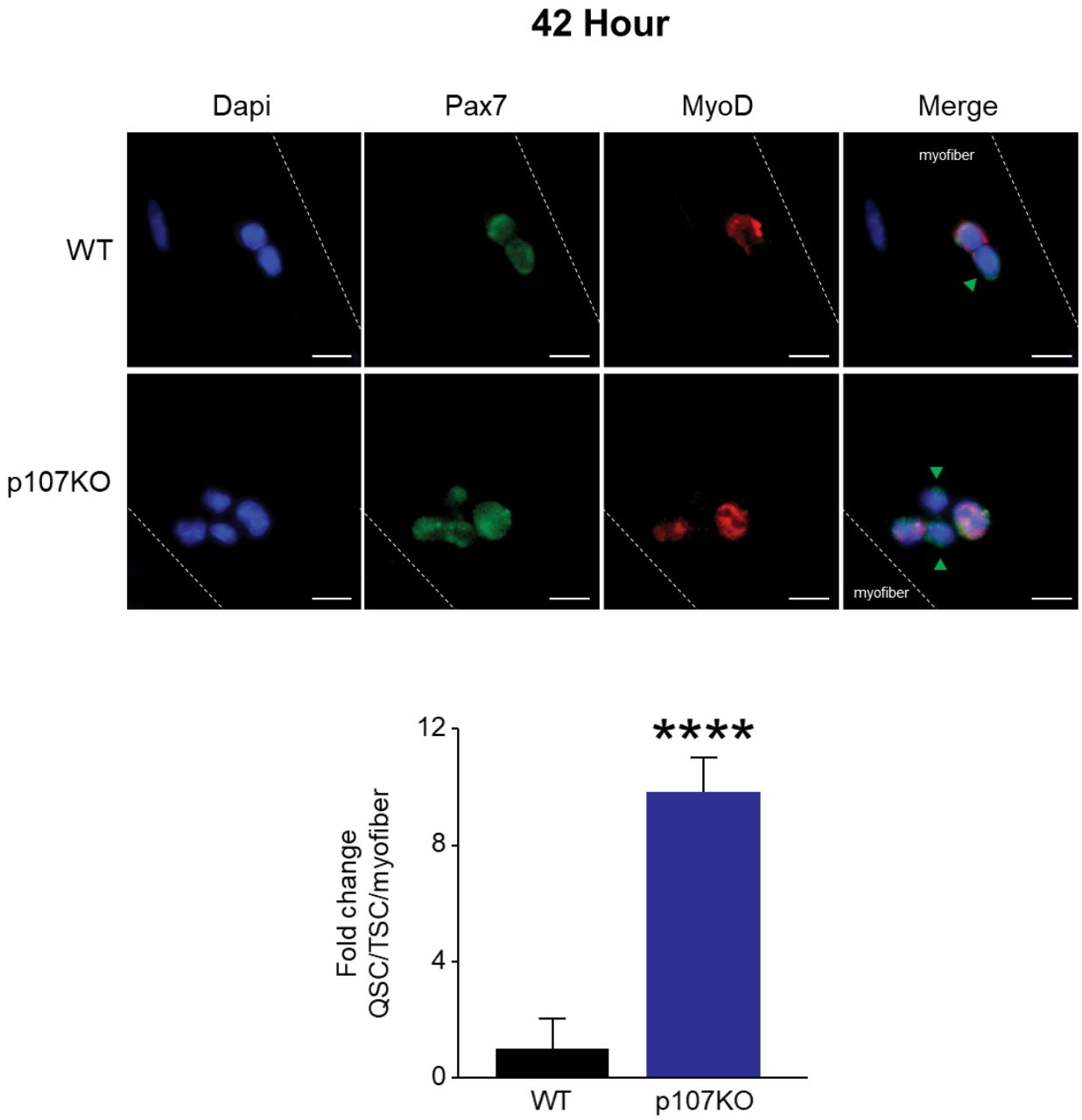

Figure 4.16. p107 regulates self-renewal capacity of SCs of myofibers. Representative immunohistochemistry for Dapi, Pax7, MyoD and merge of WT and p107KO myofibers cultured for 42 hours. Also, graphical representation of fold change for fraction of quiescent SCs (QSC) per total SCs (TSC) per myofiber. Green arrows denote self-renewed quiescent SCs. Scale bar represents 10μm and hashed lines are an outline of myofiber. Data are presented as mean values +/- SD. n=5 mice for each WT and p107KO. Two-tailed unpaired Student T-test, ****p<0.0001.

Figure 4.17

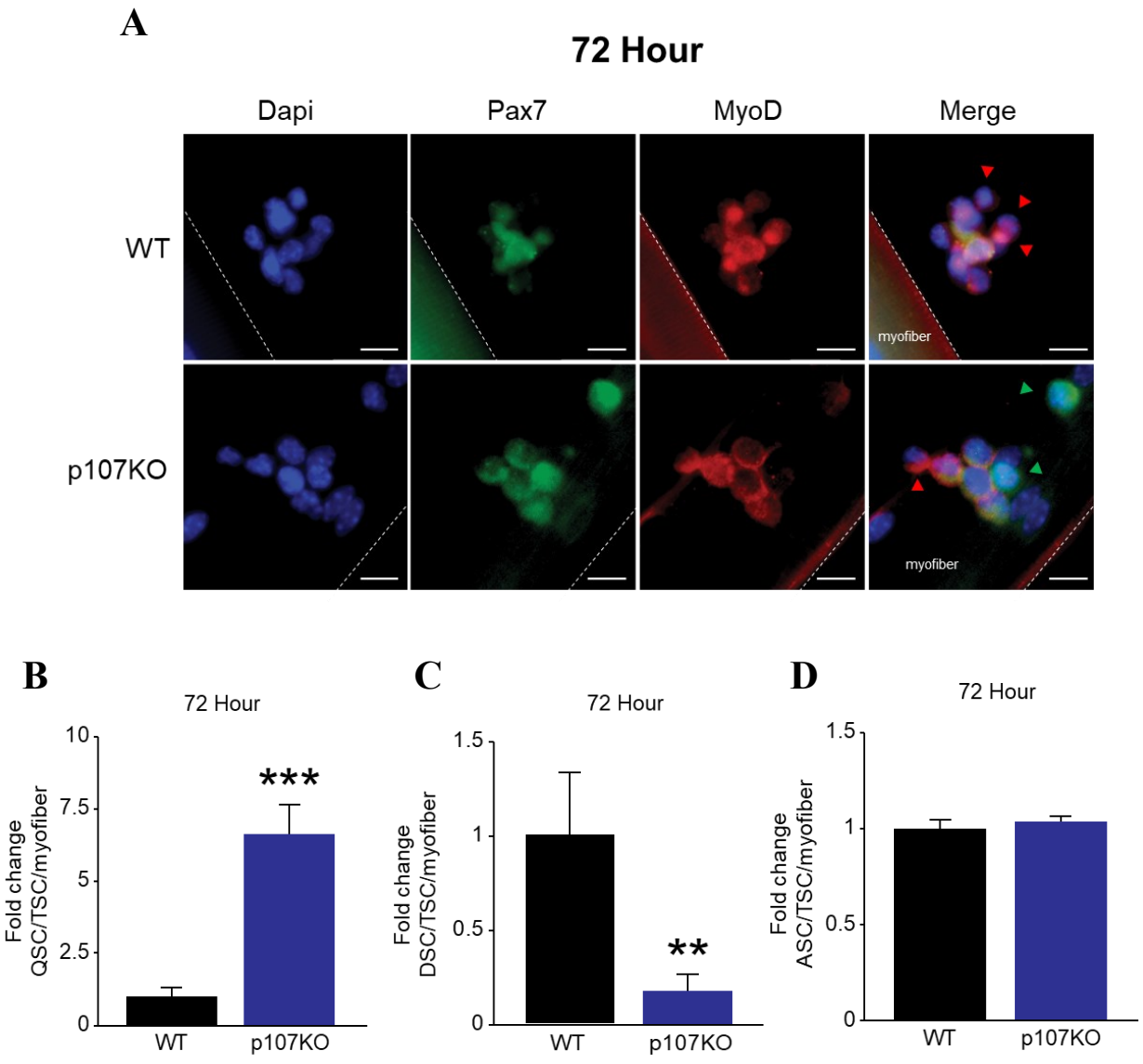

Figure 4.17. p107 regulates self-renewal capacity of myofibers. (A) Representative immunohistochemistry for Dapi, Pax7, Myod and merge of WT and p107KO myofibers cultured for 72 hours. Graphical representation of fold change for fraction **(B)** quiescent (QSC), **(C)** activated (ASC) and **(D)** differentiating (DSC) SCs per myofiber at 72 hours of culture. TSC is total satellite cells. Red arrows denote DSC, and green arrows denote self-renewed QSC. Hashed lines are an outline of myofiber. Data are presented as mean values +/- SD. n=5 mice for each WT and p107KO. Two-tailed unpaired Student T-test, $^{**}p<0.01$, $^{***}p<0.001$.

Figure 4.18

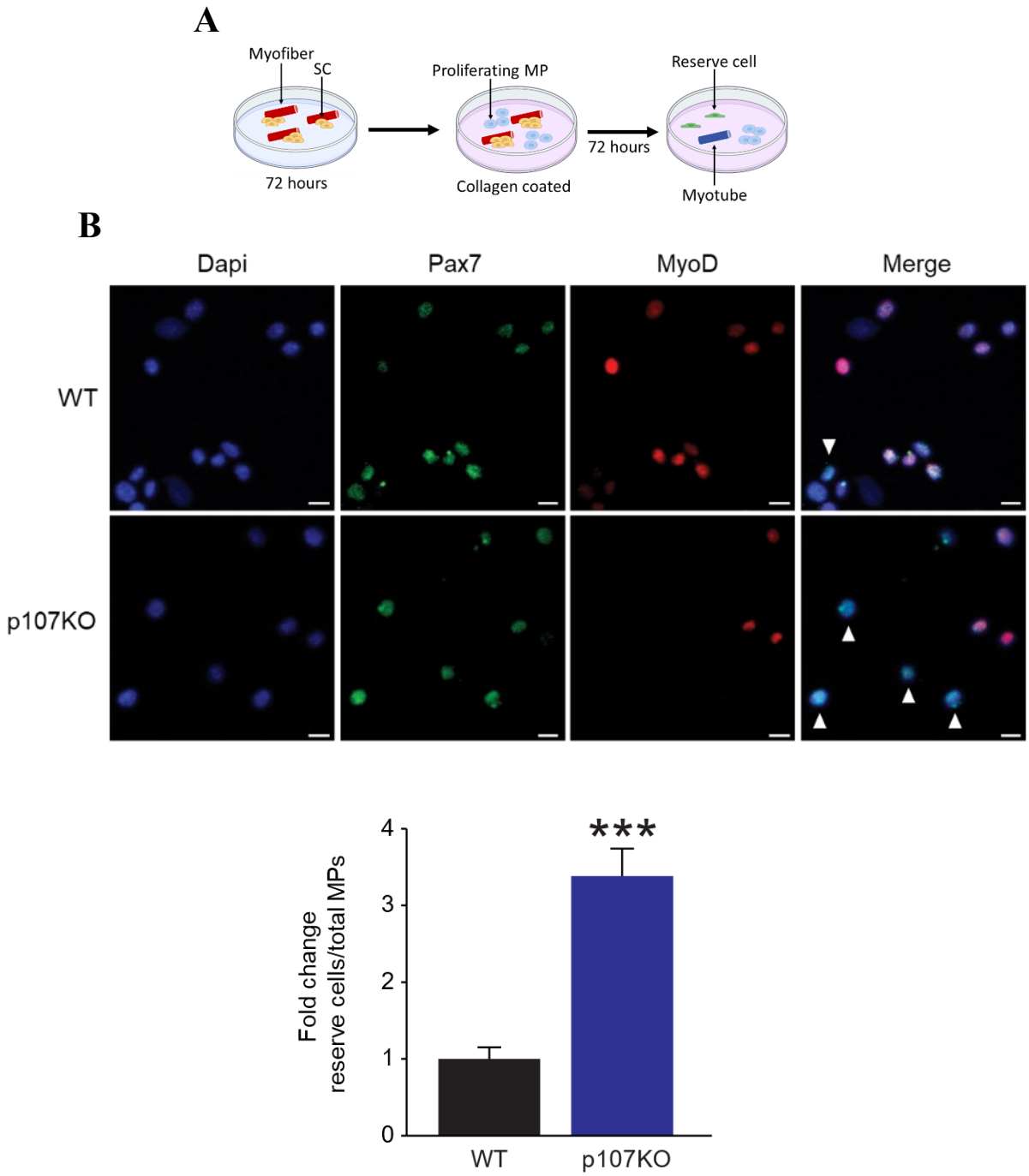

Figure 4.18. p107 effects reserve cell production. (A) Schematic approach used to obtain reserve cells. Schematic created with BioRender. **(B)** Representative immunocytochemistry of Dapi, Pax7, MyoD and merge for WT and p107KO MPs and graphical representation of fold change of the fraction of reserve cells (Pax7+MyoD-) per total MPs observed. Arrows denote reserve cells. Scale bar represents 10µm. Data are presented as mean values +/- SD. n=5 mice for each WT and p107KO. Two-tailed unpaired Student T-test, ***p<0.0001.

Figure 4.19

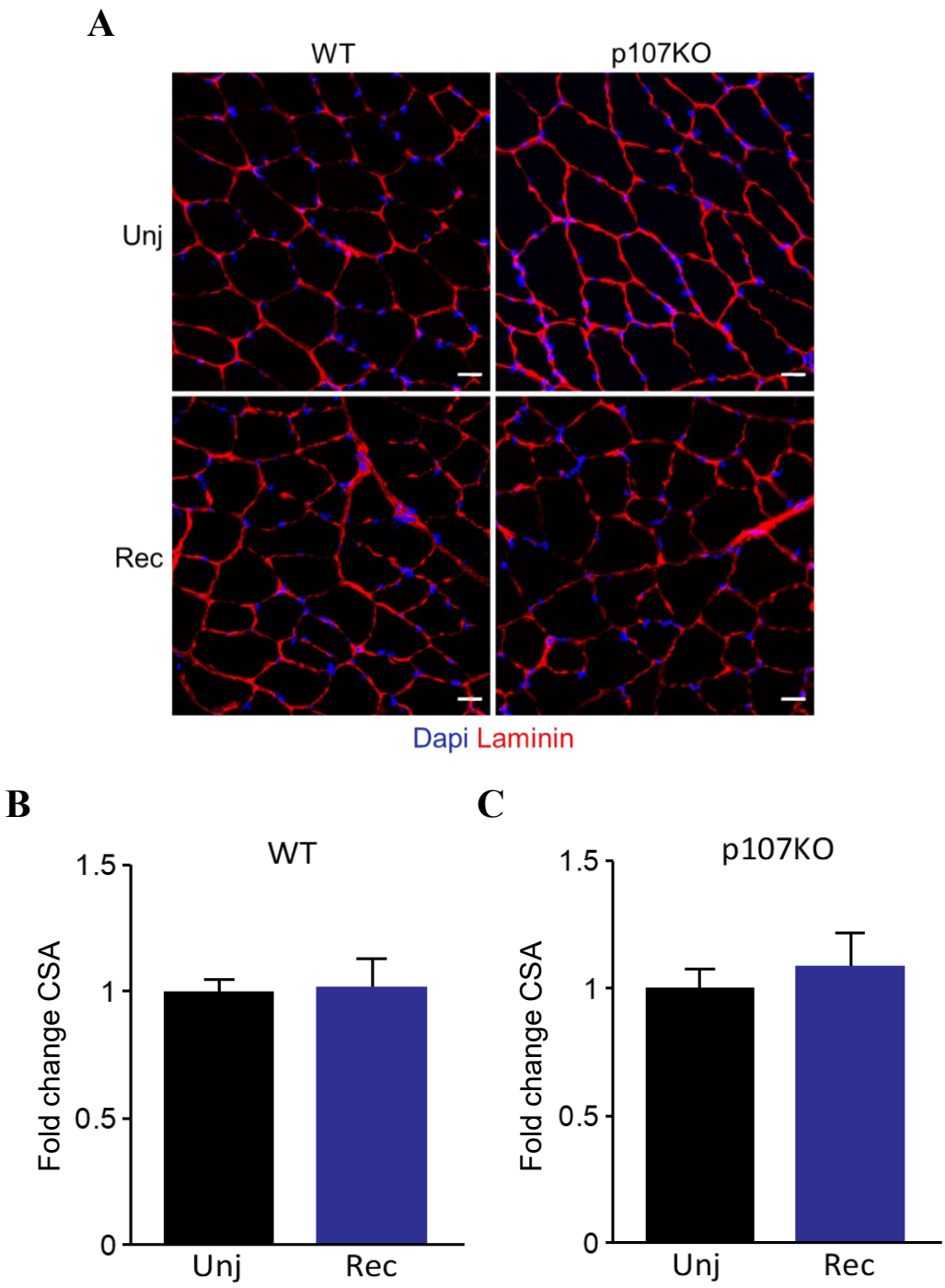

Figure 4.19. p107KO does not hinder muscle regeneration. (A) Representative merge of Dapi and Laminin and **(B)** graphical representations of fold difference of the cross-sectional area (CSA) for WT and p107KO uninjured (Unj) and contralateral recovered (Rec) from Ctx injury. Scale bar represents 20µm. Data are presented as mean values +/- SD. n=3 mice for each WT and p107KO. Two-tailed unpaired Student T-test.

Figure 4.20

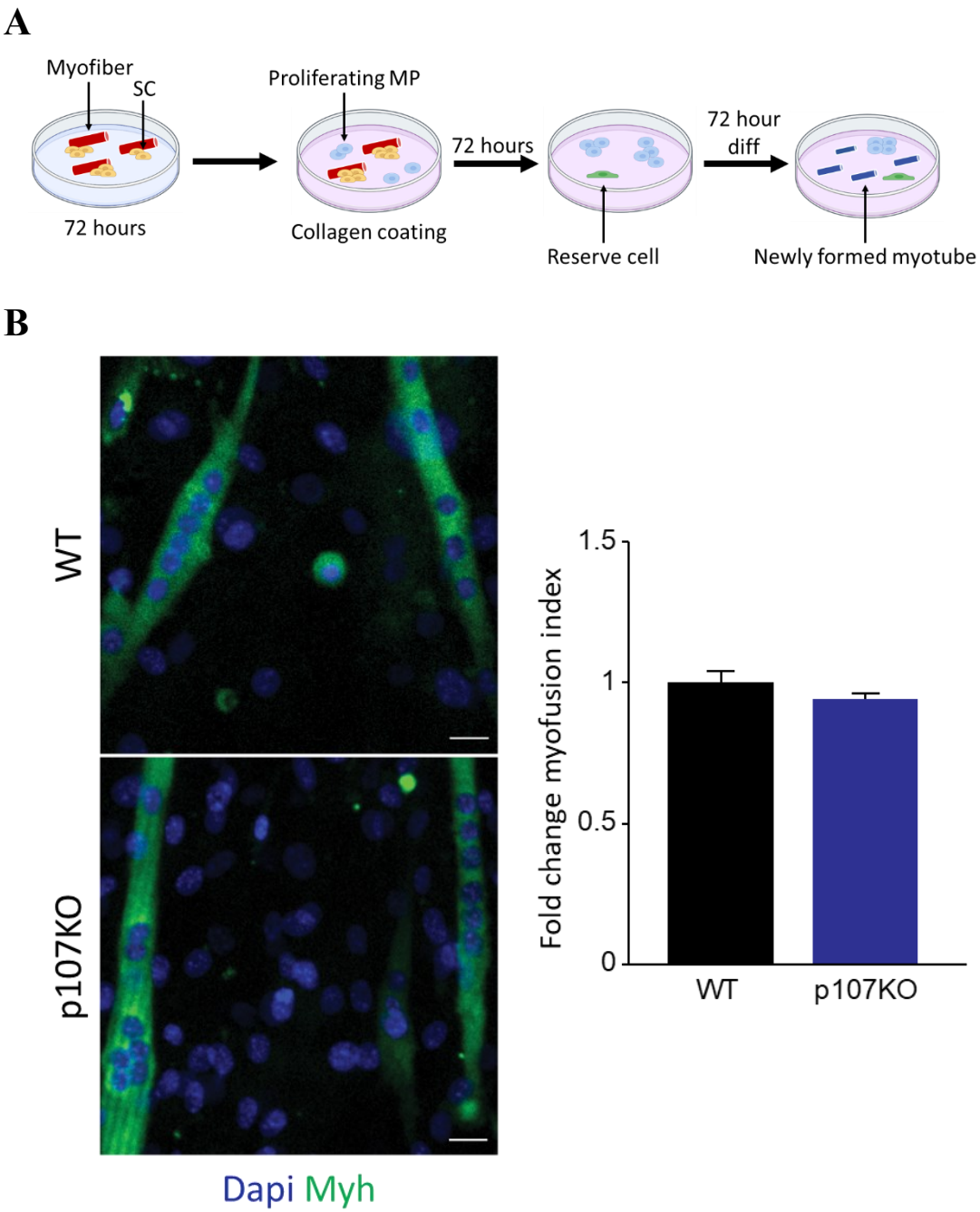

Figure 4.20. p107 deletion does not hinder MP differentiation. Schematic of methodology used to differentiate primary MPs derived from SCs of myofibers. Schematic created with BioRender. Representative merge of Dapi and myosin heavy chain (Myh) and graphical representation of the fold change of the myofusion index for WT and p107KO differentiated myotubes. Scale bars represent 10µm. Data are presented as mean values +/- SD. n=5 mice for each WT and p107KO. Two-tailed unpaired Student T-test.

Figure 4.21

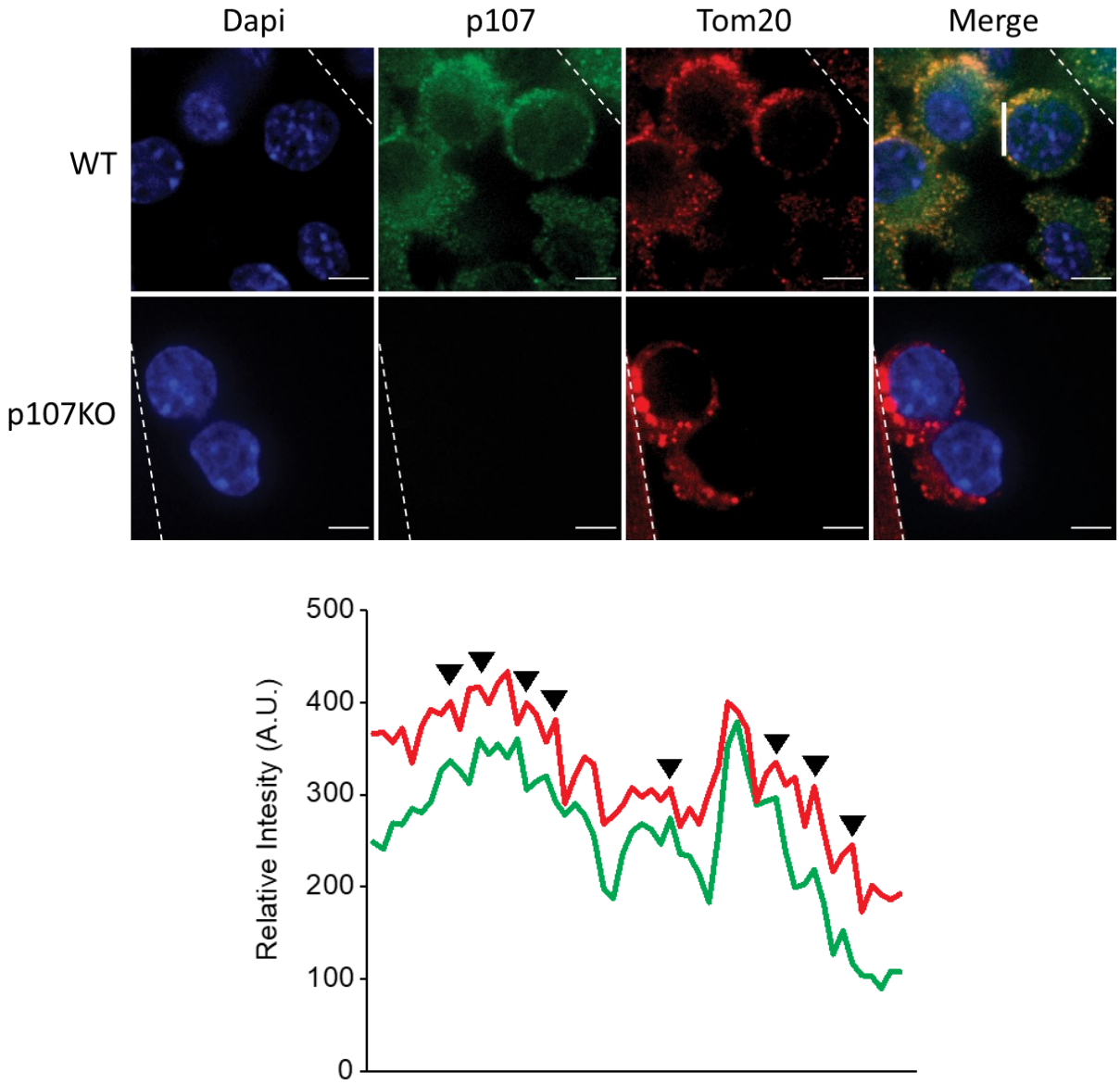

Figure 4.21. p107 is mitochondrial active in SCs. Representative confocal images for Dapi, p107, Tom20 and merge for WT and p107KO SC cluster. A line was drawn through a representative cell from merged WT confocal image to indicate relative intensity of RGB signals. The arrowheads point to areas of concurrent intensities in the images. Scale bar is 5μm. Hashed line is outline of myofiber.

Figure 4.22

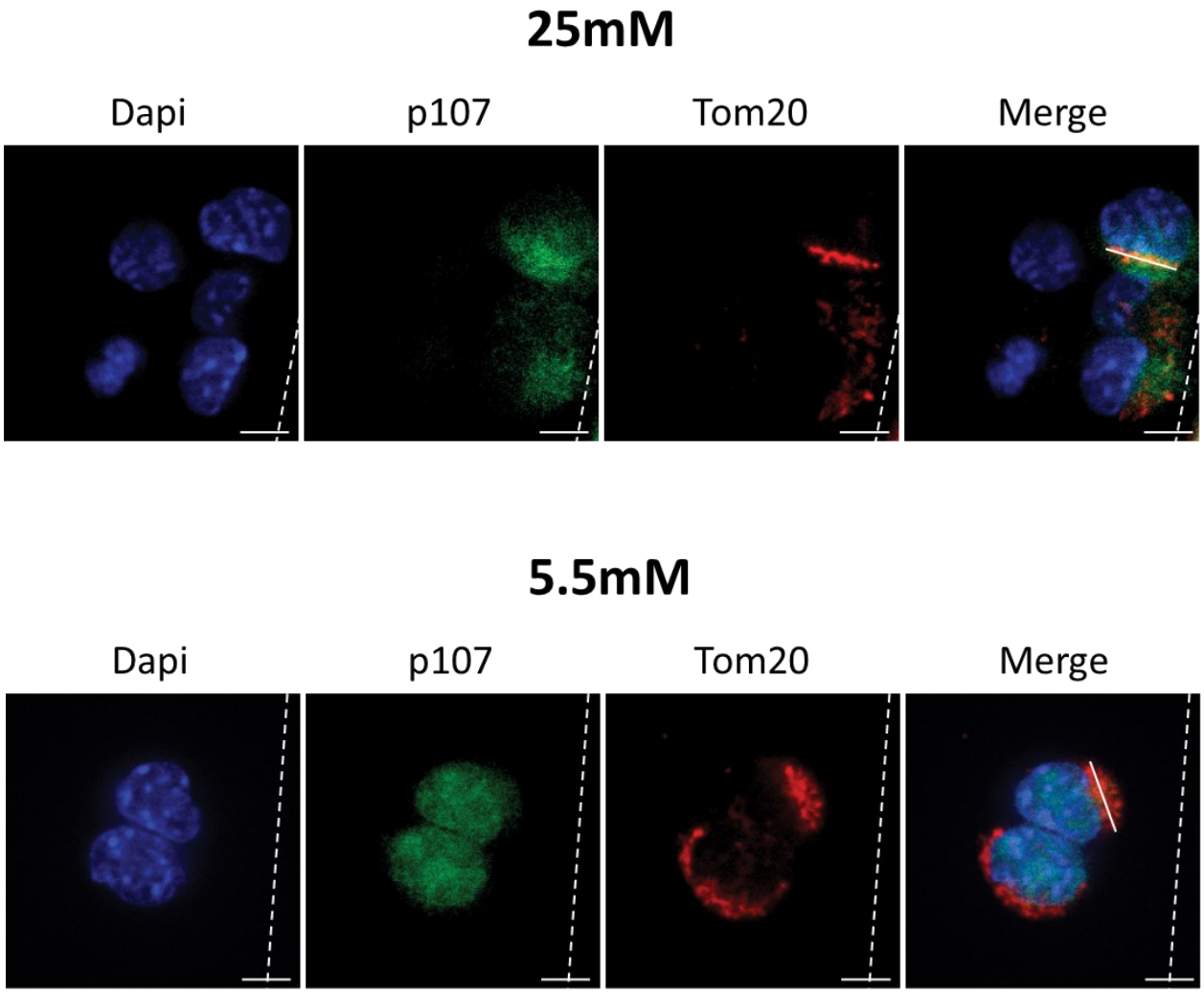

Figure 4.22. p107 mitochondrial localization is controlled by glucose levels. Representative confocal images of Dapi, p107, Tom20 and merge for myofibers cultured in 5.5mM and 25mM glucose. Scale bar is 5μm. Hashed line is outline of myofiber.

Figure 4.23

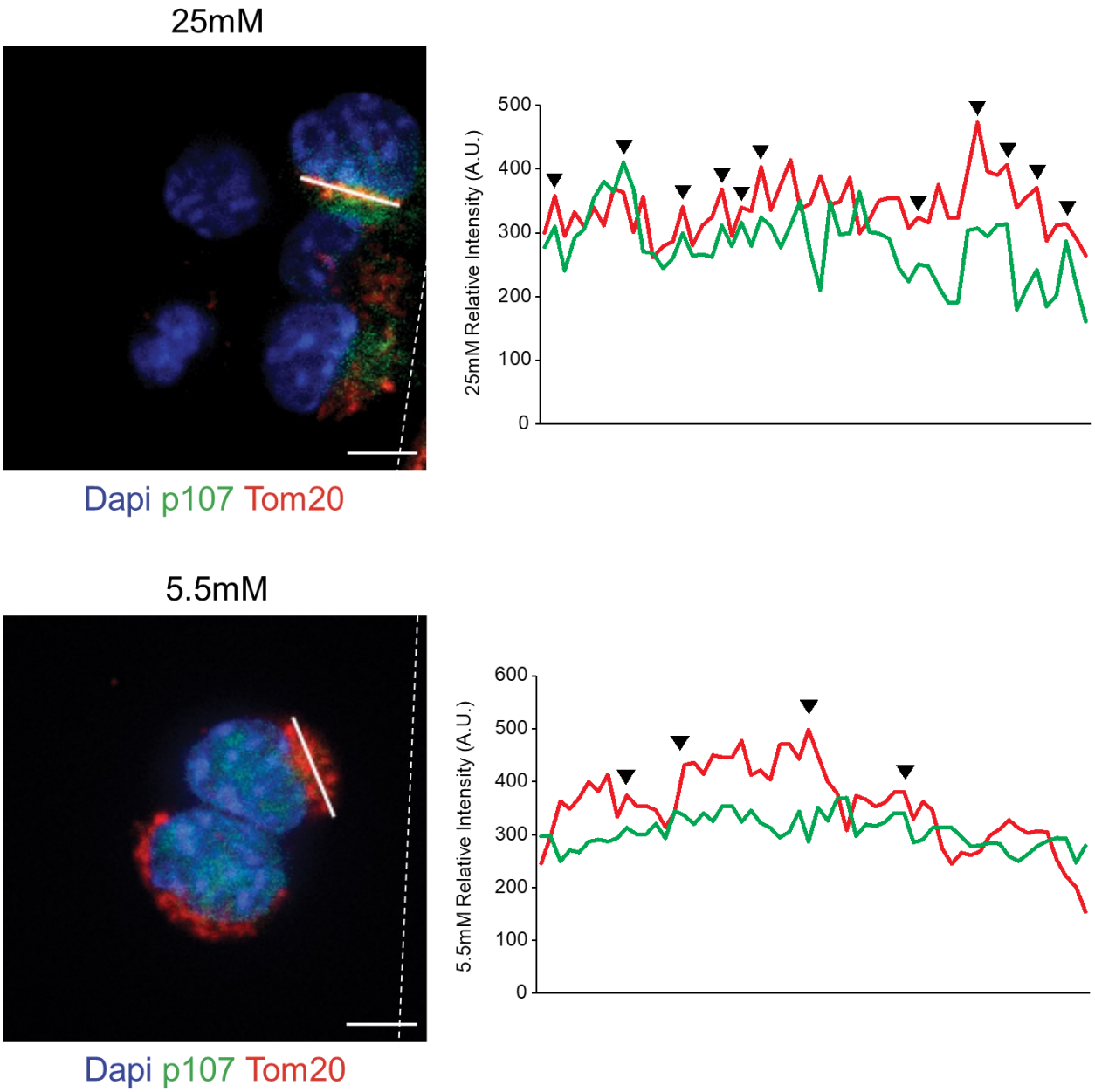

Figure 4.23. p107 mitochondrial localization in SCs is controlled by glucose concentrations. A line was drawn through a representative cell from merged confocal images for myofibers cultured in 5.5mM or 25mM glucose to indicate relative intensity of RGB signals. The arrowheads point to areas of concurrent intensities in the images. Scale bare is 5μm. Hashed line is outline of myofiber.

Figure 4.24

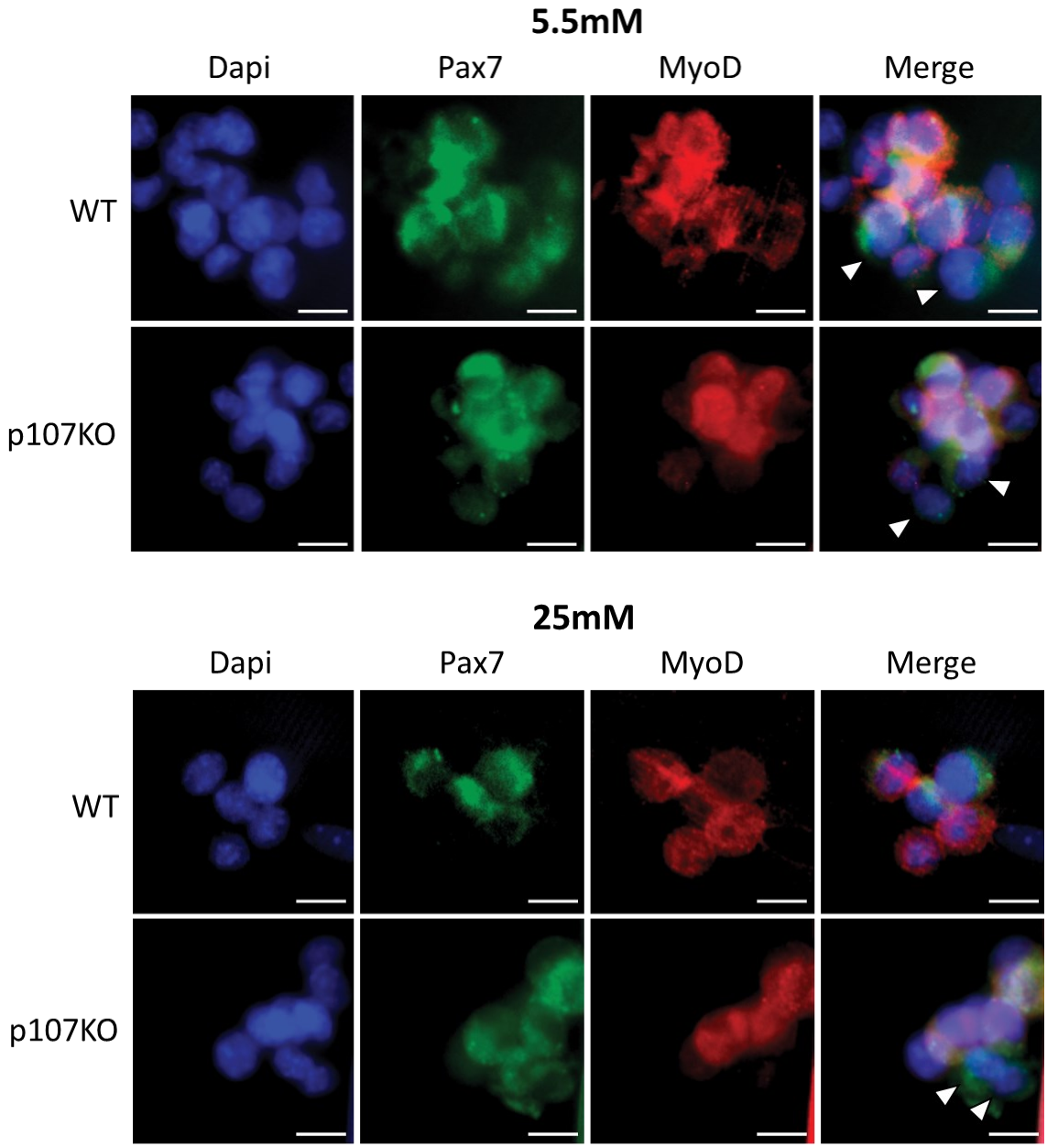

Figure 4.24. Mitochondrial p107 activity influences SC self-renewal. Representative immunohistochemistry for Dapi, Pax7, MyoD and merge of WT and p107KO myofibers cultured for 72 hours in 5.5mM and 25mM glucose. Arrows denote self-renewed SCs (Pax7+/MyoD-). Scale bar is 10μm. Hashed line is outline of myofiber.

Figure 4.25

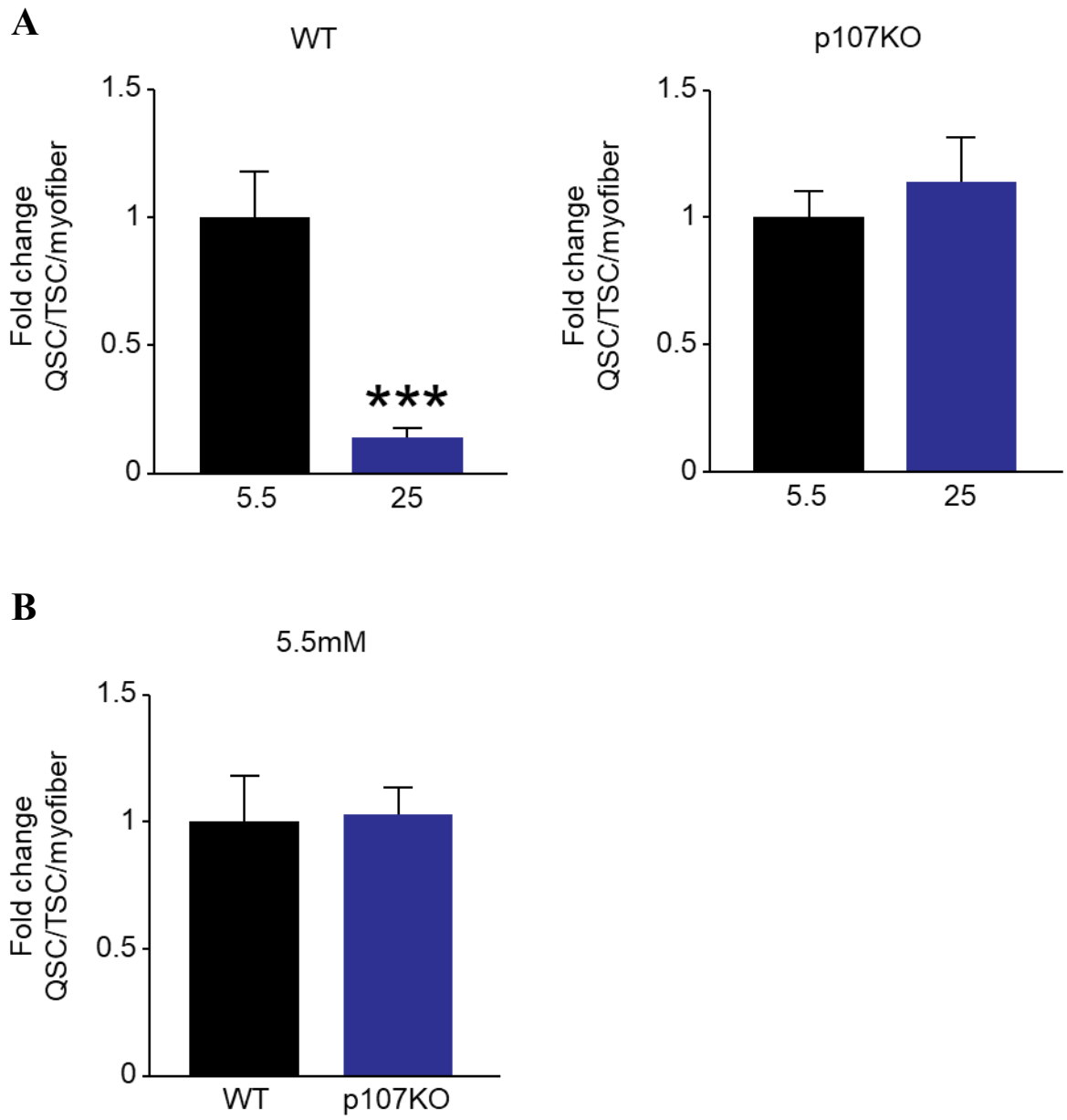

Figure 4.25. Mitochondrial p107 activity influences SC self-renewal. Graphical representations of fold change for the fraction of quiescent SCs (QSC) per total SCs (TSC) per myofiber for **(A)** WT and p107KO myofibers cultured with 5.5mM and 25mM glucose and **(B)** between WT and p107KO myofibers cultured with 5.5mM glucose. Data are presented as mean values +/- SD. n=5 mice for each WT and p107KO. Two-tailed unpaired Student T-test, ***p<0.0001.

Figure 4.26

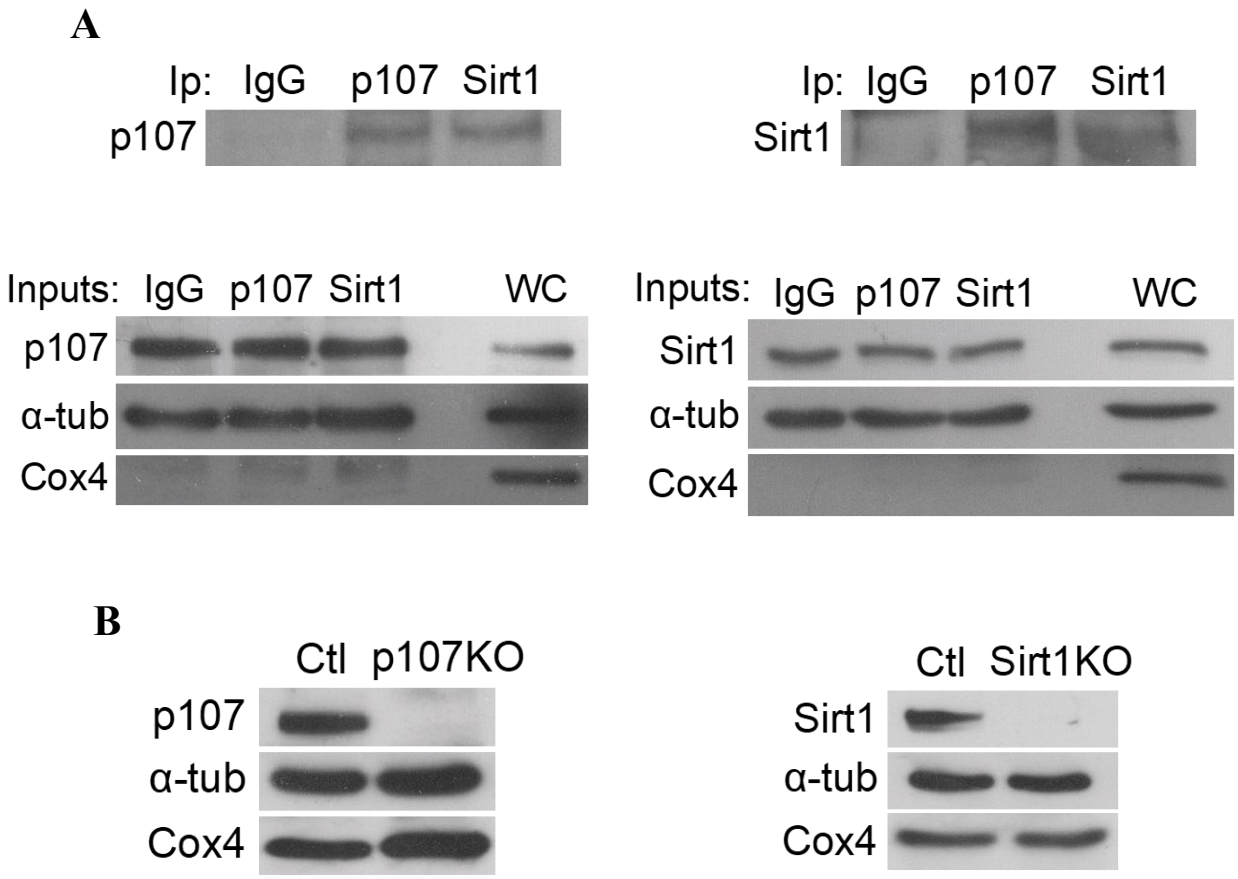

Figure 4.26. p107 interacts with Sirt1 in the cytoplasm. (A) Immunoprecipitation (IP)/Western blots for p107 and Sirt1 from cytoplasmic lysates of C2C12 cells and Ig, p107, Sirt1 IP/Westerns inputs ($1/10^{th}$) Western blotted for α-tubulin (α-tub) and Cox4 (WC is whole cell lysate). **(B)** Western blots of C2C12 control (Ctl), p107KO and Sirt1KO WC Western blotted for α-tub, Cox4 Sirt1 and p107. (Bhattacharya et al., 2021)

CHAPTER 5

DISCUSSION

In skeletal muscle, SC malfunction is commonly associated with the regenerative and functional decline observed during ageing (Almada & Wagers, 2016; W. Chen et al., 2020; Hwang & Brack, 2018). Thus, understanding SC fate decisions and the pathways that govern them may provide insight in combating the age-related decline of skeletal muscle. Our study is the first to reveal a novel role for p107, a retinoblastoma susceptibility protein family member, involvement in the SC self-renewal through a control of mitochondrial function. Notably, we found that in SCs p107 ablation results in enhanced SC self-renewal (**Fig. 4.17A and Fig. 4.17B**) and SC proliferation (**Fig. 4.10 and Fig. 4.11**) with no detriment to differentiation (**Fig. 4.17C**). Moreover, our findings indicate that p107 is the only Rb family member active in the mitochondria of activated SCs (**Fig. 4.3**) where it most likely interacts with E2f4 (**Fig. 4.5**). However, our data also indicates that p107 influences SC activation timing as p107 ablation was shown to delay SC activation (**Fig. 4.9**). We also found that p107 mitochondrial localization in SCs is regulated by the NAD^+/NADH ratio through changing glucose availability (**Fig. 4.22 and Fig. 4.23**). Indeed, increasing the NAD^+/NADH ratio reduced p107 mitochondrial localization to promote SC self-renewal (**Fig. 4.24 and Fig. 4.25**). We hypothesize that p107 mitochondrial localization regulated by the NAD^+/NADH ratio is controlled by Sirt1, as we show the two proteins interact in the cytoplasm of MPs (**Fig. 4.26**). Together, these data show that p107 regulates SC self-renewal, proliferation and quiescence through a mitochondrial function controlled by Sirt1 activity (**Fig.5.1)**.

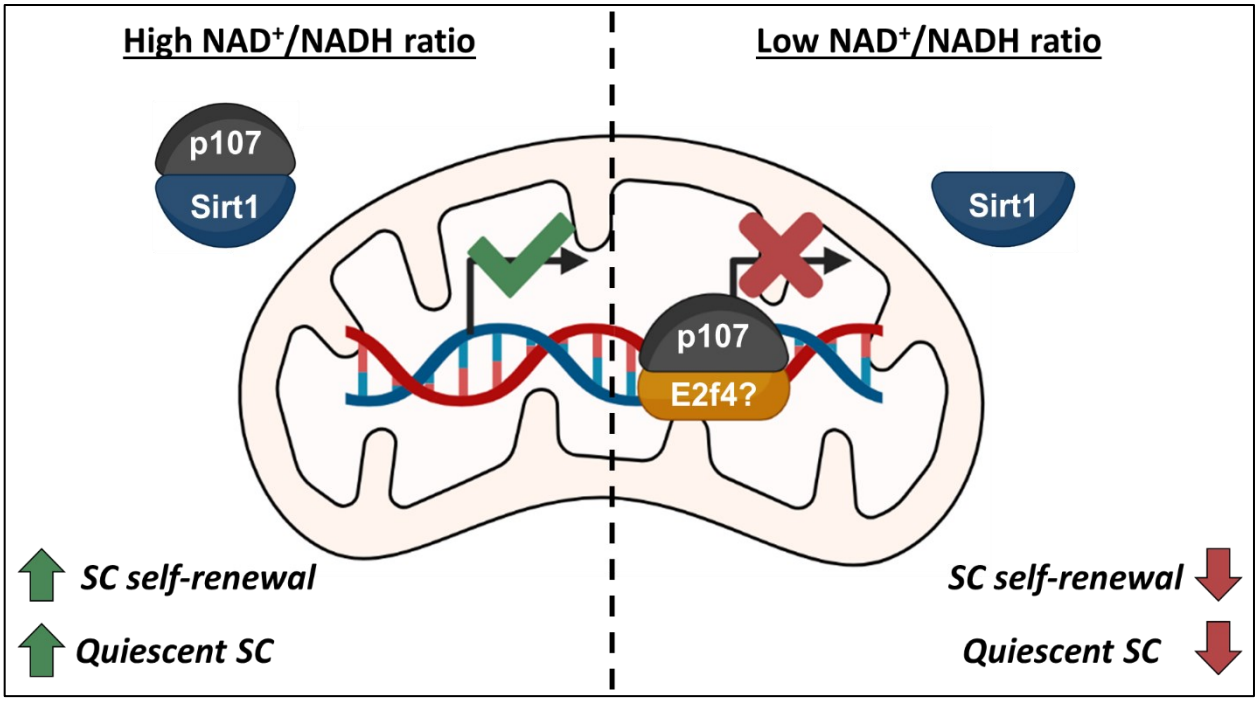

Figure 5.1: p107 controls SC self-renewal capacity through its mitochondrial function. In the presence of high NAD^+/NADH ratio, p107 interacts with Sirt1, which prevents its mitochondrial translocation. This allows for mitochondrial gene expression and enhanced OXPHOS capacity. The enhanced oxidative metabolism in SCs promotes self-renewal and results in the expansion of the quiescent SC pool. When the NAD^+/NADH ratio is reduced and Sirt1 is inactive, p107 localizes in the mitochondria of SCs. Here it represses mitochondrial gene expression and results in a diminished OXPHOS capacity. The reduction to oxidative metabolism results in decreased SC self-renewal and promotes SC activation. Figure created with BioRender.

Our findings highlight a role for p107 in controlling SC self-renewal through its mitochondrial localization. For other family members, a mitochondrial presence for p130 has not been published, but Rb has been found at the outer mitochondrial membrane and not in the matrix where p107 exerts its affect (Hilgendorf et al., 2013). Here, Rb is thought to promote mitochondrial mediated apoptosis through its interaction with BAX, the apoptosis regulator to induce permeabilization of the mitochondria (Hilgendorf et al., 2013). However, our findings show that Rb family mitochondrial presence in SCs and MPs is exclusive to p107, as Western blotting shows that Rb is not in the mitochondria of proliferating C2C12 MPs and p130 is not expressed (**Fig. 4.3**). Moreover, our findings show that a substantial proportion, approximately 28% of total p107

protein is present in the mitochondria of proliferating C2C12 MPs (**Fig. 4.1**). The high concentration of mitochondrial p107 suggests an important role that likely extends to SCs. At this time, it is unknown if this mitochondrial role is specific to muscle or other adult stem cells.

Currently, it is not fully understood how p107 is transported into the mitochondria due to the absence of a N-terminal mitochondrial targeting signal (MTS) (Wiedemann & Pfanner, 2017; Wirt & Sage, 2010). Normally proteins destined for the mitochondrial matrix contain an N-terminal MTS which facilitates the protein's interaction with the translocase of the outer membrane complex and translocase of the inner membrane complexes more commonly referred to as the mitochondrial import machinery (Wiedemann & Pfanner, 2017). However, there exists another pathway for mitochondrial protein import that recognizes internal hydrophobic amino acid domains sequences or acetylated regions (Pfanner et al., 2019; Wiedemann & Pfanner, 2017). Therefore, p107 mitochondrial import might be facilitated by a combination of internal MTS (iMTS) like sequences and post translational modifications such as acetylation or phosphorylation that are known to affect protein hydrophobicity (Garriga et al., 2004; Ree et al., 2018; Wirt & Sage, 2010). There is evidence to support this possibility as we found a high probability of an iMTS in p107 from amino acids 70-95 and 770-795 (**Fig. 4.2**) and p107 has evidence for post translational modifications. Indeed, p107 can be phosphorylated by cyclin E/Cdk2 and cyclin D/Cdk4. Cyclin E/cdk2 interaction was shown to be involved in p107 translocation from the cytoplasm to the nucleus, whereas phosphorylation at T369, S640, S964 and S975 by cyclin D/cdk4 causes p107 abrogation of E2f4 interaction (Garriga et al., 2004; Leng et al., 2002; Rodier et al., 2005).

Sirt1 a prominent deacetylase, interacts with p107 in the cytoplasm (**Fig. 4.26**) and this interaction has been shown to sequester p107 from mitochondrial localization, suggesting that

acetylation is essential for translocation (Bhattacharya et al., 2021) (**Fig. 4.22 and Fig. 4.23**). Intriguingly, an analysis of p107 with the Prediction of Acetylation on Internal Lysines (PAIL) prediction software reveals that p107 has several likely acetylation sites at K106, K156, K162 and K782, which are part of or in close proximity to the predicted iMTS that we found between amino acids 70-95 and 770-795 (**Fig. 5.2**) (**Fig. 4.2**) (Deng et al., 2016; Li et al., 2006). Thus, it is plausible that p107 acetylation status at these sites might affect iMTS recognition and p107 mitochondrial import. Other evidence for the importance of acetylation for import is from studies on highly homologous family member p130 that revealed its acetylation at K128 and K130 at its N-terminus (Schwarze et al., 2010). A BLAST search between p107 and p130 shows that K106 on p107 is strongly related to K130 on p130 (**Fig. 5.2**) (Altschul et al., 1997, 2005). It strongly suggests that K106 of p107 is acetylated and might be the Sirt1 target for deacetylation activity in the cytoplasm (**Fig. 4.26**). Thus, as acetylation is known to enhance hydrophobicity and effect protein conformation (Ree et al., 2018), the deacetylation of K106 by Sirt1 could reduce the availability of the iMTS like sequence observed between amino acids 70-95 and reduce the hydrophobicity of this region of p107. This could decrease p107 mitochondrial import by reducing interaction with the cytosolic chaperones heat shock protein 70 (Hsp70) and heat shock protein 90 (Hsp90) which recognize internal hydrophobic regions such as iMTS like sequences (Pfanner et al., 2019; Wiedemann & Pfanner, 2017).

Figure 5.2: Sequence homology of p107 and p130. A BLAST analysis of p107 and p130 reveals sequence homology of lysine (K) residue K106 at the N terminus of p107 with K130 of p130. Known p130 acetylation sites are highlighted in cyan and predicted acetylation sites of p107 are highlighted in green. Regions of high iMTS scores are highlighted in yellow. Known p107 phosphorylation sites are highlighted in pink. Note possible acetylation sites of p107 at K106, K156 and K162 are near the iMTS region from amino acids 70-95 and K782 is within the iMTS region between amino acids 770-795.

To verify the importance of iMTS and acetylation future work will need to generate mutations of p107 at its iMTS like sequences and putative acetylation sites and verify their significance for p107 mitochondrial import. If the iMTS sequences are required for p107 mitochondrial import, mutations in iMTS sequences would have reduced mitochondrial p107 localization. Moreover, cells expressing unmutated p107 could be compared with their mutated counterparts to determine if p107 interacts with the Hsp70 and Hsp90 the cytosolic chaperones. This could be done via immunoprecipitation/Western blot analysis of cytoplasmic lysates to determine if p107 interacts with the chaperones and if that interaction is dependent on the iMTS like sequences. Moreover, single point mutation of K106, K156, K162 and K782 for p107 by

replacing the lysine residue for alanine could also be conducted to test their importance to p107 mitochondrial localization. We would expect the cells expressing the mutated p107 would have enhanced p107 mitochondrial localization despite Sirt1 is activity. Additionally, mutation of the lysine residues in conjunction with mutation of the iMTS regions of p107 could be conducted to determine if p107 acetylation at those sites effects iMTS recognition. Overall, these experiments would provide evidence to establish a pathway through which p107 is imported into the mitochondria.

Mitochondrial gene expression is a very complex process that is poorly understood. The mitochondria have their own mechanism of gene transcription that relies on a combination of the transcription factors Tfam, Tfb2m and Polrmt (Farge & Falkenberg, 2019; Gustafsson et al., 2016). However, studies have shown that transcription factors and their respective co-transcriptional regulators that are active in the nucleus, can also function in mitochondria and interact with the mtDNA (Leigh-Brown et al., 2010). Until now, the E2f family of transcription factors has been shown to regulate mitochondrial activity through their interaction with nuclear genes involved in oxidative phosphorylation and the electron transport chain (Beshiri et al., 2012). More specifically, E2f4 is known to interact with the promotor for COX8, a nuclear gene that encods for a protein in the electron transport chain (Benevolenskaya & Frolov, 2015; Cam et al., 2004). However, we are the first to show that the nuclear transcription factor E2f4 is in the mitochondria of proliferating C2C12 MPs interacting at the mtDNA (**Fig. 4.4 and Fig. 4.5**). This adds E2f4 to the group of nuclear transcription factors which includes the T3 receptor p43, the tumor suppressor p53 and the estrogen receptor that are present in the mitochondria and interact with the mtDNA (Leigh-Brown et al., 2010). The interaction between p107 and E2f4 was shown to occur in the cytoplasm, but never assessed for in the mitochondria (Puri et al., 1998). To test its interaction between p107 and

E2f4 in the mitochondria, immunoprecipitation/ Western blot analysis of mitochondrial lysates should be performed. Additionally, an experiment measuring p107 mtDNA binding in a E2f4 knockdown via siRNA would help reveal if p107 mitochondrial binding partner is in fact E2f4. In this case we would expect p107 mtDNA binding to decrease in the presence of an E2f4 knockdown.

In our study we provide evidence that p107 functions to control SC self-renewal and activation timing. We propose that this phenotype is in response to a p107 mitochondrial role in SCs. Recently, our lab has shown that p107 mitochondrial activity results in decreased mitochondrial networking (fusion) and reduces mitochondrial OXPHOS (Bhattacharya et al., 2021). Intriguingly, mitochondrial activity has been implicated in the maintenance of SC quiescence and SC self-renewal (Baker et al., 2022; Hong et al., 2022). Studies have shown that enhanced mitochondrial fusion during quiescence via Opa1 activity promotes SC quiescence and Opa1 deficiency in proliferating SCs decreases self-renewal (Baker et al., 2022). Moreover, mitochondrial fission has been shown to promote SC activation and commitment while reducing self-renewal capacity (Baker et al., 2022; Hong et al., 2022). It is therefore possible that the delay to activation and enhanced SC self-renewal that is observed in the p107KO mice in our study (**Fig. 4.9 and Fig. 4.14 to 4.17**) can be explained by enhanced mitochondrial fusion that was shown in C2C12 cells (Bhattacharya et al., 2021). For SCs, this can be assessed by examining their mitochondrial network in WT and p107KO myofibers in a time course. We would expect to see enhanced mitochondrial fusion in the p107KO SCs compared to the WT counterparts. In addition, ROS signaling during quiescence has been shown to promote stem cell and SC activation (Baker et al., 2022; Khacho et al., 2016). As p107 is known to decrease mitochondrial efficiency (Bhattacharya et al., 2021), it would be beneficial to compare mitochondrial ROS levels of WT

and p107KO SCs. ROS levels can be determined with flow cytometry and the treatment of SCs or SC derived MPs with di hydrorhodamine 123, a mitochondrial ROS indicator which fluoresces upon oxidation from ROS (Cheng et al., 2018). A reduction to ROS levels in p107KO SCs in tandem with increased mitochondrial fusion would explain the delay in SC activation and enhanced self-renewal that we observe and support the published findings regarding mitochondrial fusion and SC quiescence (Baker et al., 2022; Hong et al., 2022).

It is important to note that p107 is not expressed in quiescent SCs and is only found after MyoD is expressed (**Fig. 4.6 and Fig. 4.8**). Therefore, it is unclear as to how p107 influences SC quiescence. It is possible that the absence of p107 effects the mitochondrial dynamics of quiescent SCs and is responsible for the delay in activation, as a consequence of the phenotype of the new stem cell progeny. This suggests the existence of a sub populations of SCs. The SCs that have not had the chance to observe p107 expression would not experience the same changes in mitochondrial activity and networking as their previously activated counterparts. This would cause the population of SCs that have never activated to experience conventional activation times compared to their previously activated counterpart. There is evidence for SC subpopulations in which the progeny can have different characteristics then the parent cell (Kuang et al., 2007; Rocheteau et al., 2012). One such example is the expression of Myf5. SCs that have never expressed Myf5 are considered to be a less committed population that can produce progeny that are Myf5 positive or negative (Kuang et al., 2007). On the other hand, SCs that had expressed Myf5 are characterized for their ability to more readily contribute to myogenesis (Kuang et al., 2007). In the same vein, SCs that express higher levels of Pax7 have been shown to be able to produce asymmetric progeny where one daughter cell maintains higher levels of quiescence marker Pax7 and the other daughter cell expressing differentiation markers such as myogenin

(Rocheteau et al., 2012). Future experiments will have to test the Myf5 expression pattern and Pax7 levels to explain the activation phenotype in p107KO mice.

In addition to mitochondrial networking, SC function has been linked to the availability of acetyl-coA the cellular acetylation status. In SCs, acetyl-coA has been shown to promote myogenic progression by influencing Pax7 and histone acetylation status (Massenet et al., 2021; Sincennes et al., 2021). Moreover, reduced acetyl-coA mediated Pax7 acetylation has been shown to enhance SC self-renewal (Sincennes et al., 2021). Thus, controlling the levels of free acetyl-coA is important to SC fate determination. In cells the amount of free acetyl-coA is influenced by the level of OXPHOS occurring, in this case when OXPHOS demand is high the available acetyl-coA is consumed in the TCA cycle to generate the reducing agents for the ETC (Klimova et al., 2019; Yucel et al., 2019). For mitochondrial acetyl-coA to function in the cytoplasm and nucleus it must first be exported from the mitochondria as citrate and converted back into acetyl-coA by ATP-citrate lyase (Zhao et al., 2016). Therefore, enhanced OXPHOS can reduce the level of available cytoplasmic and nuclear acetyl-coA by preferentially driving acetyl-coA into the TCA cycle to support the ETC. Intriguingly, p107KO MPs have been shown to have elevated levels of OXPHOS compared to their WT counterparts (Bhattacharya et al., 2021). It is possible that SCs have the same relationship. Thus, we propose that p107 through its regulation of mitochondrial OXPHOS capacity is indirectly controlling mitochondrial citrate export to the cytoplasm and contributing to the free acetyl-coA for acetylation that would explain the enhanced SC self-renewal observed in p107KO muscle and myofibers (**Fig. 4.12 to Fig. 4.17**). To confirm that p107 controls cytoplasmic acetyl-coA levels it is important to compare the cytoplasmic citrate levels of WT and p107KO SCs with a citrate assay kit. Due to the enhanced OXPHOS likely occurring in the p107KO SCs, we would expect to see reduced levels of cytoplasmic citrate compared to their WT counterparts. This

would suggest that due to the high oxidative demand in the absence of mitochondrial p107, acetyl-coA is preferentially consumed by the TCA as opposed to being exported to the cytoplasm as citrate to be used for protein and histone acetylation.

We hypothesize that the NAD^+/NADH ratio regulates SC activity through a p107 mechanism. The NAD^+/NADH ratio acts as a measure of the relative contribution of mitochondrial OXPHOS to ATP generation (Cantó et al., 2015). A high ratio indicative of high mitochondrial contribution to ATP generation and increased free NAD^+ translates to increased sirtuin activity (Anderson et al., 2017; Lunt & vander Heiden, 2011). Increased NAD^+ and thereby Sirt1 activity would sequester p107 in the cytoplasm (**Fig. 4.22 and Fig. 4.23**) (Bhattacharya et al., 2021). Studies on Sirt1 have shown that its activity and NAD^+ levels are both raised during SC quiescence and its activity when stimulated via caloric restriction promotes SC self-renewal (Cerletti et al., 2012; Ryall et al., 2015). Also, myogenesis and SC differentiation have been observed to be inhibited by increased Sirt1 deacetylase activity, suggesting that Sirt1 is promoting self-renewal (Fulco et al., 2003, 2008). Conversely, the ablation of Sirt1 activity via a SC specific Sirt1 deletion has been shown to delay SC activation and the overexpression of Sirt1 promoted muscle regeneration in elderly mice (Myers et al., 2019; Tang & Rando, 2014). These findings suggest that Sirt1 is required for SC activation and muscle regeneration. The opposing role of Sirt1 might be due to differences in the timepoints considered to evaluate SC activation (Ryall et al., 2015; Tang & Rando, 2014). Additionally, the use of a whole body versus SC specific Sirt1KO model might explain the differences in Sirt1 activity (Myers et al., 2019; Ryall et al., 2015; Tang & Rando, 2014).

Till now the mechanism for how Sirt1 activity regulates SC self-renewal was unknown, but our findings suggest that it is through its control over p107 mitochondrial localization. We

show that p107 interacts with Sirt1 in the cytoplasm (**Fig. 4.26**) and that manipulating the NAD^+/NADH ratio to increase available NAD^+ and promote Sirt1 activity, p107 mitochondrial localization is reduced and SC self-renewal is enhanced (**Fig. 4.22 and Fig. 4.23**). Similar to our findings, Furuichi et al had observed an increase to SC self-renewal when culturing myofibers in medium with lower glucose concentrations (Furuichi et al., 2021). They show that SC self-renewal is inversely correlated with glucose concentration (Furuichi et al., 2021). Intriguingly, manipulation of the NAD^+/NADH ratio in a glucose concentration independent manner has been shown to affect p107 mitochondrial localization in a similar manner (Bhattacharya et al., 2021). In SCs we show that a manipulation of the NAD^+/NADH ratio in a glucose dependent manner results in enhanced SC self-renewal when the NAD^+/NADH ratio is high and cellular glucose concentrations are lower (**Fig. 4.24 and Fig. 4.25**). It is important to note that the other sirtuins such as Sirt2 have been implicated in increasing SC self-renewal by specific deacetylation of Pax7 (Sincennes et al., 2021). Therefore, it is possible that the enhanced SC self-renewal on ex vivo myofibers in low glucose is in part due to Sirt2 activity.

Others have shown that increased SC self-renewal comes at the cost of differentiation (Abou-Khalil et al., 2009; Sincennes et al., 2021; Wen et al., 2012). For example, increased notch signaling was shown to enhance SC self-renewal but reduce the regenerative capacity of muscle (Wen et al., 2012). Similarly, increasing autocrine signaling through angiopoietin 1 and its receptor Tie-2 reduced SC differentiation but increased the number of quiescent SCs (Abou-Khalil et al., 2009). Moreover, Sincennes et al, reveal that ablation of Pax7 acetylation via Crispr/Cas9 promotes SC self-renewal and reduced commitment while promoting the generation of oxidative type IIA myofibers (Sincennes et al., 2021). Though we had significantly more SCs in the p107KO phenotype it did not affect the regenerative capacity. In vivo, we found that when we compared

WT and p107KO TA muscles after recovery to their contralateral uninjured TAs there was no difference in muscle cross sectional area (**Fig. 4.17**). Moreover, we corroborated our findings in vitro by assessing the myofusion index of WT and p107KO MPs (that is SCs that had been derived from expanding clusters on myofibers), which showed no significant difference between the two groups (**Fig. 4.18**). These findings indicate that p107 does not affect SC differentiation. This might be due to the enhanced proliferation that is observed in the p107KO SCs (**Fig. 4.10 and Fig. 4.11**). Under normal conditions, SCs are more than capable of generating sufficient progeny for muscle repair (Snow, 1978). In our model there is a substantial increase to SC proliferation that occurs in the p107KO SCs at 42 and 72 hours of culture (**Fig. 4.10 and Fig. 4.11**). It is then possible that despite there being a decline to the proportion of differentiating SCs at 72 hours (**Fig 4.17C**), the p107KO muscle is able to generate a significant number of progeny for regeneration.

A short coming of our study is the use of a single injury/regeneration treatment with CTX, that was not able to gauge the possibility that there might be changes in muscle regenerative capacity over subsequent regenerative episodes. The use of a triple injury model where the muscle is allowed to fully recover between three injections of CTX would allow for the testing of the regenerative capacity after repetitive injury. Assuming there are no differences to the regenerative capacity for p107KO mice, we would expect to see no major difference to cross sectional area between the uninjured and contralateral TA after multiple regeneration episodes.

The TA is commonly described as a fast twitch muscle, being composed of mainly large glycolytic type IIB fibers, as well as some oxidative type IIA fibers (Schiaffino & Reggiani, 2011). However, p107 deficient mice have been shown to have higher levels of oxidative type I and type IIA muscle fibers with enhanced oxidative metabolism (Scimè et al., 2010). Moreover, the differentiation of p107KO MPs has been shown to result in the formation of oxidative myotubes

(Scimè et al., 2010). However, we did not gauge the composition of the muscle to see if p107 has any effect on the formation of the various fiber types. In future experiments the use of subsequent regeneration cycles would demonstrate that the injured/ regenerated p107KO muscle would be composed of significantly more many oxidative fibers over its uninjured TA and more than the WT control.

To investigate whether the mitochondrial role of p107 is responsible for the formation of oxidative myotubes in vitro, it would be beneficial to differentiate MPs derived from expanding SC clusters on myofibers cultured in 25mM glucose and 5.5mM glucose respectively. Fiber type content could be determined via Western blot analysis for the various myosin heavy chain isoforms. If the formation of oxidative myotubes is reliant on p107 mitochondrial activity, we would expect to see enhanced type IIA myosin heavy chain protein expression in the MPs cultured in 25mM glucose compared to 5.5mM glucose. These experiments would help further unravel the role of p107 in SC fate determination by ascertaining whether p107 activity influences fiber composition and not only regenerative capacity.

In ageing and neuromuscular disorders such as muscular dystrophies there is a malfunction to SC proliferation which leads to a diminished population of SCs required for muscle regeneration (N. C. Chang et al., 2018; Cosgrove et al., 2014; Hwang & Brack, 2018). Moreover, there is a decline to SC self-renewal capacity and thereby the quiescent SC population (Chakkalakal et al., 2012). Mitochondrial dysfunction has been implicated in both ageing and muscular dystrophies such as Duchenne muscular dystrophy (Chang et al., 2016; H. Zhang et al., 2016). As p107 has been shown to reduce mitochondrial function (Bhattacharya et al., 2021) and we show that sequestration of p107 from the mitochondria enhances self-renewal and expands the quiescent SC population, it would be beneficial to explore the p107KO in the context of aged muscle or

Duchenne muscular dystrophy models. This could be accomplished by continuing our study with aged p107KO mice or by crossing p107KO mice with mdx mice to generate p107KO mice in the context of Duchenne muscular dystrophy.

In summary, our findings establish that the transcriptional co-repressor, p107, is an important regulator of SC fate decisions (**Fig. 5.1**). Our study has unraveled a novel role of p107 in the context of its mitochondrial activity within SCs. Crucially, p107 functions by sensing NAD^+/NADH to regulate SC self-renewal capacity. We show that p107 interacts with Sirt1 in the cytoplasm and propose that this interaction influenced by the NAD^+/NADH ratio allows for the sequestration of p107 from the mitochondria, which results in enhanced SC self-renewal. Importantly, we show that the increase to SC self-renewal does not come at the detriment of muscle regeneration. These novel findings establish p107 as a regulator of SC self-renewal and potentially implicate p107 as a target to combat age and muscle disease related SC decline.

CHAPTER 6

REFERENCES

Abdel Khalek, W., Cortade, F., Ollendorff, V., Lapasset, L., Tintignac, L., Chabi, B., & Wrutniak-Cabello, C. (2014). SIRT3, a Mitochondrial NAD+-Dependent Deacetylase, Is Involved in the Regulation of Myoblast Differentiation. *PLoS ONE*, *9*(12), e114388. https://doi.org/10.1371/journal.pone.0114388

Abou-Khalil, R., le Grand, F., & Chazaud, B. (2013). *Human and Murine Skeletal Muscle Reserve Cells* (pp. 165–177). https://doi.org/10.1007/978-1-62703-508-8_14

Abou-Khalil, R., le Grand, F., Pallafacchina, G., Valable, S., Authier, F.-J., Rudnicki, M. A., Gherardi, R. K., Germain, S., Chretien, F., Sotiropoulos, A., Lafuste, P., Montarras, D., & Chazaud, B. (2009). Autocrine and Paracrine Angiopoietin 1/Tie-2 Signaling Promotes Muscle Satellite Cell Self-Renewal. *Cell Stem Cell*, *5*(3), 298–309. https://doi.org/10.1016/j.stem.2009.06.001

Almada, A. E., & Wagers, A. J. (2016). Molecular circuitry of stem cell fate in skeletal muscle regeneration, ageing and disease. In *Nature Reviews Molecular Cell Biology* (Vol. 17, Issue 5, pp. 267–279). Nature Publishing Group. https://doi.org/10.1038/nrm.2016.7

Altschul, S. F., Madden, T. L., Schäffer, A. A., Zhang, J., Zhang, Z., Miller, W., & Lipman, D. J. (1997). Gapped BLAST and PSI-BLAST: a new generation of protein database search programs. *Nucleic Acids Research*, *25*(17), 3389–3402. https://doi.org/10.1093/nar/25.17.3389

Altschul, S. F., Wootton, J. C., Gertz, E. M., Agarwala, R., Morgulis, A., Schäffer, A. A., & Yu, Y.-K. (2005). Protein database searches using compositionally adjusted substitution matrices. *The FEBS Journal*, *272*(20), 5101–5109. https://doi.org/10.1111/j.1742-4658.2005.04945.x

Anderson, K. A., Madsen, A. S., Olsen, C. A., & Hirschey, M. D. (2017). Metabolic control by sirtuins and other enzymes that sense NAD+, NADH, or their ratio. *Biochimica et Biophysica Acta. Bioenergetics*, *1858*(12), 991–998. https://doi.org/10.1016/j.bbabio.2017.09.005

Backes, S., Hess, S., Boos, F., Woellhaf, M. W., Gödel, S., Jung, M., Mühlhaus, T., & Herrmann, J. M. (2018). Tom70 enhances mitochondrial preprotein import efficiency by binding to internal targeting sequences. *The Journal of Cell Biology*, *217*(4), 1369–1382. https://doi.org/10.1083/jcb.201708044

Baker, N., Wade, S., Triolo, M., Girgis, J., Chwastek, D., Larrigan, S., Feige, P., Fujita, R., Crist, C., Rudnicki, M. A., Burelle, Y., & Khacho, M. (2022). The mitochondrial protein OPA1 regulates the quiescent state of adult muscle stem cells. *Cell Stem Cell*, *29*(9), 1315-1332.e9. https://doi.org/10.1016/j.stem.2022.07.010

Beijersbergen, R. L., Carlée, L., Kerkhoven, R. M., & Bernards, R. (1995). Regulation of the retinoblastoma protein-related p107 by G1 cyclin complexes. *Genes & Development*, *9*(11), 1340–1353. https://doi.org/10.1101/gad.9.11.1340

Benevolenskaya, E. v, & Frolov, M. v. (2015). Emerging links between E2F control and mitochondrial function. *Cancer Research*, *75*(4), 619–623. https://doi.org/10.1158/0008-5472.CAN-14-2173

Beshiri, M. L., Holmes, K. B., Richter, W. F., Hess, S., Islam, A. B. M. M. K., Yan, Q., Plante, L., Litovchick, L., Gévry, N., Lopez-Bigas, N., Kaelin, W. G., & Benevolenskaya, E. v. (2012). Coordinated repression of cell cycle genes by KDM5A and E2F4 during differentiation. *Proceedings of the National Academy of Sciences of the United States of America*, *109*(45), 18499–18504. https://doi.org/10.1073/pnas.1216724109

Bhattacharya, D., & Scimè, A. (2020). Mitochondrial Function in Muscle Stem Cell Fates. In *Frontiers in Cell and Developmental Biology* (Vol. 8). Frontiers Media S.A. https://doi.org/10.3389/fcell.2020.00480

Bhattacharya, D., Shah, V., Oresajo, O., & Scimè, A. (2021). p107 mediated mitochondrial function controls muscle stem cell proliferative fates. *Nature Communications*, *12*(1), 5977. https://doi.org/10.1038/s41467-021-26176-0

Boutant, M., & Cantó, C. (2014). SIRT1 metabolic actions: Integrating recent advances from mouse models. *Molecular Metabolism*, *3*(1), 5–18. https://doi.org/10.1016/j.molmet.2013.10.006

Bustin, S. A., Benes, V., Garson, J. A., Hellemans, J., Huggett, J., Kubista, M., Mueller, R., Nolan, T., Pfaffl, M. W., Shipley, G. L., Vandesompele, J., & Wittwer, C. T. (2009). The MIQE guidelines: minimum information for publication of quantitative real-time PCR experiments. *Clinical Chemistry*, *55*(4), 611–622. https://doi.org/10.1373/clinchem.2008.112797

Cam, H., Balciunaite, E., Blais, A., Spektor, A., Scarpulla, R. C., Young, R., Kluger, Y., & Dynlacht, B. D. (2004). A Common Set of Gene Regulatory Networks Links Metabolism and Growth Inhibition. *Molecular Cell*, *16*(3), 399–411. https://doi.org/10.1016/j.molcel.2004.09.037

Cantó, C., Houtkooper, R. H., Pirinen, E., Youn, D. Y., Oosterveer, M. H., Cen, Y., Fernandez-Marcos, P. J., Yamamoto, H., Andreux, P. A., Cettour-Rose, P., Gademann, K., Rinsch, C., Schoonjans, K., Sauve, A. A., & Auwerx, J. (2012). The NAD(+) precursor nicotinamide riboside enhances oxidative metabolism and protects against high-fat diet-induced obesity. *Cell Metabolism*, *15*(6), 838–847. https://doi.org/10.1016/j.cmet.2012.04.022

Cantó, C., Menzies, K. J., & Auwerx, J. (2015). NAD(+) Metabolism and the Control of Energy Homeostasis: A Balancing Act between Mitochondria and the Nucleus. *Cell Metabolism*, *22*(1), 31–53. https://doi.org/10.1016/j.cmet.2015.05.023

Carelli, V., & Chan, D. C. (2014). Mitochondrial DNA: impacting central and peripheral nervous systems. *Neuron*, *84*(6), 1126–1142. https://doi.org/10.1016/j.neuron.2014.11.022

Cerletti, M., Jang, Y. C., Finley, L. W. S., Haigis, M. C., & Wagers, A. J. (2012). Short-term calorie restriction enhances skeletal muscle stem cell function. *Cell Stem Cell*, *10*(5), 515–519. https://doi.org/10.1016/j.stem.2012.04.002

Cerutti, R., Pirinen, E., Lamperti, C., Marchet, S., Sauve, A. A., Li, W., Leoni, V., Schon, E. A., Dantzer, F., Auwerx, J., Viscomi, C., & Zeviani, M. (2014). NAD+-Dependent Activation of Sirt1 Corrects the Phenotype in a Mouse Model of Mitochondrial Disease. *Cell Metabolism*, *19*(6), 1042–1049. https://doi.org/10.1016/j.cmet.2014.04.001

Chakkalakal, J. v, Jones, K. M., Basson, M. A., & Brack, A. S. (2012). The aged niche disrupts muscle stem cell quiescence. *Nature*, *490*(7420), 355–360. https://doi.org/10.1038/nature11438

Chandel, N. S. (2018). Mitochondria: back to the future. *Nature Reviews Molecular Cell Biology*, *19*(2), 76. https://doi.org/10.1038/nrm.2017.133

Chang, H.-C., & Guarente, L. (2014). SIRT1 and other sirtuins in metabolism. *Trends in Endocrinology and Metabolism: TEM*, *25*(3), 138–145. https://doi.org/10.1016/j.tem.2013.12.001

Chang, N. C., Chevalier, F. P., & Rudnicki, M. A. (2016). Satellite Cells in Muscular Dystrophy - Lost in Polarity. *Trends in Molecular Medicine*, *22*(6), 479–496. https://doi.org/10.1016/j.molmed.2016.04.002

Chang, N. C., Sincennes, M.-C., Chevalier, F. P., Brun, C. E., Lacaria, M., Segalés, J., Muñoz-Cánoves, P., Ming, H., & Rudnicki, M. A. (2018). The Dystrophin Glycoprotein Complex Regulates the Epigenetic Activation of Muscle Stem Cell Commitment. *Cell Stem Cell*, *22*(5), 755-768.e6. https://doi.org/10.1016/j.stem.2018.03.022

Chen, C.-R., Kang, Y., Siegel, P. M., & Massagué, J. (2002). E2F4/5 and p107 as Smad Cofactors Linking the TGFβ Receptor to c-myc Repression. *Cell*, *110*(1), 19–32. https://doi.org/10.1016/S0092-8674(02)00801-2

Chen, D., Livne-bar, I., Vanderluit, J. L., Slack, R. S., Agochiya, M., & Bremner, R. (2004). Cell-specific effects of RB or RB/p107 loss on retinal development implicate an intrinsically death-resistant cell-of-origin in retinoblastoma. *Cancer Cell*, *5*(6), 539–551. https://doi.org/10.1016/j.ccr.2004.05.025

Chen, W., Datzkiw, D., & Rudnicki, M. A. (2020). Satellite cells in ageing: use it or lose it. *Open Biology*, *10*(5), 200048. https://doi.org/10.1098/rsob.200048

Cheng, G., Zielonka, M., Dranka, B., Kumar, S. N., Myers, C. R., Bennett, B., Garces, A. M., Dias Duarte Machado, L. G., Thiebaut, D., Ouari, O., Hardy, M., Zielonka, J., & Kalyanaraman, B. (2018). Detection of mitochondria-generated reactive oxygen species in

cells using multiple probes and methods: Potentials, pitfalls, and the future. *The Journal of Biological Chemistry*, *293*(26), 10363–10380. https://doi.org/10.1074/jbc.RA118.003044

Collu-Marchese, M., Shuen, M., Pauly, M., Saleem, A., & Hood, D. A. (2015). The regulation of mitochondrial transcription factor A (Tfam) expression during skeletal muscle cell differentiation. *Bioscience Reports*, *35*(3). https://doi.org/10.1042/BSR20150073

Cosgrove, B. D., Gilbert, P. M., Porpiglia, E., Mourkioti, F., Lee, S. P., Corbel, S. Y., Llewellyn, M. E., Delp, S. L., & Blau, H. M. (2014). Rejuvenation of the muscle stem cell population restores strength to injured aged muscles. *Nature Medicine*, *20*(3), 255–264. https://doi.org/10.1038/nm.3464

Costa-Machado, L. F., & Fernandez-Marcos, P. J. (2019). The sirtuin family in cancer. *Cell Cycle*, *18*(18), 2164–2196. https://doi.org/10.1080/15384101.2019.1634953

Crist, C. G., Montarras, D., & Buckingham, M. (2012). Muscle satellite cells are primed for myogenesis but maintain quiescence with sequestration of Myf5 mRNA targeted by microRNA-31 in mRNP granules. *Cell Stem Cell*, *11*(1), 118–126. https://doi.org/10.1016/j.stem.2012.03.011

de Morrée, A., van Velthoven, C. T. J., Gan, Q., Salvi, J. S., Klein, J. D. D., Akimenko, I., Quarta, M., Biressi, S., & Rando, T. A. (2017). Staufen1 inhibits MyoD translation to actively maintain muscle stem cell quiescence. *Proceedings of the National Academy of Sciences*, *114*(43). https://doi.org/10.1073/pnas.1708725114

de Sousa, M., Porras, D. P., Perry, C. G. R., Seale, P., & Scimè, A. (2014). p107 is a crucial regulator for determining the adipocyte lineage fate choices of stem cells. *Stem Cells (Dayton, Ohio)*, *32*(5), 1323–1336. https://doi.org/10.1002/stem.1637

DeBerardinis, R. J., Lum, J. J., Hatzivassiliou, G., & Thompson, C. B. (2008). The biology of cancer: metabolic reprogramming fuels cell growth and proliferation. *Cell Metabolism*, *7*(1), 11–20. https://doi.org/10.1016/j.cmet.2007.10.002

Deng, W., Wang, C., Zhang, Y., Xu, Y., Zhang, S., Liu, Z., & Xue, Y. (2016). GPS-PAIL: prediction of lysine acetyltransferase-specific modification sites from protein sequences. *Scientific Reports*, *6*(1), 39787. https://doi.org/10.1038/srep39787

Díaz-Vegas, A., Eisner, V., & Jaimovich, E. (2019). Skeletal muscle excitation-metabolism coupling. *Archives of Biochemistry and Biophysics*, *664*, 89–94. https://doi.org/10.1016/j.abb.2019.01.037

D'Souza, A. R., & Minczuk, M. (2018). Mitochondrial transcription and translation: overview. *Essays in Biochemistry*, *62*(3), 309–320. https://doi.org/10.1042/EBC20170102

Dumont, N. A., Bentzinger, C. F., Sincennes, M.-C., & Rudnicki, M. A. (2015). Satellite Cells and Skeletal Muscle Regeneration. *Comprehensive Physiology*, *5*(3), 1027–1059. https://doi.org/10.1002/cphy.c140068

Dumont, N. A., Wang, Y. X., von Maltzahn, J., Pasut, A., Bentzinger, C. F., Brun, C. E., & Rudnicki, M. A. (2015). Dystrophin expression in muscle stem cells regulates their polarity and asymmetric division. *Nature Medicine*, *21*(12), 1455–1463. https://doi.org/10.1038/nm.3990

Eales, K. L., Hollinshead, K. E. R., & Tennant, D. A. (2016). Hypoxia and metabolic adaptation of cancer cells. *Oncogenesis*, *5*, e190. https://doi.org/10.1038/oncsis.2015.50

Emanuelsson, O., Brunak, S., von Heijne, G., & Nielsen, H. (2007). Locating proteins in the cell using TargetP, SignalP and related tools. *Nature Protocols*, *2*(4), 953–971. https://doi.org/10.1038/nprot.2007.131

Farge, G., & Falkenberg, M. (2019). Organization of DNA in Mammalian Mitochondria. *International Journal of Molecular Sciences*, *20*(11). https://doi.org/10.3390/ijms20112770

Feige, P., Brun, C. E., Ritso, M., & Rudnicki, M. A. (2018). Orienting Muscle Stem Cells for Regeneration in Homeostasis, Aging, and Disease. *Cell Stem Cell*, *23*(5), 653–664. https://doi.org/10.1016/j.stem.2018.10.006

Ferecatu, I., le Floch, N., Bergeaud, M., Rodríguez-Enfedaque, A., Rincheval, V., Oliver, L., Vallette, F. M., Mignotte, B., & Vayssière, J.-L. (2009). Evidence for a mitochondrial localization of the retinoblastoma protein. *BMC Cell Biology*, *10*(1), 50. https://doi.org/10.1186/1471-2121-10-50

Fischer, M., & Müller, G. A. (2017). Cell cycle transcription control: DREAM/MuvB and RB-E2F complexes. *Critical Reviews in Biochemistry and Molecular Biology*, *52*(6), 638–662. https://doi.org/10.1080/10409238.2017.1360836

Folmes, C. D. L., Dzeja, P. P., Nelson, T. J., & Terzic, A. (2012). Metabolic Plasticity in Stem Cell Homeostasis and Differentiation. *Cell Stem Cell*, *11*(5), 596–606. https://doi.org/10.1016/j.stem.2012.10.002

Frederick, D. W., Loro, E., Liu, L., Davila, A., Chellappa, K., Silverman, I. M., Quinn, W. J., Gosai, S. J., Tichy, E. D., Davis, J. G., Mourkioti, F., Gregory, B. D., Dellinger, R. W., Redpath, P., Migaud, M. E., Nakamaru-Ogiso, E., Rabinowitz, J. D., Khurana, T. S., & Baur, J. A. (2016). Loss of NAD Homeostasis Leads to Progressive and Reversible Degeneration of Skeletal Muscle. *Cell Metabolism*, *24*(2), 269–282. https://doi.org/10.1016/j.cmet.2016.07.005

Fulco, M., Cen, Y., Zhao, P., Hoffman, E. P., McBurney, M. W., Sauve, A. A., & Sartorelli, V. (2008). Glucose restriction inhibits skeletal myoblast differentiation by activating SIRT1 through AMPK-mediated regulation of Nampt. *Developmental Cell*, *14*(5), 661–673. https://doi.org/10.1016/j.devcel.2008.02.004

Fulco, M., Schiltz, R. L., Iezzi, S., King, M. T., Zhao, P., Kashiwaya, Y., Hoffman, E., Veech, R. L., & Sartorelli, V. (2003). Sir2 Regulates Skeletal Muscle Differentiation as a Potential Sensor of the Redox State. *Molecular Cell*, *12*(1), 51–62. https://doi.org/10.1016/S1097-2765(03)00226-0

Furuichi, Y., Kawabata, Y., Aoki, M., Mita, Y., Fujii, N. L., & Manabe, Y. (2021). Excess Glucose Impedes the Proliferation of Skeletal Muscle Satellite Cells Under Adherent Culture Conditions. *Frontiers in Cell and Developmental Biology*, *9*, 640399. https://doi.org/10.3389/fcell.2021.640399

García-Prat, L., Martínez-Vicente, M., Perdiguero, E., Ortet, L., Rodríguez-Ubreva, J., Rebollo, E., Ruiz-Bonilla, V., Gutarra, S., Ballestar, E., Serrano, A. L., Sandri, M., & Muñoz-Cánoves, P. (2016). Autophagy maintains stemness by preventing senescence. *Nature*, *529*(7584), 37–42. https://doi.org/10.1038/nature16187

Garriga, J., Jayaraman, A. L., Limón, A., Jayadeva, G., Sotillo, E., Truongcao, M., Patsialou, A., Wadzinski, B. E., & Grana, X. (2004). A Dynamic Equilibrium between CDKs and PP2A Modulates Phosphorylation of pRB, p107 and p130. *Cell Cycle*, *3*(10), 1320–1330. https://doi.org/10.4161/cc.3.10.1183

Gerhart-Hines, Z., Rodgers, J. T., Bare, O., Lerin, C., Kim, S.-H., Mostoslavsky, R., Alt, F. W., Wu, Z., & Puigserver, P. (2007). Metabolic control of muscle mitochondrial function and fatty acid oxidation through SIRT1/PGC-1alpha. *The EMBO Journal*, *26*(7), 1913–1923. https://doi.org/10.1038/sj.emboj.7601633

Ginsberg, D., Vairo, G., Chittenden, T., Xiao, Z. X., Xu, G., Wydner, K. L., DeCaprio, J. A., Lawrence, J. B., & Livingston, D. M. (1994). E2F-4, a new member of the E2F transcription factor family, interacts with p107. *Genes & Development*, *8*(22), 2665–2679. https://doi.org/10.1101/gad.8.22.2665

Giordani, L., Parisi, A., & le Grand, F. (2018). Satellite Cell Self-Renewal. *Current Topics in Developmental Biology*, *126*, 177–203. https://doi.org/10.1016/bs.ctdb.2017.08.001

Guja, K. E., & Garcia-Diaz, M. (2012). Hitting the brakes: termination of mitochondrial transcription. *Biochimica et Biophysica Acta*, *1819*(9–10), 939–947. https://doi.org/10.1016/j.bbagrm.2011.11.004

Gundersen, K. (2011). Excitation-transcription coupling in skeletal muscle: the molecular pathways of exercise. *Biological Reviews of the Cambridge Philosophical Society*, *86*(3), 564–600. https://doi.org/10.1111/j.1469-185X.2010.00161.x

Gustafsson, C. M., Falkenberg, M., & Larsson, N.-G. (2016). Maintenance and Expression of Mammalian Mitochondrial DNA. *Annual Review of Biochemistry*, *85*, 133–160. https://doi.org/10.1146/annurev-biochem-060815-014402

Hansen, J. B., Jørgensen, C., Petersen, R. K., Hallenborg, P., de Matteis, R., Bøye, H. A., Petrovic, N., Enerbäck, S., Nedergaard, J., Cinti, S., te Riele, H., & Kristiansen, K. (2004). Retinoblastoma protein functions as a molecular switch determining white versus brown adipocyte differentiation. *Proceedings of the National Academy of Sciences of the United States of America*, *101*(12), 4112–4117. https://doi.org/10.1073/pnas.0301964101

Henley, S. A., & Dick, F. A. (2012). The retinoblastoma family of proteins and their regulatory functions in the mammalian cell division cycle. *Cell Division*, *7*(1), 10. https://doi.org/10.1186/1747-1028-7-10

Hilgendorf, K. I., Leshchiner, E. S., Nedelcu, S., Maynard, M. A., Calo, E., Ianari, A., Walensky, L. D., & Lees, J. A. (2013). The retinoblastoma protein induces apoptosis directly at the mitochondria. *Genes & Development*, *27*(9), 1003–1015. https://doi.org/10.1101/gad.211326.112

Hillen, H. S., Morozov, Y. I., Sarfallah, A., Temiakov, D., & Cramer, P. (2017). Structural Basis of Mitochondrial Transcription Initiation. *Cell*, *171*(5), 1072-1081.e10. https://doi.org/10.1016/j.cell.2017.10.036

Hoffmann, C., Höckele, S., Kappler, L., Hrabě de Angelis, M., Häring, H.-U., & Weigert, C. (2018). The effect of differentiation and TGFβ on mitochondrial respiration and mitochondrial enzyme abundance in cultured primary human skeletal muscle cells. *Scientific Reports*, *8*(1), 737. https://doi.org/10.1038/s41598-017-18658-3

Hong, X., Isern, J., Campanario, S., Perdiguero, E., Ramírez-Pardo, I., Segalés, J., Hernansanz-Agustín, P., Curtabbi, A., Deryagin, O., Pollán, A., González-Reyes, J. A., Villalba, J. M., Sandri, M., Serrano, A. L., Enríquez, J. A., & Muñoz-Cánoves, P. (2022). Mitochondrial dynamics maintain muscle stem cell regenerative competence throughout adult life by regulating metabolism and mitophagy. *Cell Stem Cell*, *29*(9), 1298-1314.e10. https://doi.org/10.1016/j.stem.2022.07.009

Hori, S., Hiramuki, Y., Nishimura, D., Sato, F., & Sehara-Fujisawa, A. (2019). PDH-mediated metabolic flow is critical for skeletal muscle stem cell differentiation and myotube formation during regeneration in mice. *FASEB Journal : Official Publication of the Federation of American Societies for Experimental Biology*, *33*(7), 8094–8109. https://doi.org/10.1096/fj.201802479R

Hwang, A. B., & Brack, A. S. (2018). Muscle Stem Cells and Aging. *Current Topics in Developmental Biology*, *126*, 299–322. https://doi.org/10.1016/bs.ctdb.2017.08.008

Kane, D. A. (2014). Lactate oxidation at the mitochondria: a lactate-malate-aspartate shuttle at work. *Frontiers in Neuroscience*, *8*, 366. https://doi.org/10.3389/fnins.2014.00366

Khacho, M., Clark, A., Svoboda, D. S., Azzi, J., MacLaurin, J. G., Meghaizel, C., Sesaki, H., Lagace, D. C., Germain, M., Harper, M.-E., Park, D. S., & Slack, R. S. (2016). Mitochondrial Dynamics Impacts Stem Cell Identity and Fate Decisions by Regulating a Nuclear Transcriptional Program. *Cell Stem Cell*, *19*(2), 232–247. https://doi.org/10.1016/j.stem.2016.04.015

Klimova, N., Long, A., Scafidi, S., & Kristian, T. (2019). Interplay between NAD+ and acetyl-CoA metabolism in ischemia-induced mitochondrial pathophysiology. *Biochimica et Biophysica Acta. Molecular Basis of Disease*, *1865*(8), 2060–2067. https://doi.org/10.1016/j.bbadis.2018.09.025

Kuang, S., Kuroda, K., le Grand, F., & Rudnicki, M. A. (2007). Asymmetric self-renewal and commitment of satellite stem cells in muscle. *Cell*, *129*(5), 999–1010. https://doi.org/10.1016/j.cell.2007.03.044

Latil, M., Rocheteau, P., Châtre, L., Sanulli, S., Mémet, S., Ricchetti, M., Tajbakhsh, S., & Chrétien, F. (2012). Skeletal muscle stem cells adopt a dormant cell state post mortem and retain regenerative capacity. *Nature Communications*, *3*(1), 903. https://doi.org/10.1038/ncomms1890

Laumonier, T., Bermont, F., Hoffmeyer, P., Kindler, V., & Menetrey, J. (2017). Human myogenic reserve cells are quiescent stem cells that contribute to muscle regeneration after intramuscular transplantation in immunodeficient mice. *Scientific Reports*, *7*(1), 3462. https://doi.org/10.1038/s41598-017-03703-y

le Grand, F., Jones, A. E., Seale, V., Scimè, A., & Rudnicki, M. A. (2009). Wnt7a activates the planar cell polarity pathway to drive the symmetric expansion of satellite stem cells. *Cell Stem Cell*, *4*(6), 535–547. https://doi.org/10.1016/j.stem.2009.03.013

LeCouter, J. E., Kablar, B., Hardy, W. R., Ying, C., Megeney, L. A., May, L. L., & Rudnicki, M. A. (1998). Strain-dependent myeloid hyperplasia, growth deficiency, and accelerated cell cycle in mice lacking the Rb-related p107 gene. *Molecular and Cellular Biology*, *18*(12), 7455–7465. https://doi.org/10.1128/MCB.18.12.7455

Leigh-Brown, S., Enriquez, J., & Odom, D. T. (2010). Nuclear transcription factors in mammalian mitochondria. *Genome Biology*, *11*(7), 215. https://doi.org/10.1186/gb-2010-11-7-215

Leng, X., Noble, M., Adams, P. D., Qin, J., & Harper, J. W. (2002). Reversal of Growth Suppression by p107 via Direct Phosphorylation by Cyclin D1/Cyclin-Dependent Kinase 4. *Molecular and Cellular Biology*, *22*(7), 2242–2254. https://doi.org/10.1128/MCB.22.7.2242-2254.2002

Li, A., Xue, Y., Jin, C., Wang, M., & Yao, X. (2006). Prediction of Nε-acetylation on internal lysines implemented in Bayesian Discriminant Method. *Biochemical and Biophysical Research Communications*, *350*(4), 818–824. https://doi.org/10.1016/j.bbrc.2006.08.199

Lodeiro, M. F., Uchida, A., Bestwick, M., Moustafa, I. M., Arnold, J. J., Shadel, G. S., & Cameron, C. E. (2012). Transcription from the second heavy-strand promoter of human mtDNA is repressed by transcription factor A in vitro. *Proceedings of the National Academy of Sciences of the United States of America*, *109*(17), 6513–6518. https://doi.org/10.1073/pnas.1118710109

Lunt, S. Y., & vander Heiden, M. G. (2011). Aerobic glycolysis: meeting the metabolic requirements of cell proliferation. *Annual Review of Cell and Developmental Biology*, *27*, 441–464. https://doi.org/10.1146/annurev-cellbio-092910-154237

Mann, C. J., Perdiguero, E., Kharraz, Y., Aguilar, S., Pessina, P., Serrano, A. L., & Muñoz-Cánoves, P. (2011). Aberrant repair and fibrosis development in skeletal muscle. *Skeletal Muscle*, *1*(1), 21. https://doi.org/10.1186/2044-5040-1-21

Martínez-Reyes, I., & Chandel, N. S. (2020). Mitochondrial TCA cycle metabolites control physiology and disease. *Nature Communications*, *11*(1), 102. https://doi.org/10.1038/s41467-019-13668-3

Martínez-Reyes, I., Diebold, L. P., Kong, H., Schieber, M., Huang, H., Hensley, C. T., Mehta, M. M., Wang, T., Santos, J. H., Woychik, R., Dufour, E., Spelbrink, J. N., Weinberg, S. E., Zhao, Y., DeBerardinis, R. J., & Chandel, N. S. (2016). TCA Cycle and Mitochondrial Membrane Potential Are Necessary for Diverse Biological Functions. *Molecular Cell*, *61*(2), 199–209. https://doi.org/10.1016/j.molcel.2015.12.002

Massenet, J., Gardner, E., Chazaud, B., & Dilworth, F. J. (2021). Epigenetic regulation of satellite cell fate during skeletal muscle regeneration. *Skeletal Muscle*, *11*(1), 4. https://doi.org/10.1186/s13395-020-00259-w

Mauro, A. (1961). Satellite cell of skeletal muscle fibers. *The Journal of Biophysical and Biochemical Cytology*, *9*, 493–495. https://doi.org/10.1083/jcb.9.2.493

Morozov, Y. I., Parshin, A. v, Agaronyan, K., Cheung, A. C. M., Anikin, M., Cramer, P., & Temiakov, D. (2015). A model for transcription initiation in human mitochondria. *Nucleic Acids Research*, *43*(7), 3726–3735. https://doi.org/10.1093/nar/gkv235

Moss, F. P., & Leblond, C. P. (1970). NATURE OF DIVIDING NUCLEI IN SKELETAL MUSCLE OF GROWING RATS. *Journal of Cell Biology*, *44*(2), 459–461. https://doi.org/10.1083/jcb.44.2.459

Myers, M. J., Shepherd, D. L., Durr, A. J., Stanton, D. S., Mohamed, J. S., Hollander, J. M., & Alway, S. E. (2019). The role of SIRT1 in skeletal muscle function and repair of older mice. *Journal of Cachexia, Sarcopenia and Muscle*, *10*(4), 929–949. https://doi.org/10.1002/jcsm.12437

Nguyen, J. H., Chung, J. D., Lynch, G. S., & Ryall, J. G. (2019). The Microenvironment Is a Critical Regulator of Muscle Stem Cell Activation and Proliferation. *Frontiers in Cell and Developmental Biology*, *7*. https://doi.org/10.3389/fcell.2019.00254

Olguin, H. C., Yang, Z., Tapscott, S. J., & Olwin, B. B. (2007). Reciprocal inhibition between Pax7 and muscle regulatory factors modulates myogenic cell fate determination. *The Journal of Cell Biology*, *177*(5), 769–779. https://doi.org/10.1083/jcb.200608122

Oresajo, O. J. (2021). *A Mitochondrial Role for p130 During Adipocyte Differentiation*.

Pala, F., di Girolamo, D., Mella, S., Yennek, S., Chatre, L., Ricchetti, M., & Tajbakhsh, S. (2018). Distinct metabolic states govern skeletal muscle stem cell fates during prenatal and postnatal myogenesis. *Journal of Cell Science*, *131*(14). https://doi.org/10.1242/jcs.212977

Pfanner, N., Warscheid, B., & Wiedemann, N. (2019). Mitochondrial proteins: from biogenesis to functional networks. *Nature Reviews. Molecular Cell Biology*, *20*(5), 267–284. https://doi.org/10.1038/s41580-018-0092-0

Pfeiffer, T., Schuster, S., & Bonhoeffer, S. (2001). Cooperation and Competition in the Evolution of ATP-Producing Pathways. *Science*, *292*(5516), 504–507. https://doi.org/10.1126/science.1058079

Porras, D. P., Abbaszadeh, M., Bhattacharya, D., D'Souza, N. C., Edjiu, N. R., Perry, C. G. R., & Scimè, A. (2017). p107 Determines a Metabolic Checkpoint Required for Adipocyte Lineage Fates. *Stem Cells (Dayton, Ohio)*, *35*(5), 1378–1391. https://doi.org/10.1002/stem.2576

Puri, P. L., Cimino, L., Fulco, M., Zimmerman, C., la Thangue, N. B., Giordano, A., Graessmann, A., & Levrero, M. (1998). Regulation of E2F4 mitogenic activity during terminal differentiation by its heterodimerization partners for nuclear translocation. *Cancer Research*, *58*(7), 1325–1331.

Rahbani, J. F., Roesler, A., Hussain, M. F., Samborska, B., Dykstra, C. B., Tsai, L., Jedrychowski, M. P., Vergnes, L., Reue, K., Spiegelman, B. M., & Kazak, L. (2021). Creatine kinase B controls futile creatine cycling in thermogenic fat. *Nature*, *590*(7846), 480–485. https://doi.org/10.1038/s41586-021-03221-y

Ramachandran, A., Basu, U., Sultana, S., Nandakumar, D., & Patel, S. S. (2017). Human mitochondrial transcription factors TFAM and TFB2M work synergistically in promoter melting during transcription initiation. *Nucleic Acids Research*, *45*(2), 861–874. https://doi.org/10.1093/nar/gkw1157

Ree, R., Varland, S., & Arnesen, T. (2018). Spotlight on protein N-terminal acetylation. *Experimental & Molecular Medicine*, *50*(7), 1–13. https://doi.org/10.1038/s12276-018-0116-z

Reznik, M. (1969). Thymidine-3H uptake by satellite cells of regenerating skeletal muscle. *The Journal of Cell Biology*, *40*(2), 568–571. https://doi.org/10.1083/jcb.40.2.568

Rocheteau, P., Gayraud-Morel, B., Siegl-Cachedenier, I., Blasco, M. A., & Tajbakhsh, S. (2012). A subpopulation of adult skeletal muscle stem cells retains all template DNA strands after cell division. *Cell*, *148*(1–2), 112–125. https://doi.org/10.1016/j.cell.2011.11.049

Rodier, G., Makris, C., Coulombe, P., Scime, A., Nakayama, K., Nakayama, K. I., & Meloche, S. (2005). p107 inhibits G1 to S phase progression by down-regulating expression of the F-box protein Skp2. *Journal of Cell Biology*, *168*(1), 55–66. https://doi.org/10.1083/jcb.200404146

Ryall, J. G., Dell'Orso, S., Derfoul, A., Juan, A., Zare, H., Feng, X., Clermont, D., Koulnis, M., Gutierrez-Cruz, G., Fulco, M., & Sartorelli, V. (2015). The NAD(+)-dependent SIRT1 deacetylase translates a metabolic switch into regulatory epigenetics in skeletal muscle stem cells. *Cell Stem Cell*, *16*(2), 171–183. https://doi.org/10.1016/j.stem.2014.12.004

Ryzhkova, A., Sazonova, M., Sinyov, V., Galitsyna, E., Chicheva, M., Melnichenko, A., Grechko, A., Postnov, A., Orekhov, A., & Shkurat, T. (2018). Mitochondrial diseases caused by mtDNA mutations: a mini-review. *Therapeutics and Clinical Risk Management*, *Volume 14*, 1933–1942. https://doi.org/10.2147/TCRM.S154863

Schiaffino, S., & Reggiani, C. (2011). Fiber types in mammalian skeletal muscles. *Physiological Reviews*, *91*(4), 1447–1531. https://doi.org/10.1152/physrev.00031.2010

Schwarze, F., Meraner, J., Lechner, M., Loidl, A., Stasyk, T., Laich, A., & Loidl, P. (2010). Cell cycle-dependent acetylation of Rb2/p130 in NIH3T3 cells. *Oncogene*, *29*(42), 5755–5760. https://doi.org/10.1038/onc.2010.311

Scimè, A., Grenier, G., Huh, M. S., Gillespie, M. A., Bevilacqua, L., Harper, M.-E., & Rudnicki, M. A. (2005). Rb and p107 regulate preadipocyte differentiation into white versus brown fat through repression of PGC-1alpha. *Cell Metabolism*, *2*(5), 283–295. https://doi.org/10.1016/j.cmet.2005.10.002

Scimè, A., Soleimani, V. D., Bentzinger, C. F., Gillespie, M. A., le Grand, F., Grenier, G., Bevilacqua, L., Harper, M.-E., & Rudnicki, M. A. (2010). Oxidative status of muscle is determined by p107 regulation of PGC-1α. *Journal of Cell Biology*, *190*(4), 651–662. https://doi.org/10.1083/jcb.201005076

Shefer, G., van de Mark, D. P., Richardson, J. B., & Yablonka-Reuveni, Z. (2006). Satellite-cell pool size does matter: Defining the myogenic potency of aging skeletal muscle. *Developmental Biology*, *294*(1), 50–66. https://doi.org/10.1016/j.ydbio.2006.02.022

Shintaku, J., Peterson, J. M., Talbert, E. E., Gu, J.-M., Ladner, K. J., Williams, D. R., Mousavi, K., Wang, R., Sartorelli, V., & Guttridge, D. C. (2016). MyoD Regulates Skeletal Muscle Oxidative Metabolism Cooperatively with Alternative NF-κB. *Cell Reports*, *17*(2), 514–526. https://doi.org/10.1016/j.celrep.2016.09.010

Sincennes, M.-C., Brun, C. E., Lin, A. Y. T., Rosembert, T., Datzkiw, D., Saber, J., Ming, H., Kawabe, Y., & Rudnicki, M. A. (2021). Acetylation of PAX7 controls muscle stem cell self-renewal and differentiation potential in mice. *Nature Communications*, *12*(1), 3253. https://doi.org/10.1038/s41467-021-23577-z

Snow, MikelH. (1978). An autoradiographic study of satellite cell differentiation into regenerating myotubes following transplantation of muscles in young rats. *Cell and Tissue Research*, *186*(3). https://doi.org/10.1007/BF00224941

Sousa-Victor, P., García-Prat, L., & Muñoz-Cánoves, P. (2022). Control of satellite cell function in muscle regeneration and its disruption in ageing. *Nature Reviews Molecular Cell Biology*, *23*(3), 204–226. https://doi.org/10.1038/s41580-021-00421-2

Tang, A. H., & Rando, T. A. (2014). Induction of autophagy supports the bioenergetic demands of quiescent muscle stem cell activation. *The EMBO Journal*, *33*(23), 2782–2797. https://doi.org/10.15252/embj.201488278

vander Heiden, M. G., & DeBerardinis, R. J. (2017). Understanding the Intersections between Metabolism and Cancer Biology. *Cell*, *168*(4), 657–669. https://doi.org/10.1016/j.cell.2016.12.039

Wen, Y., Bi, P., Liu, W., Asakura, A., Keller, C., & Kuang, S. (2012). Constitutive Notch Activation Upregulates Pax7 and Promotes the Self-Renewal of Skeletal Muscle Satellite Cells. *Molecular and Cellular Biology*, *32*(12), 2300–2311. https://doi.org/10.1128/MCB.06753-11

Wiedemann, N., & Pfanner, N. (2017). Mitochondrial Machineries for Protein Import and Assembly. *Annual Review of Biochemistry*, *86*(1), 685–714. https://doi.org/10.1146/annurev-biochem-060815-014352

Wirt, S. E., & Sage, J. (2010). p107 in the public eye: an Rb understudy and more. *Cell Division*, *5*, 9. https://doi.org/10.1186/1747-1028-5-9

Xiao, W., Wang, R.-S., Handy, D. E., & Loscalzo, J. (2018). NAD(H) and NADP(H) Redox Couples and Cellular Energy Metabolism. *Antioxidants & Redox Signaling*, *28*(3), 251–272. https://doi.org/10.1089/ars.2017.7216

Yablonka-Reuveni, Z. (2011). The skeletal muscle satellite cell: still young and fascinating at 50. *The Journal of Histochemistry and Cytochemistry : Official Journal of the Histochemistry Society*, *59*(12), 1041–1059. https://doi.org/10.1369/0022155411426780

Yin, H., Price, F., & Rudnicki, M. A. (2013). Satellite cells and the muscle stem cell niche. *Physiological Reviews*, *93*(1), 23–67. https://doi.org/10.1152/physrev.00043.2011

Yoshida, N., Yoshida, S., Koishi, K., Masuda, K., & Nabeshima, Y. (1998). Cell heterogeneity upon myogenic differentiation: down-regulation of MyoD and Myf-5 generates 'reserve cells.' *Journal of Cell Science*, *111*(6), 769–779. https://doi.org/10.1242/jcs.111.6.769

Yucel, N., Wang, Y. X., Mai, T., Porpiglia, E., Lund, P. J., Markov, G., Garcia, B. A., Bendall, S. C., Angelo, M., & Blau, H. M. (2019). Glucose Metabolism Drives Histone Acetylation Landscape Transitions that Dictate Muscle Stem Cell Function. *Cell Reports*, *27*(13), 3939-3955.e6. https://doi.org/10.1016/j.celrep.2019.05.092

Zammit, P. S., Golding, J. P., Nagata, Y., Hudon, V., Partridge, T. A., & Beauchamp, J. R. (2004). Muscle satellite cells adopt divergent fates: a mechanism for self-renewal? *The Journal of Cell Biology*, *166*(3), 347–357. https://doi.org/10.1083/jcb.200312007

Zammit, P. S., Relaix, F., Nagata, Y., Ruiz, A. P., Collins, C. A., Partridge, T. A., & Beauchamp, J. R. (2006). Pax7 and myogenic progression in skeletal muscle satellite cells. *Journal of Cell Science*, *119*(Pt 9), 1824–1832. https://doi.org/10.1242/jcs.02908

Zhang, H., Ryu, D., Wu, Y., Gariani, K., Wang, X., Luan, P., D'Amico, D., Ropelle, E. R., Lutolf, M. P., Aebersold, R., Schoonjans, K., Menzies, K. J., & Auwerx, J. (2016). NAD^+ repletion improves mitochondrial and stem cell function and enhances life span in mice. *Science (New York, N.Y.)*, *352*(6292), 1436–1443. https://doi.org/10.1126/science.aaf2693

Zhang, J., Xiang, H., Liu, J., Chen, Y., He, R.-R., & Liu, B. (2020). Mitochondrial Sirtuin 3: New emerging biological function and therapeutic target. *Theranostics*, *10*(18), 8315–8342. https://doi.org/10.7150/thno.45922

Zhao, S., Torres, A., Henry, R. A., Trefely, S., Wallace, M., Lee, J. V., Carrer, A., Sengupta, A., Campbell, S. L., Kuo, Y.-M., Frey, A. J., Meurs, N., Viola, J. M., Blair, I. A., Weljie, A. M., Metallo, C. M., Snyder, N. W., Andrews, A. J., & Wellen, K. E. (2016). ATP-Citrate Lyase Controls a Glucose-to-Acetate Metabolic Switch. *Cell Reports*, *17*(4), 1037–1052. https://doi.org/10.1016/j.celrep.2016.09.069

Zollo, O., Tiranti, V., & Sondheimer, N. (2012). Transcriptional requirements of the distal heavy-strand promoter of mtDNA. *Proceedings of the National Academy of Sciences of the United States of America*, *109*(17), 6508–6512. https://doi.org/10.1073/pnas.1118594109